Bedform appearance and dimension in the nearshore under mixed wave and current conditions

J.W.Q. Brockhus

MSc thesis

04-01-2011

Supervisor:

Dr. B.G. Ruessink

Physical Geography

Utrecht University

Table of content

List of figures

Summary

In autumn 2009 a field campaign was done in the nearshore near a secondary tidal inlet, the Slufter, which is located on the most southern Wadden island Texel of the Netherlands. The aim of this research was to get a better understanding of the behaviour, appearance and geometry, of bedforms in the nearshore under combined wave and current conditions. Due to the presence of the Slufter tidal larger current effects were expected.

The wave conditions at the instrument location during the campaign were mostly just prior to breaking having shoaling characteristics, due to its location behind an inner bar at roughly the same height as the bar. The bedforms varied in length between 0.17 and 3 m and between 0.01 and 0.23 m in height. The transition from ripples to larger bedforms is observed to depend on a small range of Hm0 and the mean current, with the mean current playing a key role. 2D bedforms are found for low intensity wave conditions and 3D bedforms for more intense mixed wave current conditions. The wave and mixed wave-current bedforms/conditions are best separated by the criteria of Li & Amos (1998). The occasional observed sheet flow conditions were best separated with a ciritial Shiels number of 0.8 and the wave current Shields number combining method $\theta_{\mathrm{wc}} = \theta_w + \theta_c$ (Allen & Leeder, 1980).

The evolution of bedforms is found to differ for increasing versus decreasing condition, hysteresis, being more pronounced for rapid changing conditions. For increasing conditions the bedforms evolve equal rapidly although some relaxation is often present. For decreasing conditions the bedform dimensions delay the conditions significantly and may, for a decrease in Hm0 of 0.2 m and mean current of 0.2 m/s per hour, ‘freeze’. This freeze may be a temporarily result of the process of split.

Four bedform predictors are tested against the observed bedform dimensions, two wave and two wave/current based. Little difference between the predictions of wave and wave/current induced bedforms is found. The wave/current predictor of Khelifa & Ouellet (2000) performs the best, even for wave only conditions. Disregarding the bedforms from the first fifth and fifth fifth duration of each tide, which are expected to deviate due to relaxation, did not lead to major improvements of the predictors.

1. Introduction

This chapter gives an introduction to the research. Section 1.1 clarifies the relevance of this study. In section 1.2 a brief overview of the relevant literature is given. Based on this literature overview, research questions are formulated in section 1.3. Section 1.4 presents the thesis outline.

1.1 Motivation

In this thesis the bedform appearance and dimensions under wave and current conditions in the nearshore is treated. Specifically, near the secondary tidal inlet the Slufter which is expected to induce large current effects. For the prediction of seabed changes, coastal evolution and the morphological impact of human interference in the coastal zone, the wave induced sediment suspension and more importantly, the net sediment transport needs to be known. For predicting this sediment suspension and net sediment transport, the appearance and geometry (dimension and bedform pattern) of bedforms is of fundamental importance (Wiberg & Harris, 1994; O'Donoghue et al., 2006). Bedforms affect the flow regime in two ways; firstly, bedforms represent roughness elements, determining the structure of the bottom boundary layer; secondly, certain bedforms can generate near-bed turbulence (vortex) significantly affecting the vertical profile of suspended sediment (Vincent et al., 1991).

Bedforms have already been intensively researched for decades. Although numerous bedform, mainly ripple, predictors have been proposed (e.g. Nielsen, 1981; Grant &Madsen 1982; van Rijn, 1993; Wiberg & Harris, 1994; or more recently, Soulsby & Whitehouse, 2005), none is widely accepted. This indicates that the process of bedform formation and the dependence of the bedforms on the flow conditions is not fully understood or not is not yet captured adequately within a predictor. One source of discrepancy between predicted and observed bedforms is the difference in flow, both wave and current, conditions on which the predictor is based and which flow conditions are observed. Early research took place in laboratories with flume or oscillatory plate experiments (among others, Bagnold, 1946). The later field studies were besides in the nearshore often performed on the continental shelf. Nearshore conditions are expected to show; wave skewness caused by wave shoaling which lacks in both laboratory as continental shelf conditions; wave irregularity often lacking in laboratory conditions; an additional mean current like a wave induced cross or longshore current or a tidal current usually not present in laboratory conditions; and close to the shore rapid changing conditions due to tidal induced changing water levels which can lead to hysteresis, were laboratory but also continental shelf (due to the larger waterdepth) conditions are more constant in time. The focus of this thesis will lie on the effect of an additional mean current and hysteresis on the bedform appearance and dimensions.

This thesis is done as part of the Master research program of the master Physical Geography at Utrecht University. It is part of a larger research project conducted at the Slufter in getting a better understanding in the morpho- and hydrodynamic behaviour of secondary tidal inlets.

1.2 Literature review

In this section a review of the research of the past decades on bedforms is given. The research on wave induced bedforms, many ripples, is extensive but under combined wave and current conditions is not. Therefore some wave only condition subjects relevant for the expected nearshore conditions are treaded first where after current influences and hysteresis will be discussed.

First, the bed is not always covered with bedforms. Three different bed stages can be distinguished:

- Lower stage plane bed
- Bed covered with bedforms
- Upper stage plane bed (sheet flow conditions)

Lower stage plane bed refers to a plane bed with no or negligible sand motion (excluding biogenic features) (Kleinhans, 2005). The topography will be flat or dominated with relict bedforms and or bioturbation (Nielsen, 1992). Upper stage plane bed refers to a plane bed which is due to such intense flow, both wave as current, conditions characterised with a suspension layer of several grains thick (Kleinhans, 2005). Ripples develop during times when the bed material is primarily moving as bed load and are assumed to be washed out during very intense flow conditions when most of the moving bed material is carried in suspension (Wiberg and Harris, 1994). The critical Shields parameter θ_{cr}, indicating the critical flow conditions for which the initiation of motion occurs is therefore often used to distinguish between the lower stage plan bed and a bed covered with bedforms. Varies equations and diagrams have been developed to determine the critical Shields parameter, one recent equation is proposed by Soulsby (1997) (In Camenen, 2009):

$$\theta_{cr} = \frac{0.30}{1+1.2d_*} + 0.055 \cdot [1 - \exp(-0.02 d_*)] \tag{1.1}$$

Where d_* is the dimensionless grain size:

$$d_* = \left(\frac{(s-1) \cdot g}{\nu^2} \right)^{1/3} \cdot d_{50} \tag{1.2}$$

with ν the kinematic viscosity. A lower stage plane bed will be present if the Shields parameter θ is smaller than the critical Shields parameter. The Shield parameter:

$$\theta = \frac{0.5 \cdot f_w \cdot \hat{U}_\delta^2}{(s-1) \cdot g \cdot d} \tag{1.3}$$

Here, f_w is the wave friction factor, for which varies empirical formulas exist. $\hat{U}_\delta$ is the near bed peak orbital velocity, s is the relative density of sediment, g is the acceleration of gravity and d is the sediment grain diameter (usually d_{50}). Besides the equation of Soulsby and Whitehouse (1997), less complex equations are often used for the critical Shields parameter, e.g. Nielsen (1992), $\theta_{2.5} < 0.05$. Here $\theta_{2.5}$ refers to the grain related Shields parameter. Although differences exist between the different equations by different authors, the principle for distinguishing between a lower stage plane bed and a bed covered with bedforms based on the critical Shields parameter is widely accepted (e.g. Nielsen, 1992; van Rijn, 1993; Kleinhans, 2005; Camenen, 2009).

Sheet flow conditions are assumed to be present in the surf zone (nearshore) where breaking waves are dominant (van Rijn, 1993). Several criteria are proposed to separate a bed covered with bedforms from an upper stage plane bed; critical values for the Shield parameter, mobility parameter, orbital Reynolds number and ratio $\hat{A}_\delta/d_{50}$. Most commonly used criteria are critical values for the Shield parameter and mobility parameter. The mobility number reads:

$$\psi = \frac{\hat{U}_\delta^2}{(s-1)\cdot g \cdot d} \tag{1.4}$$

Some criteria from different authors for which an upper plane stage bed is predicted:

$\theta > 0.8$ (Camenen, 2009; van Rijn, 1993) (1.5)

$\theta_{2.5} > 1$ (Nielsen, 1992) (1.6)

$\psi > 100$ (Camenen, 2009) (1.7)

$\psi > 250$ (van Rijn, 1993) (1.8)

$\psi > 156$ (Grasmeijer and Kleinhans, 2004) (1.9)

The differences in criteria, especially for the mobility number, are rather large indicating the upper stage plane bed occurrence is likely to be influenced by yet another flow characteristic. One flow characteristic possible influencing the criteria is wave irregularity, present in natural wave conditions. For conditions with $\psi > 25$ / $\psi > 30$ wave irregularity results in smaller and less steep bedforms according to van Rijn (1993) and van der Werf (2006) respectively. The effect is more pronounced for more intense conditions and can according to O'Donoghue et al. (2006) lead for very intense conditions ($\psi > 190$) to a different bedform regime than for the equivalent regular flow. The highest velocities in the irregular flow regime induce flat bed conditions, while in the regular flow case the bedforms keep growing. Criteria incorporating wave irregularity are not found.

The initial bedform type after a lower stage plane bed condition is rolling grain ripples, named after the back and forth rolling of the grains. Rolling grain ripples are a transitory regime always evolving into vortex ripples in which the evolution time depends on the flow conditions (Stegner & Westfreid, 1999). O'Donoghue & Clubb (2001) observed evolution times of only a few minutes for natural like (irregular but still laboratory) conditions (T, 2-10 and $\hat{A}_\delta$ 0.16-2.2m). Rolling grain ripples are therefore not expected to be recorded during the field campaign. Vortex ripples are ripples which may develop a vortex at the lee-side of the ripple and detach form the crest each half oscillation (Yoshikawa et al., 2004; van der Werf et al., 2007). A further differentiation in vortex ripples, based on their spatial pattern 2D or 3D, is often made (e.g. O'Donghue et al., 2006; van der Werf, 2006; Dolphin & Vincent, 2009). The 2D pattern refers to wave ripples with long crests sometimes referred to as linearly ripples, see figure 1.1. Within the 3D ripple a further distinction in irregular ripples, characterised by an irregular pattern with short crested ripples with frequent bifurcations, and cross shore ripples, characterized by two sets of ripples, short- and longwave crested, can be made see figure 1.1. (Osborne & Vincent, 1993; van Rijn, 1993; Hay & Mudge, 2005).

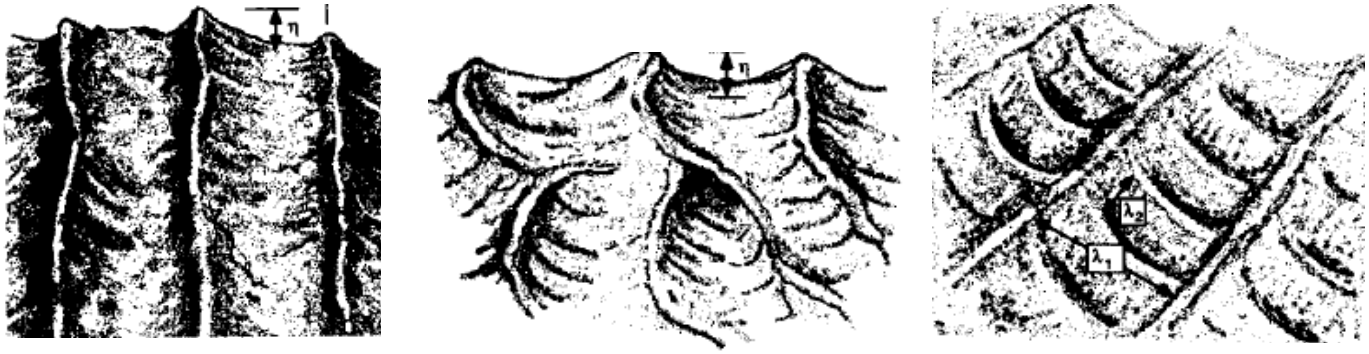

Fig. 1.1, Sketches of different ripple patterns. From right to left; 2D (linear) ripple pattern, irregular (3D) ripple pattern and cross shore (3D) ripple pattern. (Osborne & Vincent, 1993)

Besides ripples, larger bedform features are found in laboratory and field conditions. The larger bedforms have greater lengths than normal wave ripples (>>0.2m), are often sub-imposed on ripples and are associated with more intense flow conditions (e.g. Nielsen 1992; Osborne & Vincent, 1993; van Rijn, 1993, Ribberink & Al-Salem, 1994; Li & Amos, 1999; Hay & Mudge, 2005; Kleinhans, 2005; Masselink et al., 2007). Furthermore, larger bedform features are generally associated with much sediment suspension but not with vortex shedding (e.g. Kleinhans, 2005). For the 'classification' of larger bedforms several names are in use by different authors, like long wave ripples (LWR) (e.g. Masselink et al., 2007; Dolphin & Vincent, 2009), or megaripples (Osborne & Vincent, 1993). Some even further differentiate the larger bedfroms based on 2D or 3D shape. This differentiation and naming is not straightforward and consistent between different authors.

For determining the type of bedform/pattern being present for certain wave conditions little predictors exist. However, two wave induced flow characteristics are suggested to influence the appearance of different bedform types, the orbital flow velocity and wave skewness. But, different authors do not agree upon the degree of influence of those flow characteristics. Hay & Mudge (2005) state, based on their field data, that the bedform type depends on the orbital velocity while being insensitive to wave skewness and wave asymmetry (sawtooth shaped waves), see figure 1.2. However, large overlap between the different bedform types is still present; note the carefully chosen order foreground /background of the different colours/bedform types. The large flume data of O'Donoghue et al. (2006) gives a similar result, being able to distinguish between flat bed and bedforms, but unable to clearly distinct between bedform types based on the highest flow velocity. Osborne & Vincent (1993) and van Rijn (1993) observed a bedform sequence for increasing skewness; irregular ripples (3D pattern), cross ripples, lunate megaripples and flat bed. But since the increasing wave skewness is simultaneously accompanied with orbital velocity, the direct relation between wave skewness and bed form type is not proven.

Besides wave characteristics O'Donoghue & Clubb (2001), O'Donoghue et al. 2006 and van der Werf (2006) indicate dependency of the bedform type on the grain size, 2D ripples when D50 > 0.30 mm and 3D when the D50 is less than 0.22 mm. O'Donoghue et al. (2006) explain this phenomenon by the fact

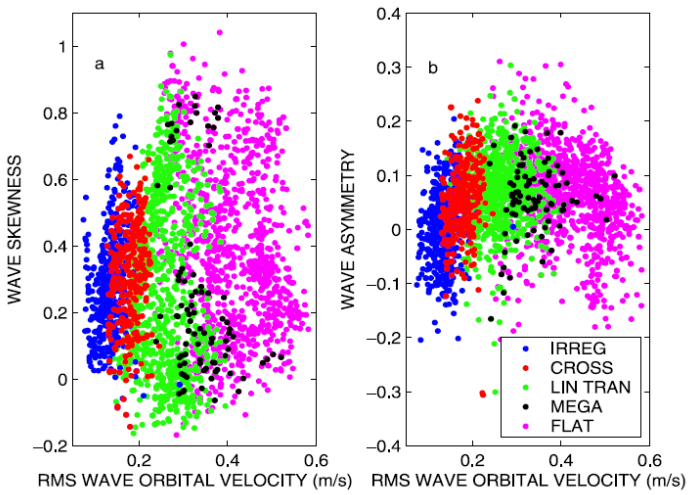

Fig. 1.2, The bedform types plotted for the wave orbital velocity against wave skewness and asymmetry respectively, with irregular ripples, cross shore ripples, linear transition ripples (2D pattern), megaripples and flat bed (Hay & Mudge, 2005).

that fine sand is more susceptibility to turbulent fluid motions. This combining with the fact that the main flow is mainly 2D oriented while turbulence is 3D, leads to the argument that the coarse sand will tend follow the 2D main flow while fine sand will also be influenced by the 3D turbulence motion, thus resulting in more 3D bedforms for finer sands.

For the bedform dimensions however, many empirical predictors exist mainly focussing on ripples. Although different authors use different relationships to predict the wavelength like the Shields number (θ), the mobility number (ψ) or the ratio between the orbital excursion and the grain diameter $\hat{A}_\delta/d$, a similar tendency in the length can to some extent be found. For low flow conditions the (vortex) ripple length (λ) scales to the near bed orbital excursion, called orbital ripples by Clifton (1976) adopted by e.g. Wiberg & Harris (1994), Williams et al. (2005) and Camenen (2009), or called the equilibrium range by Grand & Madsen (1982) and Li & Amos (1998). For more intense flow conditions the sediment is more transported as suspended load, which due to its diffusive character results in a smoothing of the ripples (Nielsen, 1981; Grant & Madsen, 1982; van Rijn, 1993; Wiberg & Harris, 1994; Li & Amos, 1998) and the relation between the orbital excursion and ripple length becomes 'decoupled' (Grant & Madsen, 1982; Li & Amos, 1998). This transition is referred to the break-off point (Grant & Madsen, 1982; Li & Amos, 1998) or to suborbital ripples (Clifton, 1976; van Rijn, 1993; Wiberg & Harris, 1994). For flow conditions above this transition the two different theories/approaches deviate from each other. Above the break-off point, the break-off region, the ripple length still grows/evolves defined by a different relation as for the equilibrium range. While, anorbital ripples refer to ripples having lengths proportional to the sediment size being constant for increasing conditions (Clifton, 1976). This theory is confirmed by Wiberg & Harris (1994), but other authors (e.g. Hay & Mudge, 2005; O'Donoghue et al., 2006; Camenen, 2009) do find increasing ripple lengths. An explanation for this discrepancy can be found in the earlier quoted irregularity; wave irregularity results in smaller bedforms with a more pronounced effect for more intense conditions. This effect can be observed in figure 1.3, used by Wiberg & Harris (1994) to argue for (an)orbital ripple:

comparing the left and right figure where the anorbital ripples coincide with the field (irregular) data and orbital ripples coincide with lab (regular) data.

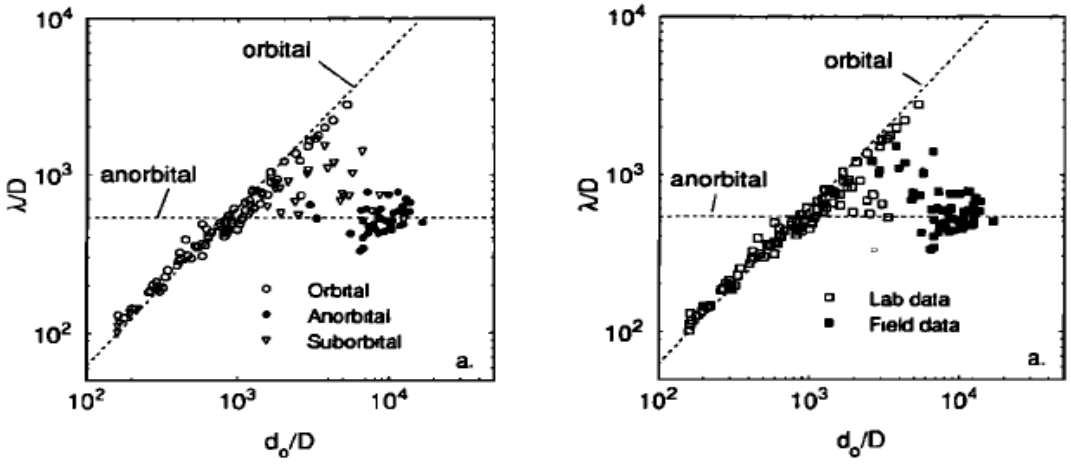

Fig. 1.3, Measured wavelength (λ/d) against orbital diameter ($\hat{A}_\delta/d$) with two different legends (Wiberg & Harris, 1994).

The bedform height is often predicted using the length and steepness (e.g Grant & Madsen 1982; Wiberg & Harris, 1994. Grasmeijer & Kleinhans, 2004), because the steepness shows a more distinctive 'evolution' with respect to the flow conditions than the height. Rolling grain ripples have a small steepness < 0.10 while vortex ripples are found to have a steepness of 0.15-0.2 (Nielsen, 1981; Grant & Madsen, 1982; Wiberg & Harris, 1994; Li & Amos, 1999; Stegner & Westfreid, 1999; Styles & Glenn, 2002). This vortex steepness is found to be the maximum or near maximum steepness, bounded by the angle of response of the bed sediment. For more intense flow conditions the bedforms are smoothed and the steepness decreases, ultimately to the upper stage plane bed (e.g. Nielsen, 1981; Wiberg & Harris, 1994; Li & Amos, 1999; Styles & Glenn, 2002). Furthermore, O'Donoghue et al. (2006) and van der Werf (2006) found that bedforms showing a 3D pattern (or shape) are generally smaller than 2D bedforms. For the case of ripples, O'Donoghue et al. (2006) propose to multiply the height and length of 2D ripple with 0.55 and 0.73 respectively to obtain the dimensions of a 3D rippled bed.

Three common used and reviewed wave induced bedform (ripple) predictors spanning the different relationships used to predict the bedform dimensions:

Grant & Madsen, 1982

Grant & Madsen distinguish between ripples in equilibrium and break-off range based on the break-off point:

$$\left(\frac{\theta'}{\theta_{cr}}\right)_B = 1.8 \cdot \left(\frac{d_*^{1.5}}{4}\right)^{0.6} \tag{1.10}$$

Where the superscript ' stands for grain (skin) related. For the equilibrium range, when $(\theta'/\theta_{cr}) < (\theta'/\theta_{cr})_b$;

$$\frac{\eta}{\lambda} = 0.16 \cdot \left(\frac{\theta'}{\theta_{cr}} \right)^{-0.04} \tag{1.11}$$

$$\frac{\eta}{\hat{A}_\delta} = 0.22 \cdot \left(\frac{\theta'}{\theta_{cr}} \right)^{-0.16} \tag{1.12}$$

For the breakoff range, when $(\theta'/\theta_{cr}) > (\theta'/\theta_{cr})_b$:

$$\frac{\eta}{\hat{A}_\delta} = 0.48 \cdot \left(\frac{d_*^{1.5}}{4} \right)^{0.8} \cdot \left(\frac{\theta'}{\theta_{cr}} \right)^{-1.5} \tag{1.13}$$

$$\frac{\eta}{\lambda} = 0.28 \cdot \left(\frac{d_*^{1.5}}{4} \right)^{0.6} \cdot \left(\frac{\theta'}{\theta_{cr}} \right)^{-1.0} \tag{1.14}$$

Nielsen, 1981

Nielsen uses the mobility number to predict the ripple length and distinct between laboratory (regular) and irregular (field) conditions. Only the ones for irregular conditions are given.

$$\frac{\lambda}{\hat{A}_\delta} = \exp\left(\frac{6936 - 0.37 \cdot \ln^8 \psi}{1000 + 0.75 \cdot \ln^7 \psi} \right) \tag{1.15}$$

$$\frac{\eta}{\hat{A}_\delta} = 0.275 - 0.022 \cdot \psi^{0.5} \tag{1.16}$$

Soulsby & Whitehouse 2005

Soulsby & Whitehouse use after extensive comparison with different data sets and different predictors Δ, $\hat{A}_\delta/d$.

$$\frac{\lambda}{A} = \left[1 + 1.87 \cdot 10^{-3} \cdot \Delta \cdot \left(1 - \exp\left\{ -\left(2.0 \cdot 10^{-4} \cdot \Delta \right)^{1.5} \right\} \right) \right]^{-1} \tag{1.17}$$

$$\frac{\eta}{\lambda} = 0.15 \cdot \left[1 - \exp\cdot \left\{ -\left(5000/\Delta \right)^{3.5} \right\} \right] \tag{1.18}$$

In nearshore field conditions the bed is often subjected to a steady current 'superimposed' on the wave motion. Such current is found to influences the bedform type/pattern (Sherman & Greenwood, 1984; van Rijn, 1993; Li & Amos, 1998; Andersen & Faraci, 2002; Kleinhans, 2005; Dolphin & Vincent, 2009) and/or bedform dimensions (Nielsen, 1981, van Rijn, 1993; Li & Amos, 1998; Khelifa & Ouellet, 2000).

According to the laboratory experiments of Andersen & Faraci (2002) leads an addition mean current perpendicular to the wave direction for increasing current strength to serpentine, segmented and finally irregular (current) ripples, see figure 1.4.a. The segmented pattern is a pattern in between serpentine and irregular, where the serpentine wavy pattern is still visible but with discontinues ripple crests (irregular). An appearance of the serpentine pattern for a perpendicular current is also found by Lee Young & Sleath (1990). The occurrence of an irregular pattern for a large mean current is expected since pure current ripples show a irregular (3D) pattern as well (van Rijn, 1993; Li & Amos, 1998; Kleinhans, 2005). Hay & Mudge (2005) do not support this coupling between the mean current strength and ripple pattern, based on their field data, see figure 1.4.b. Their data shows that every bedform type is present for a

significant range of longshore currents and that the bedform type is more likely to be depended on de orbital diameter.

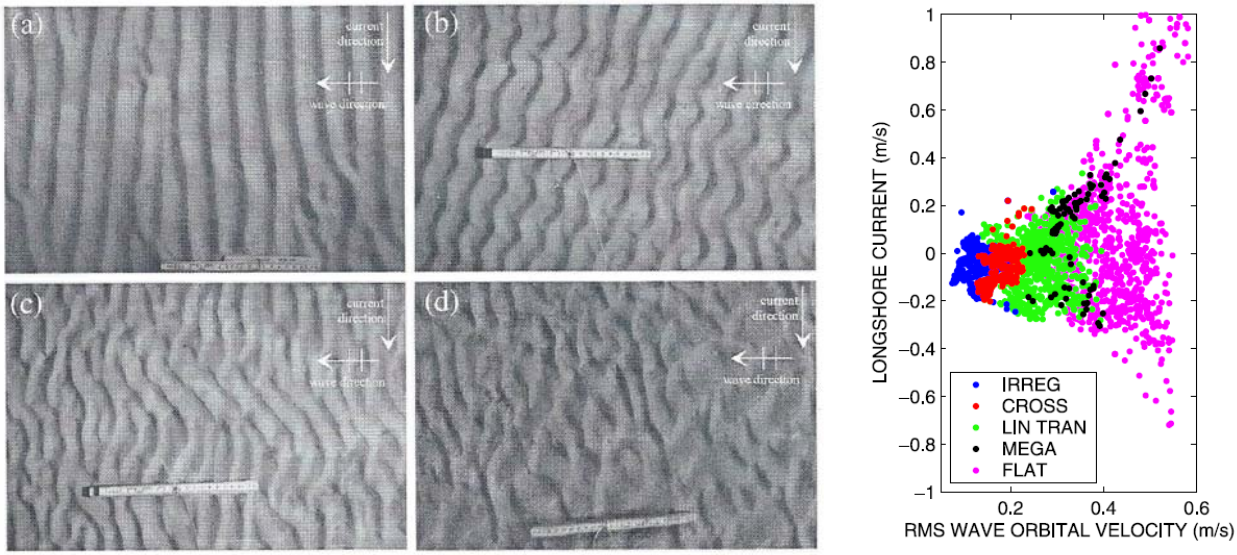

Fig. 1.4. a) (left) Ripple pattern for increasing current strength: a) 2D (U_c/U_w = 0.13), b) serpentine (U_c/U_w = 0.5), c) segmented (U_c/U_w = 0.9), d. Irregular (U_c/U_w = 1.5). b) (right) The bedform types plotted for the wave orbital velocity against longshore current, (Hay & Mudge, 2005).

Current induced ripples differ besides the always irregular pattern from wave induced ripples by being asymmetrical shaped and therefore having a strongly three-dimensional, often linguoid, shape (van Rijn, 1993; Kleinhans, 2005). Wave induced ripples can also show an asymmetrical shape induced by wave skewness (e.g. Ribberink & Al-Salem, 1994; Wiberg and Harris 1994; Hay & Mudge, 2005) for $\Delta\hat{U}_\delta$ (orbital velocity asymmetry) > 0.05 m/s according to van Rijn (1993). Furthermore, current and mixed (current and wave) induced ripples are lower and therefore less steep than purely wave induced ripples, according to field observations of Li & Amos (1998). This could directly result from the asymmetry when the steepness is bounded by the angle of response, since asymmetrical shaped bedforms (lee side bounded by angle of response) need to be relatively longer than symmetrical (lee and stoss side bounded by angle of response) shaped bedforms.

Different criteria are proposed to distinct between current, wave or mixed induced ripples or between the resulting ripple pattern. Li & Amos (1998) proposed the ratio between the skin (grain related) friction wave shear velocity to skin friction current shear velocity $U_{*,w}/U_{*,c}$

$U_{*,w}/U_{*,c} > 2$	wave ripples
$1.25 < U_{*,w}/U_{*,c} < 2$	wave-dominant ripples
$0.75 < U_{*,w}/U_{*,c} < 1.25$	combined wave-current ripples
$U_{*,w}/U_{*,c} < 0.75$	current dominated ripples

With the shear velocity:

$$U_* = \sqrt{\frac{\tau}{\rho}} = \sqrt{0.5 \cdot f \cdot \hat{U}_\delta^2}$$

With τ the bed shear stress

$$\tau = \rho \cdot \nu_t \cdot \frac{du}{dz}$$

The different ripple types are distinguished on increasing bedform asymmetry and increasingly irregular (3D) pattern. Figure 1.5 shows the recorded bedform types of Li & Amos (1998) plotted against the proposed criteria and seems to be well separated by it. Andersen & Farci (2002) use the ratio wave orbital velocity and current velocity U_c/U_w to distinguish between their found bedform patterns. Here the ratio's are reversed

$U_w/U_c > 5$	ripples are not affected by the current (2D pattern)
$1.6 < U_w/U_c < 5$	serpentine pattern
$0.9 < U_w/U_c < 1.6$	segmented pattern
$0.9 < U_w/U_c$	irregular pattern (current ripples)

Since the shear velocity is significantly different than just velocity, the criteria of Li & Amos (1998) and Andersen & Faraci (2002) are difficult to compare. Besides, the data of Li & Amos is based on field conditions while the data of Andersen & Faraci (2002) is based on laboratory experiments with a T of 1.1 sec and maximal water depth of 0.45m.

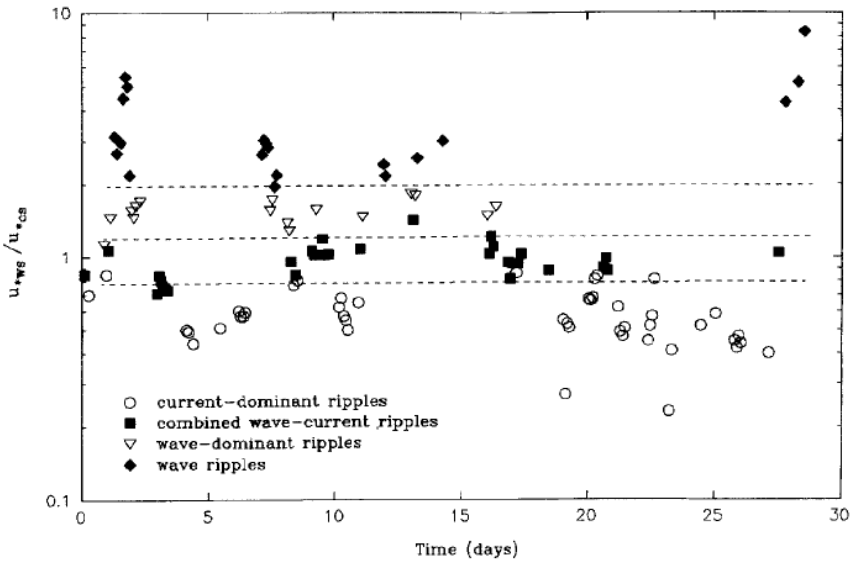

Fig. 1.5, Bedform type plotted against $U_{*,w}/U_{*,c}$ (Li & Amos, 1998).

Figure 1.6 shows the phase diagram of Kleinhans (2005) for combined wave and current conditions, based on the grain related wave Shields parameter θ'_w and grain related current Shields parameter θ'_c In this diagram Kleinhans not only tries to differentiate between wave versus current dominated bedforms but also between upper and lower stage plane bed and tries to further differentiate for different bed forms types. For the latter insufficient data is available for this to be verified. But, the general

transitions between wave and current dominated conditions seem to be captured, although some overlap (scatter) is present. Kleinhans (2005) distinguish between wave, wave dominated, current dominated and wave ripples based on the criteria of Zanke (2003). To compare the ratio's with Li & Amos (1998) the square root of the ratio's are taken to give the skin friction shear velocities.

$U_{*,w}/U_{*,c} > 2.24$	wave only ripples
$1 < U_{*,w}/U_{*,c} < 2.24$	wave-dominant ripples
$0.45 < U_{*,w}/U_{*,c} < 1$	current-dominated ripples
$U_{*,w}/U_{*,c} < 0.45$	current ripples

The value to distinguish between wave and wave dominated ripples are quite similar between Li & Amos (1998) and Zanke (2003). Li & Amos (1998) also distinguish combined wave current ripples above Zanke (2003) but do not distinguish current ripples. The values to distinguish between current dominated ripples do differ.

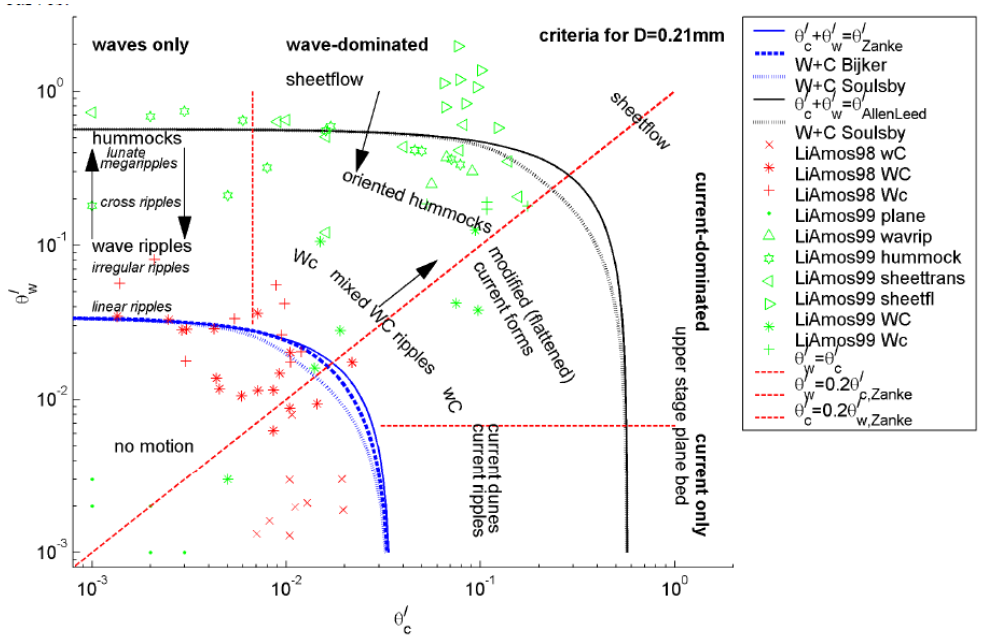

Fig. 1.6. Distinguishing between different bedform types for combined wave and current conditsion (Kleinhans, 2005).

To distinguish between lower and upper stage plan bed, the Shields parameter has be able to represent both wave, current as combined wave current conditions. One quite resent criteria also used in the diagram of Kleinhans (2005) is that of Soulsby (1997), originally in shear stress (τ) but can be substituted by θ:

$$\theta_{cw} = \sqrt{(\theta_m + \theta_w \cos\phi)^2 + (\theta_w \sin\phi)^2} \qquad (1.19)$$

In wich Φ is the angle between the waves and current and θ_m is the mean Shields number:

$$\theta_m = \theta_c(1 + 1.2(\theta_w/(\theta_c + \theta_w))^{3.2}) \qquad (1.20)$$

To other proposed criteria are

$$\theta_{wc} = \theta_w + \theta_c \qquad (1.21)$$

$$\theta_{wc} = \sqrt{(\theta_w^2 + \theta_c^2)} \qquad (1.22)$$

1.21 is proposed by Allen & Leeder (1980, in Kleinhans 2005) which may be physically incorrect when the wave and current are not co-directional, ignoring the interaction between the two components. 1.22 originates from the maximum shear stress according to Soulsby (1997) and is physically equal to adding two vector components under a 90° angle.

For predicting the dimensions of wave/current bedforms less predictors have been developed than for wave only conditions. One quite resent is proposed by Khelifa & Ouellet (2000):

$$\frac{2\cdot\lambda}{d_{wc}} = 1.9 + 0.08\cdot\ln^2\left(1+\psi_{wc}\right) - 0.74\left(1+\psi_{wc}\right) \tag{1.23}$$

$$\frac{2\cdot n}{d_{wc}} = 0.32 + 0.017\cdot\ln^2\left(1+\psi_{wc}\right) - 0.142\cdot\ln\left(1+\psi_{wc}\right) \tag{1.24}$$

The length and height depend on d_{wc}, the distanced moved by the fluid during a wave period, and on the mobility number in which the velocity is also defined by d_{wc},:

$$d_{wc} = \sqrt{\left(d_w^2 + \left(T\cdot\overline{u}_\delta\right)^2 + 2\cdot d_w\cdot\left(T\cdot\overline{u}_\delta\right)\cdot\cos\theta\right)} \tag{1.25}$$

$$U_{wc} = \frac{d_{wc}}{T} \tag{1.26}$$

The predictor of Soulsby & Whitehouse (2005) already given also has an current induced bedform part which should be applied when $\theta'_c > \theta'_w$:

$$y = d_{50}\cdot\left(500 + 1881\cdot D_*^{-1.5}\right) \tag{1.27}$$

$$\eta_{\max} = d_{50}\cdot 202\cdot D_*^{-0.554} \tag{1.28}$$

η_{max} since the bedform height is expected to be washed out for an increasing intense current. For the expected range of sediment size on the field site:

$$\theta'_{wo} = 1.66\cdot D_*^{-1.3} \quad \theta'_{sf} = 2.26\cdot D_*^{-1.3} \tag{1.29}$$

$$\eta_{eq} = \eta_{\max}\cdot\left(\frac{\theta'_{sf} - \theta'_c}{\theta'_{sf} - \theta'_{wo}}\right) \qquad \text{for } \theta'_{wo} < \theta'_c < \theta'_{sf} \tag{1.30}$$

With θ'_{wo} the wash out criteria and θ'_{sf} the sheetflow criteria. $\eta_{eq} = \eta_{max}$ for $\theta'_c < \theta'_{wo}$.

Most bedform predictors presume the bedforms to be in equilibrium with the forcing, like Nielsen (1981), Grant & Madsen (1982) and Khelifa & Ouellet (2000). However, in nearshore environments the wave conditions can change rapidly. Recent laboratory (Stegner & Westfried, 1999; Smith & Sleath, 2005; Doucette & O'Donoghue, 2006) but also field studies (Osborne & Vincent, 1993; Traykosvski, 1999; Williams et al., 2005; Austin et al., 2007; Dolphin & Vincent, 2009) indicate that it can take a significant amount of time for bedforms to evolve after a change in the wave conditions. This time, also called relaxation time, is by several authors quantified into a model. Two different approaches are adopted, modelling the bedform evolution after a stepwise change in flow conditions, showing an exponential behaviour in time, versus bedform evolution for (gradual) continuously changing flow conditions captured in a differential equation. Soulsby and Whitehouse (2005) proposed the following differential equation:

$$\frac{d\eta}{dt} = \frac{\beta}{T} \cdot (\eta_e - \eta) \tag{1.31}$$

$$\beta = \frac{2.996 \cdot \psi^{1.07}}{21700 + \psi^{1.07}} \tag{1.32}$$

in which η_e is the equilibrium and η_0 the initial height.

The model by Doucette & O'Donoghue (2006) showing exponential behaviour in time is in fact one solution to this differential equation for a stepwise change in conditions:

$$\frac{\eta(t)}{\eta_e} = 1 - \left(1 - \frac{\eta_0}{\eta_e}\right) \cdot \exp\left(-\beta \cdot \frac{t}{T}\right) \tag{1.33}$$

$$\beta = \exp(0.036 \cdot \psi - 7.44) \cdot \log\left(\frac{1 - \eta_0/\eta_e}{0.5}\right) \tag{1.34}$$

The large oscillatory flume experiments of Doucette & Donoghue (2006) reveals that their model is not always able to correctly predict the evolution of the ripple height, but is capable to correctly predict the relaxation times. The field study in the nearshore of Austin et al. (2007) do also show agreement with the relaxation time predictor of Doucette & O'Donoghue (2006), but only for increasing flow conditions. The absence of the exponential behaviour in the field data of Austin et al. (2007) could be expected since the conditions change gradually instead of stepwise, therefore the Soulsby & Whitehouse (2005), which is also validated on the Doucette & O'Donoghue (2006) flume data, is expected to perform better.

The model of Traykovski (2007), although also incorporating a dependence on the flow intensity and departure from equilibrium factor, approaches the ripple evolutions from a sediment continuity equation point of view.

$$(1 - \phi) \cdot \frac{d\eta(k)}{dt} = \frac{dQ}{dx} \frac{(\eta_{eq}(k) - \eta(k))}{n_s(k)} \tag{1.35}$$

where the term *(1-ϕ)* account for the porosity of the sand and the equilibrium ripple height spectrum (k = wavenumber) is modeled by a Gaussian distribution. For the sediment flux rate, Q, a bed load formula of Meyer-Peter and Muller (1948) is used, since the ripple evolution process is dominated by bed load flux, according to Traykovski et al. (1999). Traykovski (2007) is calibrated with and tested on continental shelf data. Figure 1.7 shows the observed (black), predicted (red) and equilibrium wavelength (bleu) for a series of field data from Traykovski. The modelled wavelength seems to follow the observed wavelength quite reasonable, but often deviates when the ripple length is stationary (wavelength does not change anymore due to subcritical conditions). From this can be concluded that the model is not able to exactly model the ripple length decay after decreasing conditions, because deviations in decay result in deviation when the length is stationary. Furthermore, Traykovski (2007) also found an exponential behavior for the bed evolution from the solution of his differential equation in the case of time-step changing conditions.

Although the reviewed models are different from each other, they all incorporate a dependency on the flow conditions, more intense flow conditions shorter relaxation time and departure from equilibrium factor, the larger the departure the shorter the relaxation time. Furthermore, the reviewed models use the bedform height to model the evolution in time. This is common because the height evolution is found to

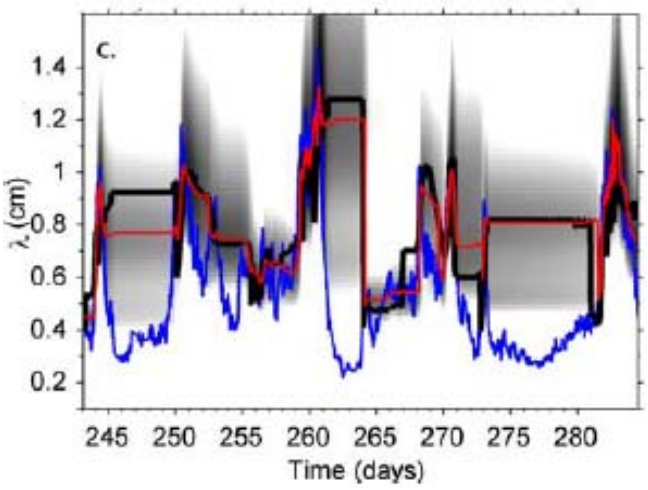

Fig. 4.2.4. Time series of model predicted spectra (gray scale intensity), model predicted wavelength (colored lines), and observed wavelength (black lines)

evolve more gradual than the bedform length. The bedform length is namely observed to change in two distinct processes after subjected to a change in flow conditions; slide and split/merge (Smith & Sleath, 2004; Doucette & O'Donoghue, 2006). Slide is the process of gradual increase or decrease in ripple length by the movement of ripple crest's either farther apart or closer together. Split refers to the process in which ripple crests appear to split into two or more ripples of shorter length reducing the bedform length. Merge refers a similar process as split only the other way around for increasing (growing) bedforms. Split/merge results therefore in a more stepped change in bedform length, especially since this process is observed to occur for multiple ripples simultaneously (Doucette & O'Donoghue, 2006). Slide and split/merge are observed to occur simultaneously but slide is dominant for gradual changing conditions while split/merge is that for stepped change or rapid changing conditions (Doucette & O'Donoghue, 2006).

Smit & Sleath (2004), Doucette & O'Donogue (2006) and Traykovski (2007) do find evolving bedforms for decreasing conditions as long as the conditions exceed the critical flow conditions although the rate may decrease. This is also reflected by the different given models. The field study of Austin et al. (2007) however, studying the ripple dimensions during 15 tidal cycles in the nearshore, found that during the falling tide as the flow conditions become less vigorous the bedform dimensions did not change significantly any more: hysteresis. This effect is clearly depicted in figure 1.8 for one tide on two locations, in which can be seen that although the hydrodynamic conditions show a more or less symmetrical behaviour for the rising and falling tide, the ripple dimensions do not. The ripple geometry is only 'reset' by the action of swash at the tail of the ebb and beginning of the flood (Austin et al., 2007). A similar hysteresis type of behaviour is also found by Stegner & Westfreid (1999). Although the study comprises a small scale laboratory experiment (an annular cell with a diameter of 7cm), the results are indicative for the process. Austin et al. (2007) explain the presence of hysteresis by the relaxation times, causing the ripple geometry to lag behind the changes in the hydrodynamic forcing. This eventually causes the ripples to become too large to be changed by the waning energy conditions and hence become decouple from the

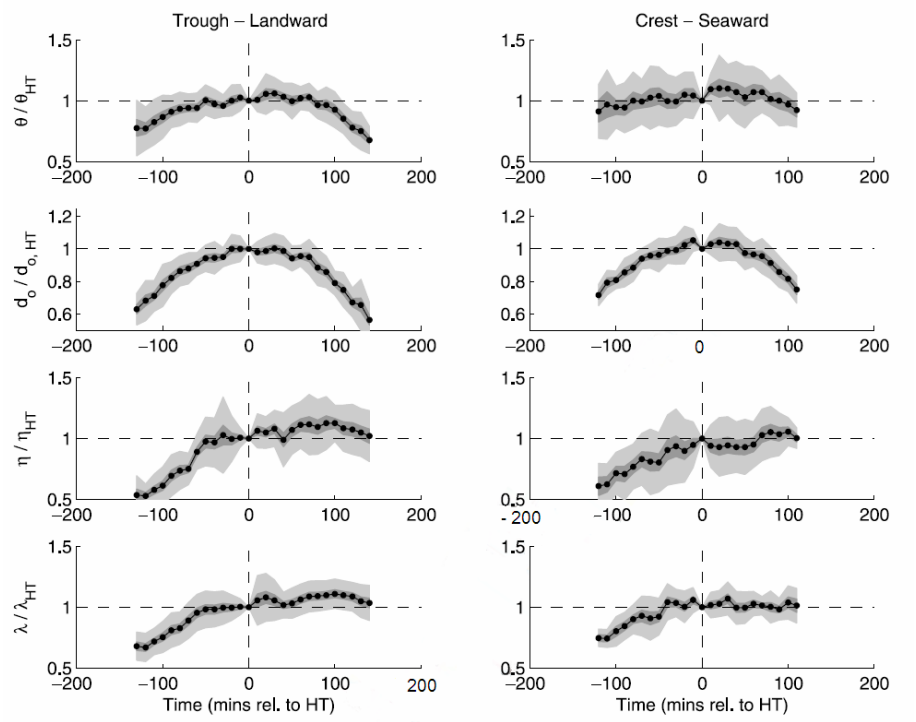

Fig. 1.9, Relative Shields parameter, orbital diameter, bedform length and height, around a high tide (Austin et al., 2007).

forcing. Austin et al., (2007) suggest that this indicates that the initial bed configuration is of critical importance to the observed hysteresis. Although the reviewed models relate the relaxation time positively to the flow intensity, meaning the bedform will evolve more and more slowly for decreasing conditions, the departure from equilibrium factor counters that effect when the 'present' and equilibrium bedform dimensions become more and more apart. This counter effect contradicts with the idea's/foundings of Austin et al (2007). The departure from equilibrium factor is based on the concept that when ripples are far from equilibrium, the transport convergence required to drive the ripples toward an equilibrium state will be maximized (Traykovski, 2007). Maybe this is only valid for increasing and not or limited for decreasing conditions. This idea is strengthened by the often observed development of superimposed ripples on larger relict bedforms, which indirectly represents decreased conditions, instead of decreasing larger bedforms. Then, the observation of Austin et al. (2007) can be explained by the models: during the rising tide the ripple dimensions are able to closely 'follow' the equilibrium dimensions due to the (exponentially) decreasing relaxation times induced by the increasing flow conditions. When the tide is falling, the conditions decreases and therefore the relaxation time increase exponentially. The faster the decrease in ψ, the faster the relaxation times increases. It becomes harder and harder for the ripples to decay. Eventually, the ripples are unable, on the timescale of half a tide, to be changed by the waning energy conditions. The field study of Hay & Mudge (2005), strengthens is theory. Hay & Mudge (2005), found a symmetrical sequence of bed states during a storm cycle (during both storm growth as decay), indicating a lack of dependence on the prior bed state. The lake of hysteresis in this field situation can be explained by the difference in the flow conditions compared to Austin et al. (2007). Since the flow conditions during the storm cycle were more intense and had a longer duration, the bedforms had more time and better (more vigorous) conditions to adept for the changing conditions than in the situation of Austin et al. (2007).

1.3 Research questions

A great number of studies about bedforms have been preformed the last decades. This has led to a much better understanding of the appearance and dimensions of bedforms. But, large anomalies between observed and predicted bedforms and differences in adopted relations between bedform appearance/ dimensions and the hydrodynamic forcing for different researches are still found. One source of discrepancy between the founding's of different authors is the flow conditions on which the model or the relation is based on and the flow conditions during the observations. Since, many research has been done under laboratory or continental shelf conditions which can differ from nearshore conditions. The conditions at the study site are expected to differ from laboratory and or continental shelf conditions by sometimes rapid changing flow conditions induced by the tidal range effects and the presence of a significant steady current induced by the Slufter. Such nearshore and combined wave and current conditions haven't been research yet for as far as I have found. The sometimes rapid changing conditions are expected to result in hysteresis, the hydrodynamic conditions versus bedform dimensions relation differing for the rising and falling tide. But, not as some researchers have observed, resulting in a freeze in bedform dimensions during the falling tide when the conditions decrease in intensity. The additional steady current is expected to affect the bedform appearance and dimensions significantly, which is not predicted by wave based bedform predictors. In order to test these hypothesizes the following research question have been formulated:

- What are the characteristics of the wave and mixed wave current bedforms for the found range of flow conditions and for which condition range do bedforms occur.

- Are wave, wave/current and current induced bedforms separated by existing criteria?

- Can the wave only and mixed wave current dimensions be predicted by a common wave based bedform predictor? And by a wave wave/current orientated predictor?

- Do (rapid) decreasing conditions lead the bedform dimensions to lack behind the flow conditions more than during increasing conditions: hysteresis? And, does the bedforms more or less freeze during decreasing conditions?

1.4 Research outline

In chapter 2, *Methodology*, the characteristics of the field site, including the external conditions during the field work, the measurement setup and data processing is discussed. Chapter 3, *Results*, is divided into different sections, first some aspects are analyzed comprising the whole campaign, the hydrodynamic conditions at the study site, the measured bedform characteristics and the type of flow conditions to get inside in the general conditions and bedforms during the campgaing. Then, the

hydrodynamic and bedform characteristics are in detail analyzed tide specific to obtain inside in the bedform response to different and different changing conditions. The hypothesized relations found within the tides are also tested on generalization for all tides. This is followed by the analysis of the performance of four wave and wave/current predictors. In chapter 4, *Discussion*, the found relations between bedform appearance and dimensions are discussed and reviewed to the found relations in the literature. In chapter 5, *Conclusion*, the most important findings are summarized.

2. Methodology

2.1 Field site

The study site was located at the wave-dominated sandy coast of Texel, one of the Netherlands its barrier islands (figure 2.1). The site was located close to the tidal channel of the Slufter, a secondary tidal inlet (figure 2.1). A secondary tidal inlet is a salt or brackish dune valley which is connected with the open sea by a tidal channel and is completely flooded for at least once a year (Durieux, 2004). In the case of the Slufter, the tidal channel is diurnally flooded and the whole system is flooded approximately 5 times a year.

Fig. 2.1. Satellite image of Texel (left) and the Slufter (right) (from Google Earth).

2.3 External conditions

The Fieldwork was executed from 17 September until 1 November 2009. Figure 2.2.a-c shows the relevant offshore wave conditions measured by a buoy at the Eierlandse Gat, the tidal inlet between Texel and Vlieland. The buoy was located approximately 20 km north of the Slufter in 26m deep water. From the significant wave height (Hm0) two storm events can be detected, on 4 and 16 October, with Hm0 up to 5 and 5.8 m respectively. Besides two other more energetic events on 12 and 26 October, with Hm0 up to 3.8 and 3.2 m respectively, the wave conditions were light to moderate with waveheights between 0.5 and 2 m. The significant wave period ($Tm\text{-}_{10}$) was maximal during the two storm events with wave periods between 7 and 8.6 sec, while varied around 5 sec (3 - 6 sec) in between. This is characteristic for continental sea waves (non-ocean).

Figure 2.2.d-e shows the astronomic water level fluctuation and the surge level. The surge level is computed from the actual water level, measured at the tidal station 'Texel North Sea' located 15 km south

of the Slufter in 26m deep water, and the astronomic water level. The tide is characterised by a mean tidal range of 1.4 m, increasing to 2.1m during spring tide and decreasing to 0.9 during neap tide. This is indicative for a micro-tide. The surge was maximal, 1m, during the storm on 4 October. The surge during the second storm was only minor (0.2 m). This difference is induced by the wave direction (fig 2.2.c). The shore normal is 300°. The wave direction on 4 October was roughly equal to this 300° while was more northerly (+/- 350°) on 16 October. The surge was usually around -0.2 / 0.2 m, but reached -0.5m with strong easterly winds.

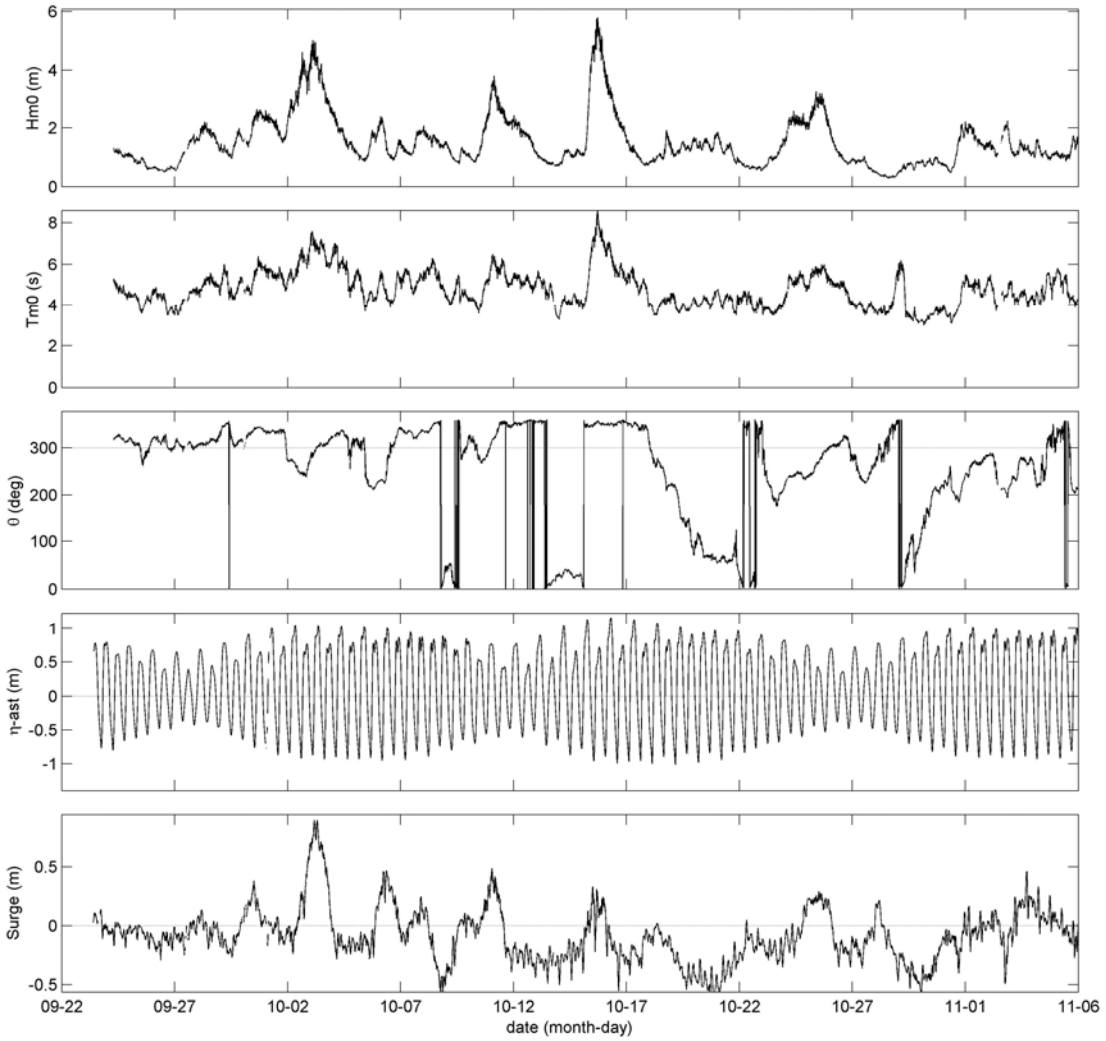

Fig. 2.2 Offshore conditions during field campaign: a) Significant wave height, b) significant wave period, c) wave direction, d) Astronomic water level fluctuations, e) Surge.

2.2 Instrumentation

The red rectangle in figure 2.1 marks the 'actual' study site. Figure 2.3a shows a DEM (Digital Elevation Model) of that area, measured at the beginning of the fieldwork. For reference, the transition between light and dark blue is indicative for the average water level at ebb tide and the minimum and

maximum heights in this figure are -2.5m and 4.3m above MSL respectively. Note that the course of the tidal channel and the beach morphology in figure 2.3.a deviates from the Google Earth image of figure 2.1 (taken at a different time), which is indicative for a dynamic system.

The black crosses on the southern beach plain in figure 2.3 represent instrument frames. The location of the instrumentation transect had to be chosen such that it matched the requirements for three MSc researches, being able to measure both wave-dominated processes as well as processes related to the inundation of the beachplain during storm. The instrument frame array consisted of three mini-tripods and one large tripod, further referred as the Truc-Vert frame (figure 2.4) and was directed shore normal +/- 300°. Only data from the Truc-Vert frame, the most extensive frame, is used in this thesis due to the presence of a ripple profiler. The Truc-Vert frame, the most seaward frame and represented by the most lower cross in figure 2.3, was located behind a trough at roughly the same elevation as the inner bar (figure 2.3.b), at +/- -0.90m above MSL. The Truc-Vert frame was located close to the tidal channel mouth, therefore influences of the tidal channel on the measurements at the Truc-Vert frame are expected.

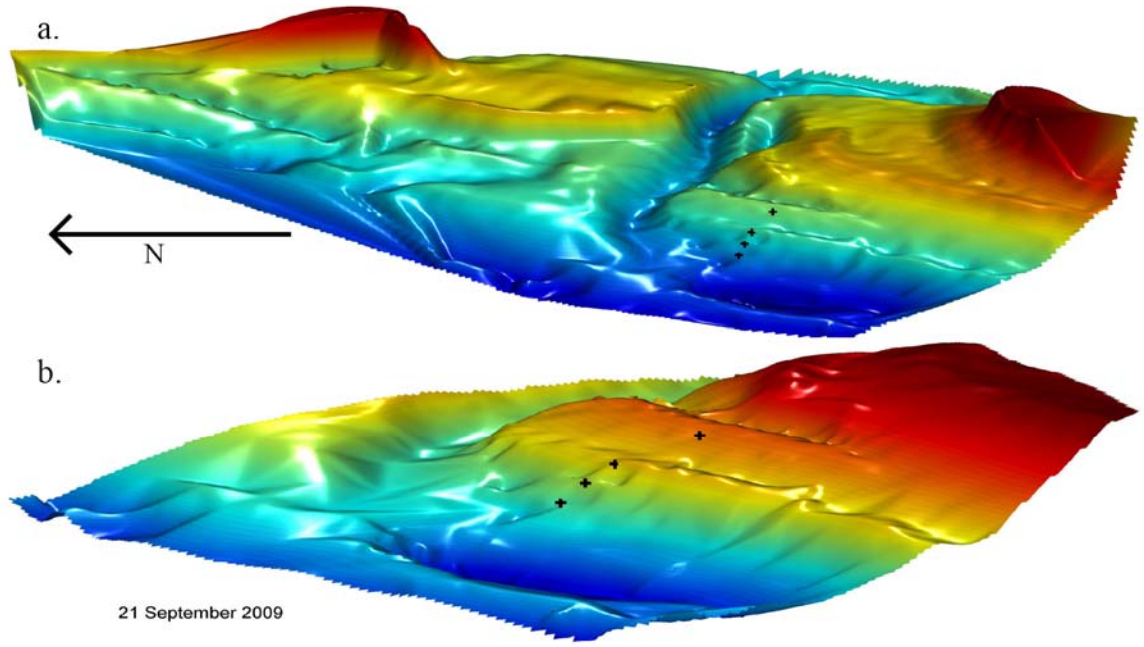

Fig.2.3. DEM of the Slufter area at the beginning of the field campaign: a). Overview over the tidal channel, north and southern beachplain; b). Enlargement of southern beachplain with the instrument frames.

The Truc-Vert frame was grounded on three pipes, manually drilled into the sand, arranged in a triangular shape with the apex directed seaward (figure 2.4). Besides a ripple profiler, the Truc-Vert frame was equipped with a several other sensors to measure hydrodynamic and sedimentary properties.

Two electromagnetic current meters (EMF), two single sediment turbidity meters (STM) and one STM-array were mounted to the most seaward pipe of the frame to obtain cross shore (x) and long-shore (y) velocities and sediment turbidity respectively. EMF1 and STM1 were mounted at +/- 30 cm above the seabed, EMF2 and STM2 at +/- 50 cm. The STM-array, consisting of 5 STM sensors above each other, was mounted at +/- 2 cm above the bed. The EMF's were mounted such that the two sensors couples (x and y)

were roughly cross-shore and long-shore directed. The exact direction was measured at 1° accuracy, in order to correct later. The sensor faces of the STM's where directed parallel to the shore normal.

One acoustic backscatter sensor (ABS) was mounted on a seaward extended 'cross' pipe (most upper left instrument in figure 2.4) at +/- 90 cm from the seabed, for obtaining (mainly quantitative) sediment turbidity in the vertical. The ABS is for this thesis only used as a seabed detector. The ripple profiler, a sand ripple profiler sonar (SRPS) for obtaining 2D cross-shore profiles of the seabed, was located just behind the ABS at +/-80 cm from the seabed. One Keller pressure transducers to obtain waterlevel fluctuations was mounted to the most northern pipe at +/- 10 from the seabed. In order to correct the pressure sensor, the air pressure was also measured with a 10 min interval.

The EMF's, STM's and the pressure transducer measured continuously with 4Hz. The ABS measured also at 4Hz, but in bursts of 29min 50s. The SRPS made 3 successive sweeps, +/- 25 seconds apart, every 5min. All heights given are measured from the actual sensor height to the bed except for the STM-array and SRPS, which are measured from the bottom of the device and from the bottom of the sensor cap respectively.

Fig.2.4. Instrument frames: Truc-Vert frame (left), mini-frame (right).

The given initial sensor heights were subjected to bedlevel fluctuations, since the frame was fixed in height in relation to the mean sea level. Only the STM-array was relocated every ebb tide when necessary and possible to maintain the 2 cm height above the bed, because this height (and sensor) was most sensitive to bedlevel changes. The actual heights during the campaign were determined in three ways, via the ABS, SRPS and manually. Manually involved measuring the sensor heights each ebb tide when possible. From the ABS and SRPS the local bed level and therefore the height of the ABS or SRPS is retrieved directly. But, since the height of each sensor is levelled multiple times with a DGPS, the heights of the other sensors could be calculated too, thereby neglecting the beach slope over those short distances.

With this DGPS system the beach section around the frame array was monitored daily with three cross-shore and three long-shore transects. Between 30 September and 6 October no DGPS measurements were made due to technical difficulties. A more extensive DEM of the beach plain, tidal channel (mouth) and the inner bar is made four times during the campaign using the DGPS: on 21 September, 8, 15 and 30 October (figure 2.3.b). Topographic levelling was used for the submerged parts, waterlevel > 0.5m. On 15 October even a larger area of the Slufter is levelled with the DGPS (figure 2.3.a).

Furthermore, sediment samples were taken along the frame transect mid October (October 13-16). The median grain size was determined from the fall velocity and from sieving. Both methods gave similar results for the sediment size around the Truc Vert frame, a *d50* of *316 μm* and *d90* of *470 μm*.

2.4 Data processing

The raw data output in minivolts from the EMF and pressure transducer data were calibrated (linearly) with an offset and multiply-factor to obtain velocities (m/s) and pressure (m). The offset and multiply-factor were determined with an experimental setting in the lab. The x and y velocities were rotated to obtain the cross-shore and long-shore velocities. Onshore cross-shore velocities as well as north going long-shore velocities are defined as positive. The sensor heights were determined from the ABS, SRPS or manual measures, in that specific order of abundance. The bedlevel heights from the ABS and SRPS were obtained by the height of maximum detection. The maximum detection was determined from smoothed (median filter) and half an hour averaged data to exclude perturbations due to bedforms. The accompanying height was only accepted when the maximum detection value exceeded the maximum background noise. In case of the SRPS, only 20cm bedprofile directly beneath the sensor was used. When necessary, the sensor heights were interpolated linearly in between. With the EMF data in (m/s) and the pressure transducer data in (m), the following parameters were computed for periods of 15min.

The waterdepth (h) was computed by adding the sensor height to the water pressure. The water pressure data was retrieved by subtracting the air-pressure from the pressure transducer data.

The significant wave height (H_{m0}) was obtained for the high frequency range. This range was set to 0.05- 1 Hz, corresponding to a wave period of 20 – 1 sec. H_{m0} was determined as four times the standard deviation of the frequency filtered surface fluctuations (sf). The surface fluctuations were obtained from correcting the pressure transducer data for linearly wave theory. The surface fluctuations were detrended with a second order polygon and finally filtered for the determined frequency range with the discrete Fourier transform.

The wave skewness for the high frequency range was computed with equation 2.1 (Butt & Russel, 1999).

$$S = \frac{\left\langle sf^3 \right\rangle}{\left\langle sf^2 \right\rangle^{3/2}} \tag{2.1}$$

where *sf* are the surface fluctuations (m) and the angle brackets denote time averaging. Asymmetry was computed with equation 2.2 (Elgar & Guza in Foster et al., 1999).

$$A = \frac{\left\langle H(sf)^3(t) \right\rangle}{\left\langle H(sf)^2(t) \right\rangle^{3/2}} \tag{2.2}$$

where *H(sf)* is the Hilbert transform of sf (m). The characteristic wave period is chosen as $Tm\text{-}_{10}$; m_{-1}/m_0 where m is the spectral moment, calculated with:

$$m_{n\cdot} = \int f^n \cdot E(f) \cdot df \tag{2.3}$$

where E is the energy a given frequency (f). The cross-shore and longs-shore root mean square velocities (u_{rms} and v_{rms}) are computed from the variance of the high frequency filtered cross- and long-shore velocity signal (u and v).

$$u_{rms} = \sqrt{\mathrm{var}(u)} \tag{2.4}$$

$$v_{rms} = \sqrt{\mathrm{var}(v)} \tag{2.5}$$

The horizontal rms velocity U_{rms} is computed with equation 2.6.

$$U_{rms} = \sqrt{u_{rms}^2 + v_{rms}^2} \tag{2.6}$$

The orbital diameter is determined form the integral of the amplitude of the first eigenvector of the high frequency filtered cross- and long-shore velocity signal. The orbital diameter is four times the standard deviation of that integral. The mean cross- ($\bar{v}$) and long-shore ($\bar{v}$) velocities are simply retrieved by taking the mean of the different velocity signals.

The mean wave angle and wave spread are obtained from principal component analysis of a detrended cross-shore and long-shore high-frequency (0.05-1 Hz) velocity signal. The mean angle is related to the orientation of the first eigenvector and the wave spread is related to the square root of the relative contribution of the second eigenvector. The wave angle is positive in the anti-clock wise direction.

Furthermore, the relative breakpoint associated with the relative waveheight (H_{m0}/h) is computed with equation 2.7 (Price and Ruessink, 2008).

$$\left(\frac{H_{m0}}{h}\right)_b = 6.1 \cdot \frac{H_{m0}}{L} + 0.31 \tag{2.7}$$

Were L is the wavelength computed according to Guo (2002).

SRPS data

The processing of the SRPS data involved many steps to obtain the bed characteristics. First, the SRPS backscatter data was converted from a polar coordinate system (angle and binrange) to a Cartesian coordinate system with to x and y coordinates. Then, the backscatter of the three successive sweeps, made every 5 min, were plotted together with a sweep containing the maximum values of those three sweeps. An example of such a plot is depicted in figure 2.5. From those four sweeps the one best representing the bedprofile for those 5 minutes was chosen, visually. When gabs were present in all three sweeps, as in figure 2.5, the 'maxima-sweep' was usually chosen. But, when a single sweeps was also complete (no gabs) and clear (no detection of sediment suspension clouds for example) that sweep was often preferred above the 'maxima-sweep' because the 'maxima-sweep' shows usually more 'scatter' (compare sweep 2 and the maxima-sweep in figure 2.5). This scatter originates from the fact that the bedprofile is subjected to sediment transport and thus bedform migration in the time the three successive sweeps (+/- 25 sec apart) are made. No sweep was saved when all four sweeps contained more than 50% gabs.

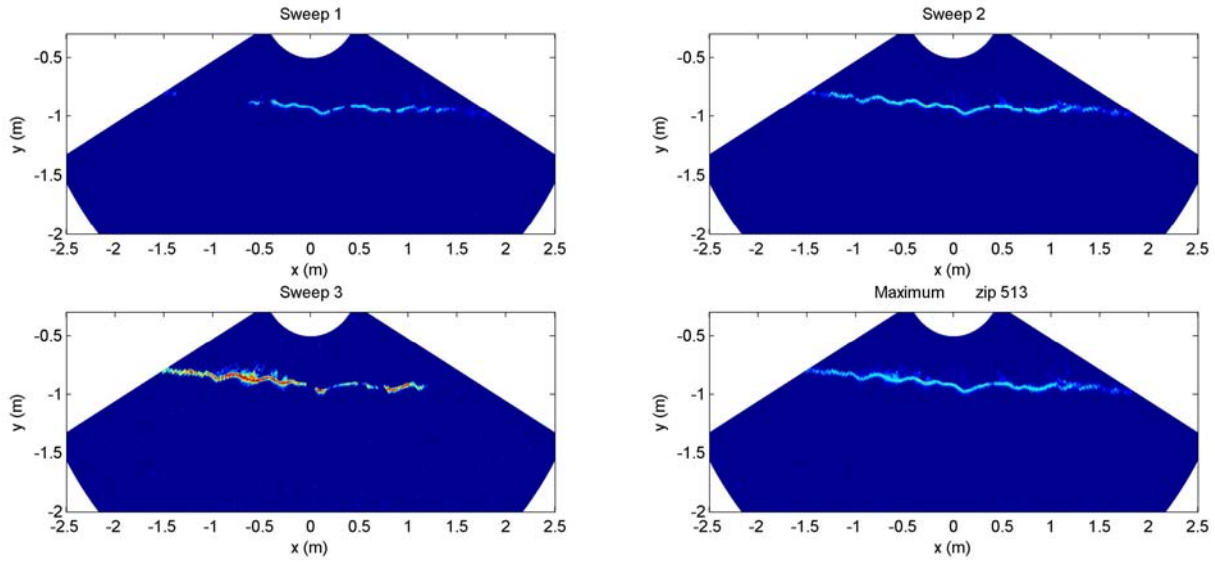

Fig.2.5. Three successive sweeps and there combined maxima on 8 October 11:30.

For the chosen sweeps the 2D backscatter data was converted to initial bedlevel profiles. The initial bed profile corresponding to the maxima-sweep of figure 2.5 is depicted in figure 2.6. To obtain this profile, maximum backscatter values for each y-axis were determined. Around each maximum a second polynomial was fitted trough 11 backscatter points (or more when necessary) centred around this maximum. The maximum of this polynomial was then determined. The y-values corresponding to this maxima represent relative bedlevel heights (z) and make up the bedlevel profile. Using the maxima from the polynomial instead of the direct maxima provides a smoother bedlevel line. When a maximum backscatter value not exceeded the threshold, the bedlevel height (z) for that x coordinate was rejected. The threshold is determined as the maximum value of the background noise. The background noise is taken as the backscatter far below the actual bedlevel. Furthermore, the bedlevel profile was normalised and z-

values exceeding the mean by more than 3.5 times the standard deviation were also rejected. All this rejecting is done to exclude noise and suspension clouds from the bed profile.

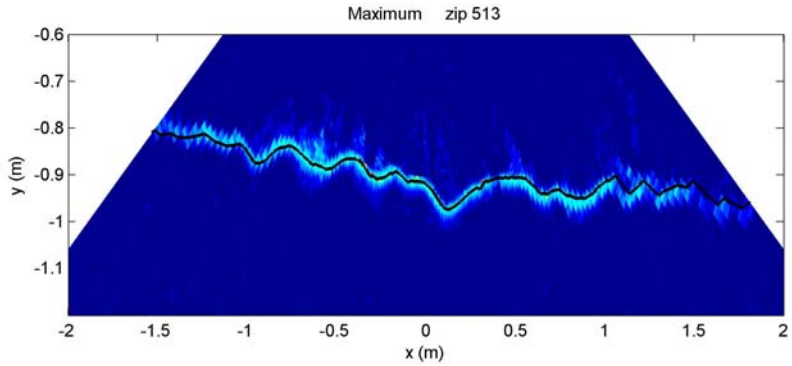

Fig.2.6. Close up of the maxima-sweep of figure 2.5 with a black solid line representing the initial bed profile.

Next, the obtained profiles were run trough a medianfilter, capable of handling Nan's (not a number), to further reduce the noise of the bed profiles. The profiles were linearly interpolated to a regular grid with a horizontal resolution of 1cm. For comparison, the horizontal resolution of the SRPS was +/- 1.4 cm straight below the SRPS sensor (*x = 0*) and +/-5.3 cm 1.5m from the SRPS sensor (*x = 1.5 / -1.5*). The horizontal span was reduced to -1.2 to +1.5 m, in order to leave the less clear and pronounced edges out of the further analysis.

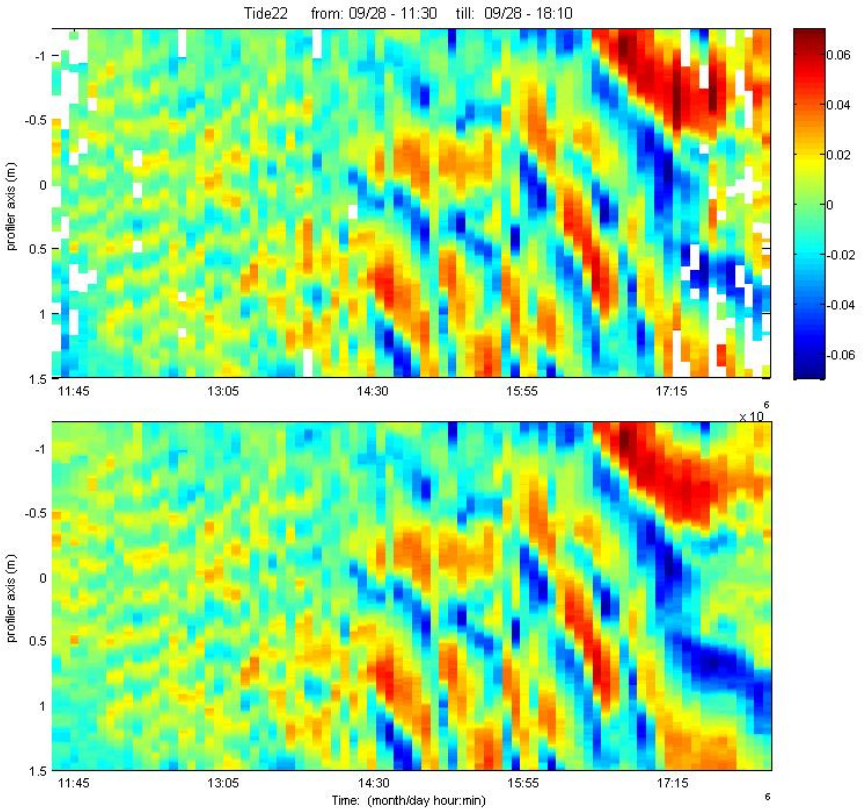

Fig.2.6. The bedprofiles for tide 22 (09/29 10:30 – 18:10) with gaps (a) and without gaps (b). The numbers at the colorbar are heights (z) in cm.

Gabs in profiles, mainly present in sweeps at the beginning and end of, were filled up with an inpaint_nan technique using a string metaphor (D'Errico, 2006), see figure 2.7. This technique fills the gaps on a tidal scale, looking in vertical (in this case, at the neighbour point in the sweep) as well as in horizontal direction (in this case, at neighbour points in time, neighbour sweeps). Figure 2.8 shows an example of a profile with filled gaps (for sweep 1 of tide 22, figure 2.7). Furthermore, a smoothed detrended average profile per tide and average height per sweep were determined and subtracted from the sweeps to obtain profiles with average height z of zero and with a tidal average beach profile of zero, as in figure 2.7.

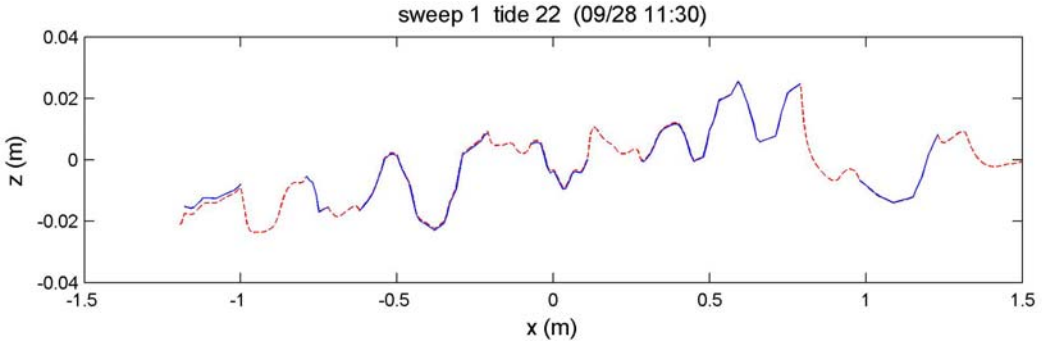

Fig. 2.7. Sweep 1 (09/28 11:30) from tide 22 with filled gaps.

The bedform length was initially determined with the auto-correlation function. According to Masselink et al. (2007) the bedform length is represented by twice the spatial lag corresponding to the strongest negative autocorrelation peak. From figure 2.8, showing the bed profiles (2.8.a) and the accompanying correlograms (2.8.b) for three sweeps from tide 22, can be seen that this relation holds in the case of regular ripples as sweep 13 represented by the blue solid line. With a lag of 1cm, the representative ripple length for sweep 13 would be 30 cm. But in the case of irregular ripple, as for sweep 1 represented by the green solid line in figure 2.8, the bedform length would be +/- 2.4m, which does not seem to be representative looking at the bedprofile. It is more convincing to take twice the spatial lag corresponding to the first local minimum (looking from lag 0) of the autocorrelation coefficient. This corresponds to a representative bedform length of +/- 25 cm for sweep 1. This method gives also the same length for sweep 13. But, in the case of sweep 1 the autocorrelation coefficient belonging to the first local minimum is not even negative, so the question arises whether this peak and therefore the found bedform length is statistical significant.

Since adjacent points in bedform profile are not independent, the significance of the obtained local minimum was tested by using a reduced number of points N_*, following Garrett & Toulany (1981) in Masselink (1995).

$$\frac{1}{N_*} = \frac{1}{N} + \frac{2}{N^2} \cdot \sum_{j=1}^{N_0} (N - j) \cdot R_s(j) \qquad (2.10)$$

Where N is the original number of points (270), R_s is the lagged auto-correlation of the sweep to be correlated, and N_0 is the number of lags until R_s experience a zero-crossing (Masselink, 1995). The reduced number of points is more or less the minimal number of points in which the shape of the profile is still

captured. In the case of tide 22, the average N_* per sweep was 12, varying between 5 and 25. The 95% confidence correlation coefficient below which to accept the local minima to represent the bedform length is then $-0.16 \cdot \left(1.96/\sqrt{N_*}\right)$ (Jenkins and Watts, 1968, in Masselink, 1995). This confidence correlation coefficient is plotted as a blue dashed line in figure 2.8.b for sweep 13. Although this correlation coefficient is different for every sweep, the range of values for tide 22 is only small (mean of -0.1 and standard deviation of 0.02), making it in this case unnecessarily to plot them for every sweep separately. So, from figure 2.8 can now be concluded that the first local minimum of sweep 1 is not statistical significant.

From figure 2.11.c showing the calculated bedform length according to the strongest negative autocorrelation peak and first local minimum method for all sweeps in tide 22, can indeed be concluded that for bedform lengths <<1m the method of strongest negative autocorrelation gives unrealistic results, while the lengths according to the first minimum method are not always statistical significant (**arced** by a red dot). This is the case for all tides.

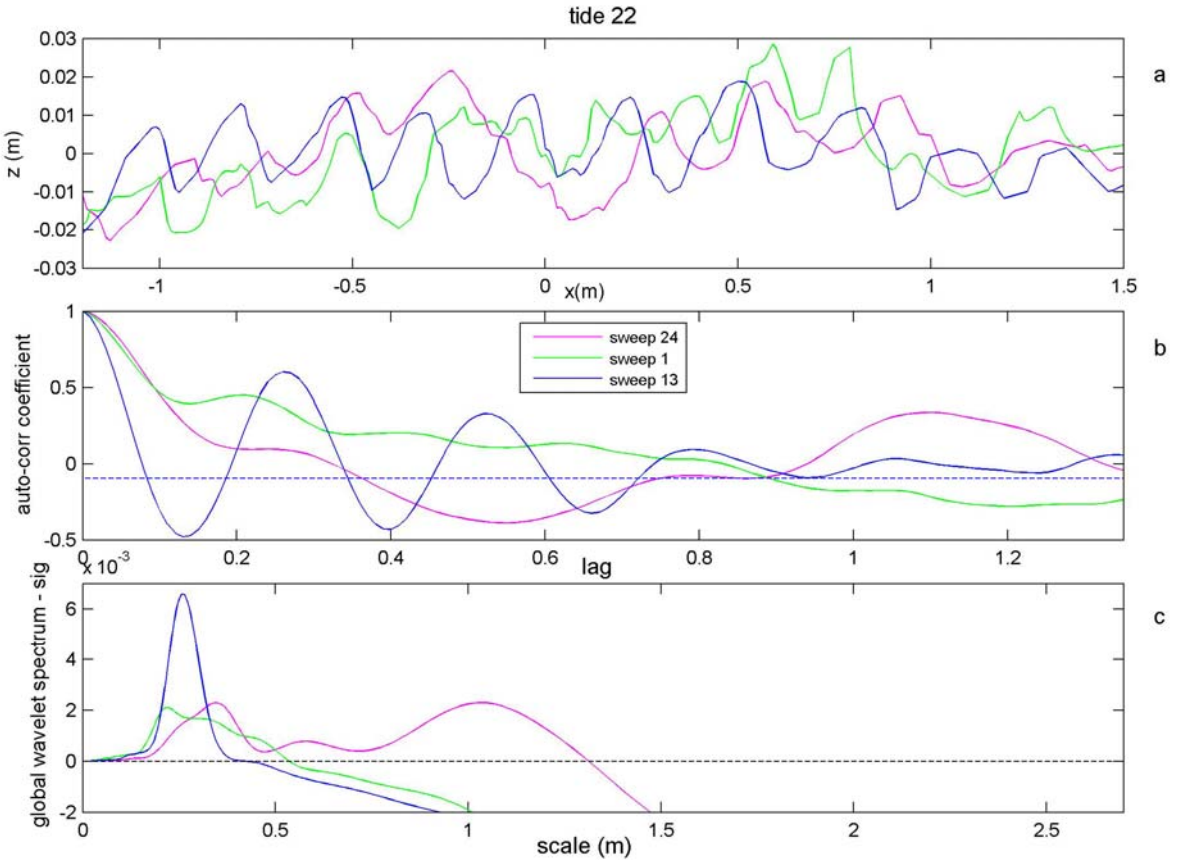

Fig.2.8. bedlevel profile (a), auto-corelation graph (b) and global wavelet spectrum – significance level (c) for sweep 1, 13 and 24 of tide 22.

To obtain statistical significant bedform lengths in the case of smaller bedforms, a different method, wavelet analysis was executed. Wavelet analysis is developed to decompose a time-series into time and frequency space simultaneously, to get information on the amplitude of any periodic signals

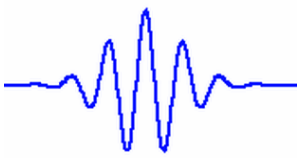

Fig.2.9. Morlet wavelet

within the series and how this amplitude varies with time. In the case of bedforms, the time series is replaced with a bedlevel profile to obtain the amplitude of any bedform length within the profile and how this amplitude varies in the profile. Wavelet analysis works with a wavelet, in this case the Morlet wavelet is used (figure 2.9), which is fitted for varies sizes (bedform lengths) trough all varies positions in the profile: Wavelet Transform, see Torrence & Campo, 1998, for all necessary equations. By squaring the result and removal of the scale based bias (Liu et al., 2007), the wavelet power spectrum was obtained (figure 2.10), in which the power (colour) indicates how well the wavelet could be fitted trough the positions in the bedlevel profile for the different scales (bedform lengths). Since the interest goes to the representative bedform length averaged over the bed profile in stead of position specific, the power spectrum was summed to obtain the global wavelet spectrum (figure 2.10).

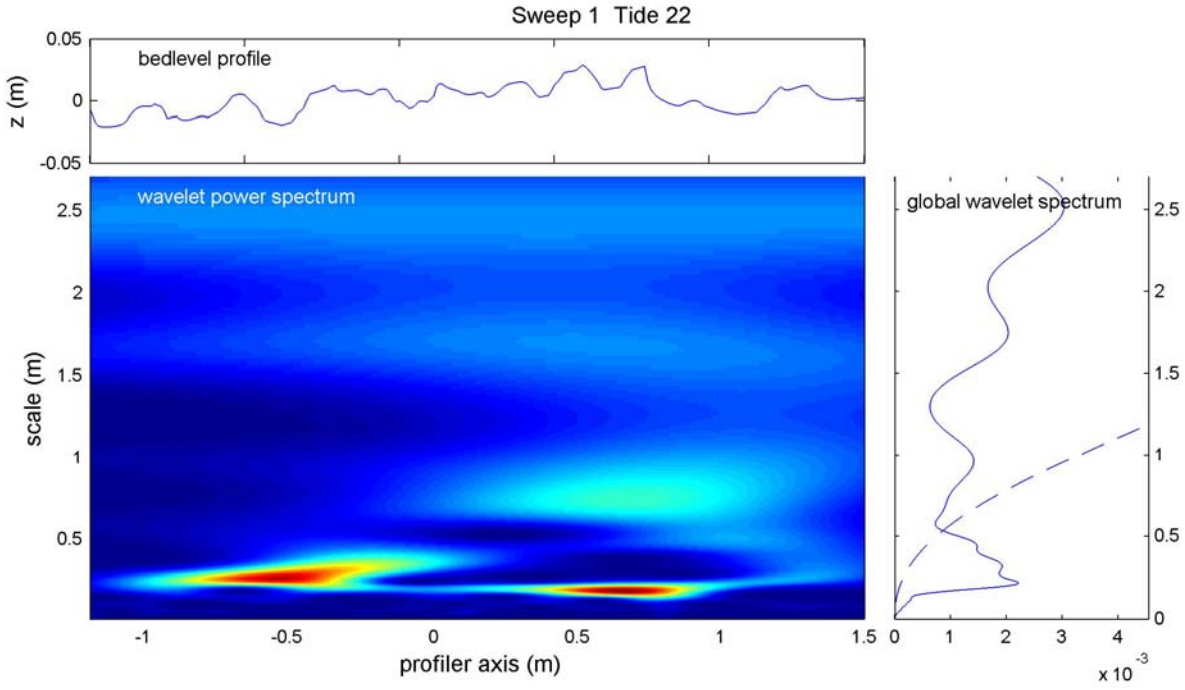

Fig.2.10. The wavelet power spectrum and global wavelet spectrum for sweep 1 of tide 22.

Before concluding on which scale (bedform length) is dominant, the significance levels of the spectrum was determined with a foulier red noise spectrum (11) and a chi-square test. The global wavelet spectrum value above which the wavelet spectrum is with 95% confidence different from noise, is given by (12) (Torrence & Campo, 1998).

$$P_k = \frac{1-\alpha^2}{1+\alpha^2-2\cdot\alpha\cdot\left(2\cdot\pi\cdot k/N\right)} \tag{2.11}$$

$$\frac{|W(s)|^2}{\sigma^2} = \frac{1}{2}\cdot P_k\cdot\chi_2^2 \tag{2.12}$$

Where α is the lag-1 autocorrelation and *k*… *N/2* is the scale (bedform length) index. *W* is the wavelet spectrum at scale *s*, σ^2 is the variance of the bedprofile and χ_2^2 is the 95th percentile value for a Chi squared distribution. This significance line is plotted in figure 2.10 as the blue dashed line. The global wavelet spectrums with significance levels are plotted for tide 22 in figure 2.11.b. The bedform length corresponding to the highest peak of the global wavelet spectrum minus the significance 'spectrum' is now chosen as the representative length (figure 2.9.c). This subtracting of the significance level is done to compensate for the larger uncertainly level at larger bedform lengths. This results in a bedform length of +/- 20cm for sweep 1, corresponding to the length found by taken twice the lag of the first local minimal of the autocorrelation coefficient.

In figure 2.9.c the global wavelet spectrum minus significance levels for sweep 13 and 24 c are also shown. The representative bedform length for sweep 13 is quite straightforward, but for sweep 24, showing a more bimodal bed profile (2.9.a), two distinct peaks occur (at +/- 35 cm and +/-105 cm). The peak at +/-105 cm is slightly larger, but choosing for one representative bedform length does not cover all characters of the profile. Therefore, the bedform lengths corresponding to a second peak are also determined when the peak is larger than half the size of the largest peak. In figure 2.11.d these lengths, when present, are indicated with a green dot.

In figure 2.11.d are besides the bedfrom lengths from the wavelet analysis also the lengths from the autocorrelation method (first local max) plotted (pink dots). From this graph can be concluded that both methods give similar results, although the autocorrelation method does seem to consequently result in a little larger length. To test how similar the results really are, the different lengths are plotted against each other (figure 2.12.a) on which linear regression is applied. A gradient of 0.86 indeed indicates that lengths from the auto-correlation are larger, on average +/-14%. A intersect of 0.03 deviates only 3cm from zero, being not relevant. With a R^2 of 0.92, the two methods can be indentified as similar with a small deviation (14%). To test weather this is also the case for tides other than 22, linear regression was applied to the bedfrom length estimations of a selection of 10 tides, figure 2.11.b. With a gradient of 0.91, intersect of -0.04 and R^2 of 0.77 it is similar to the results of tide 22 only more outliers are present which lower the R^2.

However, from all tides (figure 2.12.b) can be seen that the bedform length from wavelet analysis shows clustering around 2.5 and 1.7m length with no bedforms in between. This is rather unlikely to be natural. The bedform lengths from the autocorrelation method do show a more natural distribution. This clustering probably comes form the increasing uncertainty for larger length, but how exactly is unclear.

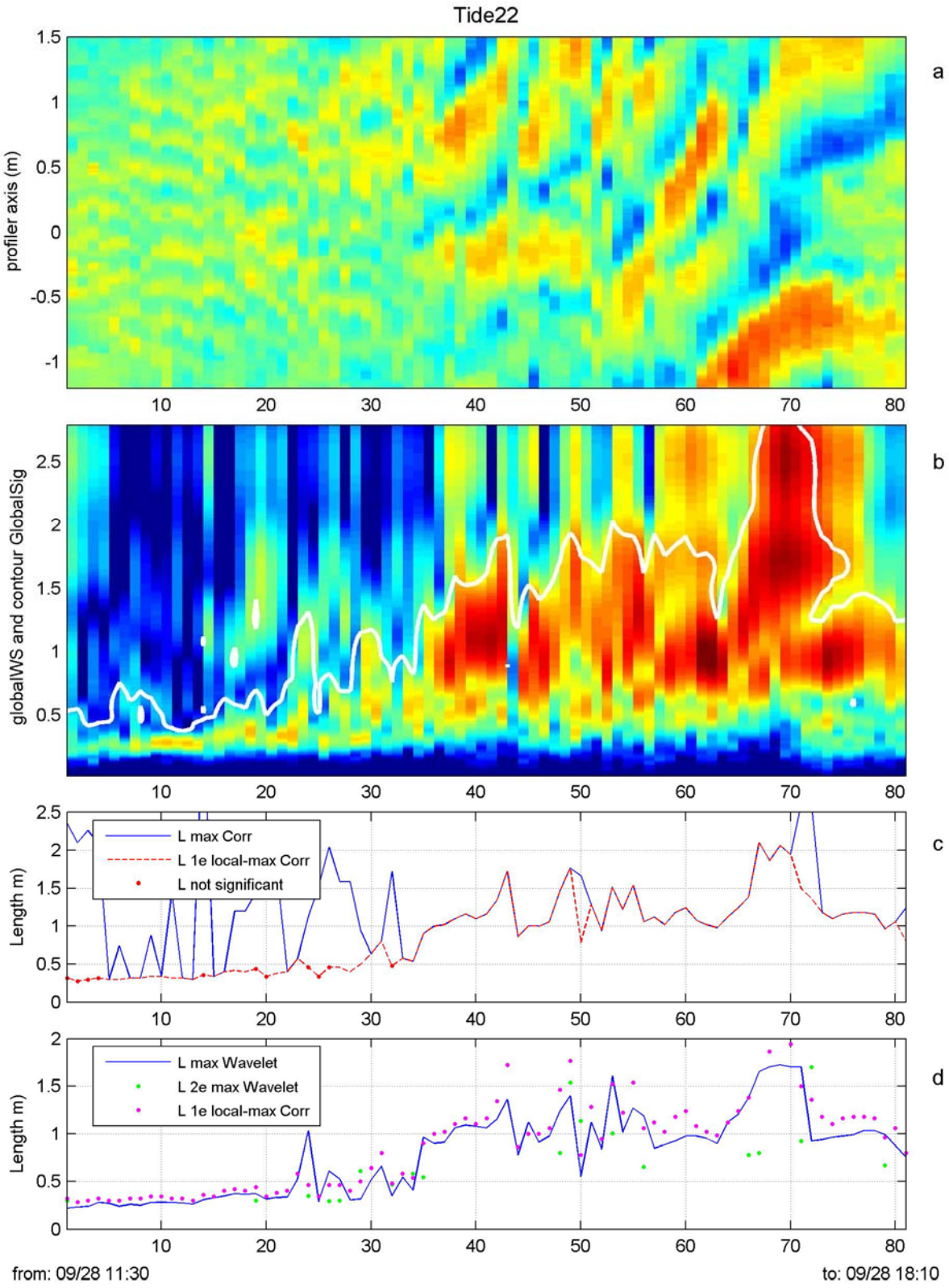

Fig.2.11. Bedlevel profiles (a), global wavelet spectrum and significance contour levels (plotted on log scale) (b), bedform length estimation by autocorrelation (c), bedform length estimation by wavelet analysis (d)

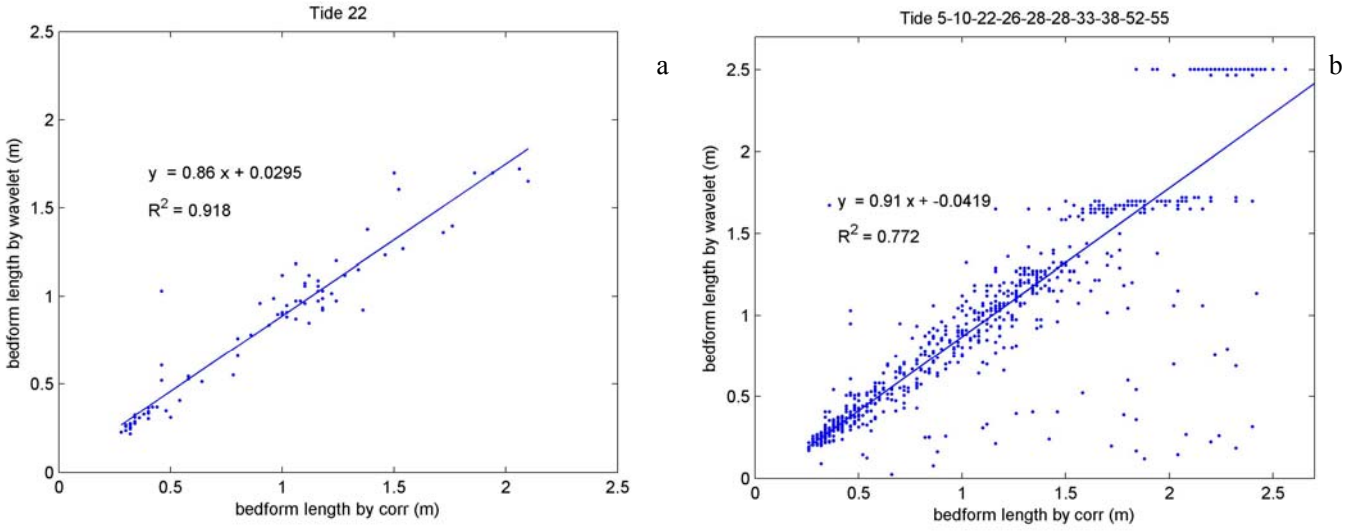

Fig.2.12. Bedform length estimated by auto-correlation and wavelet analysis, on which linear regression is applied. For tide 22 (a) and ten different tides together (b).

Concluding, both auto-correlation as wavelet analysis give similar bedform lengths. But, the auto-correlation methods fails to give significant lengths when the bedforms are < 0.5 m, while the wavelet analysis does provide significant bedform lengths but gives unrealistic clustering at lengths > 1.35m. Therefore, in this thesis the lengths from the wavelet analysis is used unless the lengths are > 1.35 m, then the lengths from the autocorrelation method are used. Unfortunate, this results in a small lag of data points with a length just larger than 1.35, since the bedform length from the autocorrelation method are slightly larger.

The bedform height was determined as $\sqrt{8}\cdot\sigma$, in which σ is the standard deviation of the bed level profile (Masselink et al., 2007). Figure 2.13.a shows the height for tide 22. The bedform skewness and asymmetry were computed similar to the wave skewness and asymmetry with equations (1) and (2), only with the bed level profile substituted for *sf*. The skewness and asymmetry are rather spiky as is shown for tide 22 in figure 2.12.b and c by the dashed green lines. Therefore, the data is smoothed with a 5 point moving average, shown by the solid blue lines in figure 2.12.b and c.

The bedform migration rate was determined using the cross-correlation function between two bedlevel profiles. The spatial lag corresponding tot the strongest positive correlation represents the migration distance, figure 2.13. The migration rate is this distance dived by the time interval between the two bedlevel profiles. The resolution of the migration rate between two adjacent sweeps is only 1cm/5min, which makes it sensitive for spikiness especially when the rate is close to 0. Therefore, the migration rate per sweep (*s*) is determined with equation (2.13) to make it smoother, see figure 2.12.d.

$$M_r = \frac{c_1\left(M_{s-1}+M_{s+1}\right)+c_2\left(M_{s-2}+M_{s+2}\right)}{2\left(c_1+c_2\right)} \qquad (2.13)$$

where M_{s-1} and M_{s+1} are the migration rates determined from cross-correlation between the present, previous and next sweep respectively; M_{s-2} and M_{s+2} represents the migration rate from the present sweep and the second previous and second next sweep respectively; c_1 and c_2 are constants with values of 1.25 and 0.75 respectively.

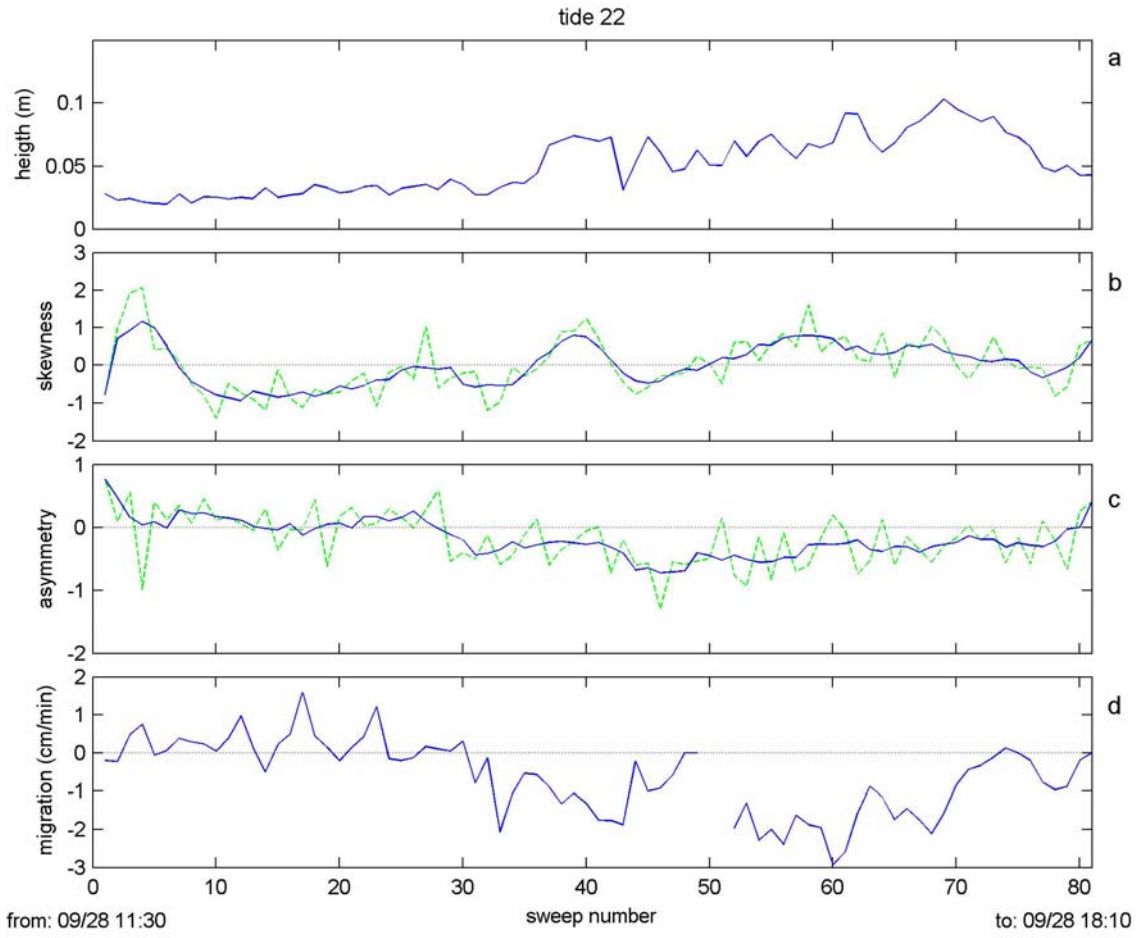

Fig.2.12. The bedform height in m (a), the bedfrom skewness (b), the bedform asymmetry (c) and the migration rate in cm/min (d).

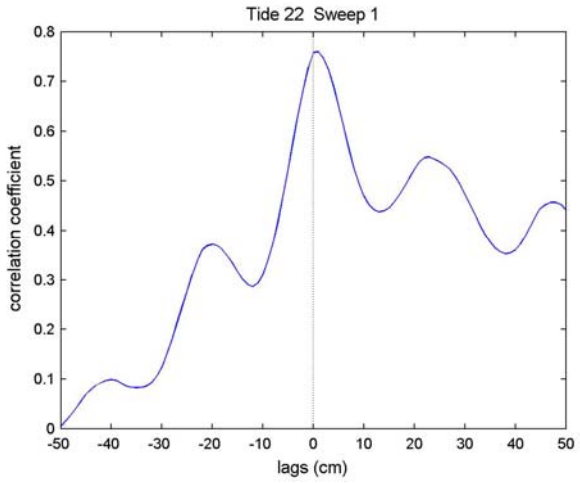

Fig.2.13. The correlation graph, of the correlation between sweep 1 and 2 of tide 22.

3. Results

3.1 Hydrodynamic Conditions

The hydrodynamic conditions at the Truc Vert frame for the whole field campaign are depicted in figure 3.1. Due to a technical defect, the data between 20 October and 1 November is useless. The significant wave height (Hm_0) varied mainly between 0.5 m and 1.0 m exceeding to 1.35 during the storm on 4 October, with a characteristic wave period ($Tm\text{-}_{10}$) varying between 5 and 10 sec. The wave period was largest during the storm on 16 October, but was also surprisingly large (8.5 sec) on 20 September while having the smallest Hm_0. Since wind waves were nearly absent due to the Easterly wind, this large $Tm\text{-}_{10}$ originates from relict swell.

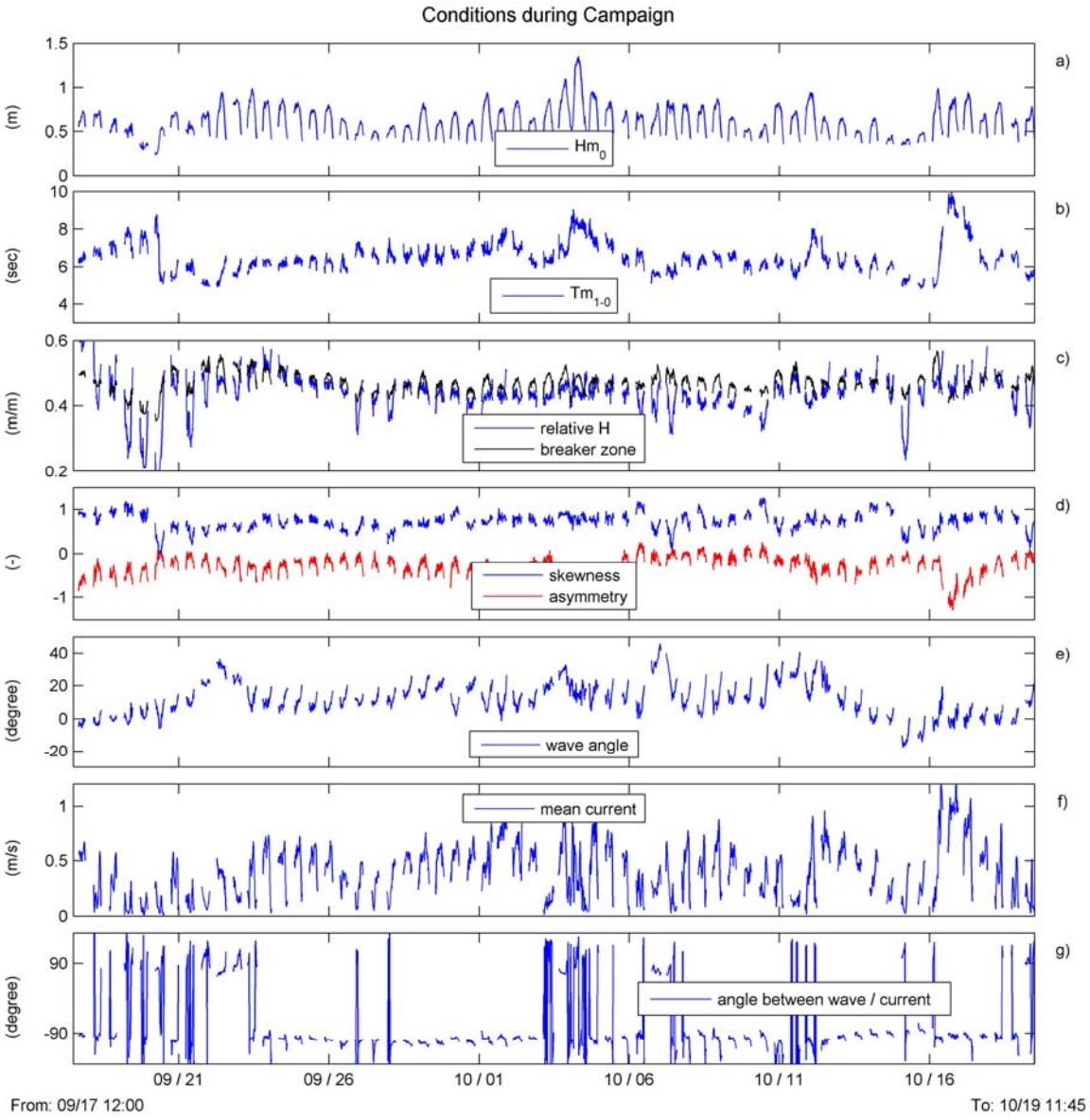

Fig.3.1. Hydrodynamic conditions during the campaign measured at the Truc Vert frame, from 09-17 till 10-19.

Hm_0 (figure 3.1.a) shows a tidal dependence, with increasing Hm_0 during the rising tide and falling Hm_0 during the falling tide. This is indicative for saturated wave conditions, with Hm_0 depending on the water depth. The relative waveheight, shown in figure 3.1.a, supports this argument, being fairly constant around 0.45m except for periods with Hm_0 smaller than 0.5m. Those periods were characterised with gentle Easterly winds. Figure 3.1.a also shows the breakpoint according to Price & Ruessink (2008), which depends on the wave steepness. Relative waveheight values (much) smaller than the breakpoint are indicative for shoaling waves, values larger than the breakpoint but smaller than the 'swashpoint' indicate the breakerzone. With an average 'swashpoint' of 1.1 and the relative waveheight mostly just below the breakpoint the waves at the Truc Vert frame were, during the periods the instruments were able to accurately operate, mostly just prior to breaking having shoaling characteristics or were at the beginning of breaking (breakerzone), according to Price & Ruessink (2008). That type of wave conditions is likely seen the location of the frame (figure 2.3), which is behind a higher seaward bar so being located in a trough. Although rollers were often visually observed at the frame suggesting being inside the breakerzone, this does not have to contradict the found type of wave conditions since the relative waveheight and breakpoint are based on average values over 20 min.

Figure 3.1.d shows the wave asymmetry and skewness. The wave skewness mainly fluctuates between 0.5 and 0.9 with an average of 0.72. Values smaller than 0.5 coincide with small values for Hm_0 and $Tm\text{-}_{10}$. Positively skewed waves have flat broad troughs and are sharply peaked crests, which is induced by wave shoaling. The wave asymmetry varies slightly more than the skewness, especially on the tidal scale, having a standard deviation of 0.23 versus 0.19 for the wave skewness. Since the average asymmetry of -0.3 is also much closer to 0, the asymmetry is less pronounced constant. Negative asymmetry means the wave becomes pitched forward with steep front faces and more gently sloping rear faces. Waves become negatively asymmetric just prior to wave breaking and continue to become more asymmetric after wave breaking. The combination of a small negative asymmetry and a more pronounced positive skewness points to just prior to wave breaking conditions on average. This support the earlier founding's of the average wave conditions at the frame being within the breakerzone but having a more shoaling like (just before breaking) wave type.

The wave angles measured at the frame (figure 3.1.e) have as expected a smaller range than the wave angle found offshore (figure 2.2), due to wave refraction when the waves approach shore. More surprisingly are the nearly constant positive angles (positive angles stand for waves approaching anticlockwise relative to the shore normal). Only the first and last couple of days show negative angles. This can be explained by the bathymetry around the Truc Vert frame. The presence of the eb tidal 'delta' of the tidal channel northwest of the frame make the waves refract around this 'delta' approaching the frame more from the south (positive angle). This effect of the tidal delta is less pronounced when the water level is high, as can be seen from the tidal pattern of the wave angle.

The mean current shown in figure 3.1.f has an average of 0.4 m/s and goes up to 1.2 m/s making the conditions mixed wave and current. The angle between the wave and mean current (figure 3.1.g.) is mostly around -100, meaning the current comes from 100 degrees northerly with respect to the waves. The

main origin of the current can therefore not be wave induced. A cross shore current is more parallel to the wave direction and a large longshore influence current would result in mostly positive and just smaller than 90° angles. Positive, since the wave direction was mostly positive and therefore the angle between wave and current should also be mainly positive when the longshore current is the main mean current component. Smaller than 90°, since a longshore current is parallel to the shore in the same 'direction' as the waves. The main source of the large mean current is therefore to be found in the influence of the tidal channel. This founding is strengthened by visual observations during the campaign.

3.2 Bedform characteristics

Figure 3.2 shows the bedform characteristics throughout the field campaign. De bedform length depicted in figure 3.2.a, show large bedform lengths, varying from 0.17 till 3m with an average of 1.0 m. Less than 20% of the time, the bedforms were smaller than 0.5. This indicates that most the time,

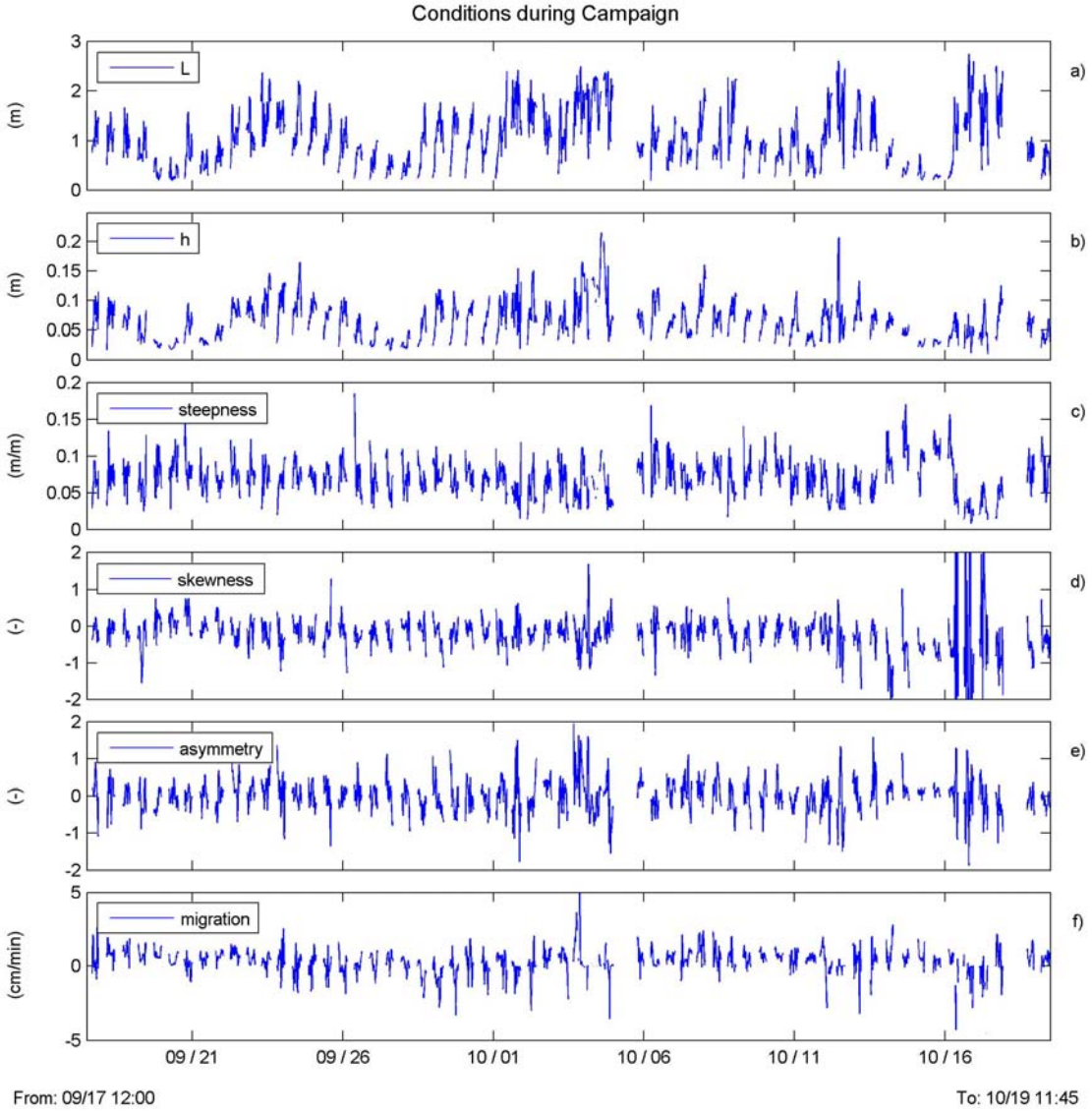

Fig.3.2. The bedform characteristics during the campaign measured at the Truc Vert frame, from 09-17 till 10-19

no ripples, but larger bedform types were present. Due to the fact that the scans were 2D, no further distinguishing in 2D/3D patterns can be made directly. Flat bed has never really been recorded.

The bedform height seems to follow more or less the same pattern as the bedform length, varying between 0.01 and 0.23 m with an average of 0.07 m. The bedform steepness is not constant and seems to show, besides tidal variation, dependence on the bedform length; the smaller the bedform length the larger the steepness. In figure 3.3 the steepness is plotted against the bedform length with the red and dashed red line representing the mean and standard deviation respectively. Those two parameters are based on the steepness for an interval of L of 0.05 m and thereafter smoothed using a 5 point moving average. Although the standard deviation range is large (scatter), a linear like relation (blue line) is present. Except for the ripple like bedforms (L = 0.15 - 0.35 m), having larger steepness. The larger bedforms (L > 2.5m) also show larger steepness, but due to the little amount of data point less significant.

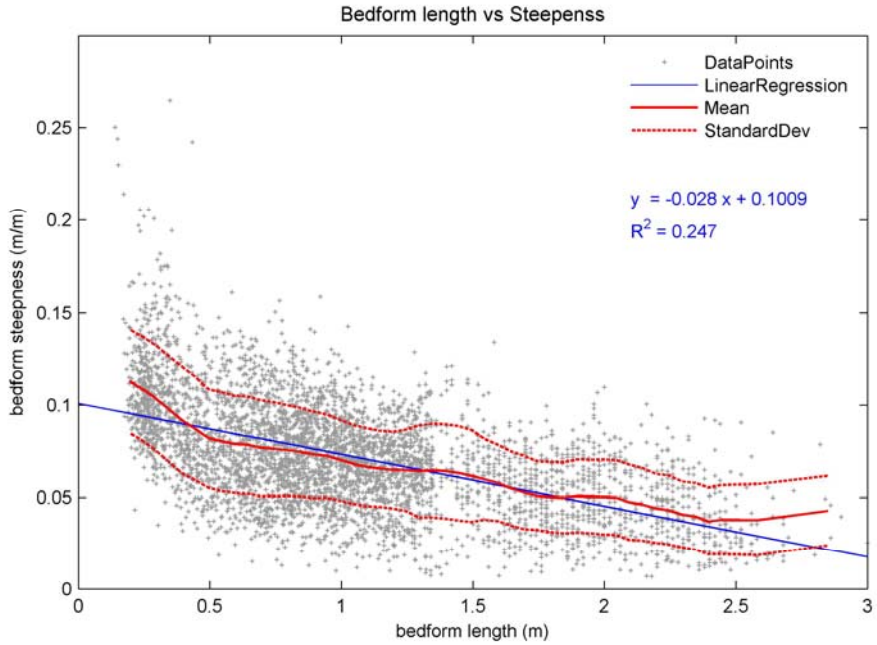

Fig.3.3. Bedform length against bedform steepness

The bedform skewness and asymmetry plotted in figure 3.2.d and e. respectively show besides some tidal variation, 3-5 periods where large peaks in both the positive as negative direction close to each other are present. The peaks from the skewness in the period from 10/11 – 10/14 even extend to > 4 and < -4. All periods with large both directional peaks collide with periods with large bedforms (L > 1.5 m). In figure 3.4 four bedprofiles with different skewness and asymmetry values are shown. Subfigure a and c show two bedprofiles belonging to a skewness of -1.2 with a small asymmetry and asymmetry of -1 with a small skewness respectively. Clearly the broad crests and sharp peaked troughs versus steep front faces and more gently sloping rear faces can be observed. In subfigures b and c the bedform lengths are so long that one bedform does not or hardly fits into one scan. Such large bedforms make the skewness and asymmetry sensitive to which part of the bed is captured by the scan. This can be seen from the large negative skewness and positive asymmetry in subfigure b and d while not necessarily being more skewed or

asymmetric in comparison with figure a and c. This explains the large both positive as negative peaks observed so close to each other for large bedforms (L > 1.5 m). The bedform asymmetry and skewness are therefore assumed to be unreliable for L > 1 m. Furthermore, the campaign average asymmetry is nearly zero (-0.0048) and the skewness close to zero (-0.23).

Subfigure 3.2.e show the migration rates. The migration rate varies between -4.5 and 5.5 cm/min having an average of 0.23 cm/min. A positive migration refers the migration of bedforms shoreward.

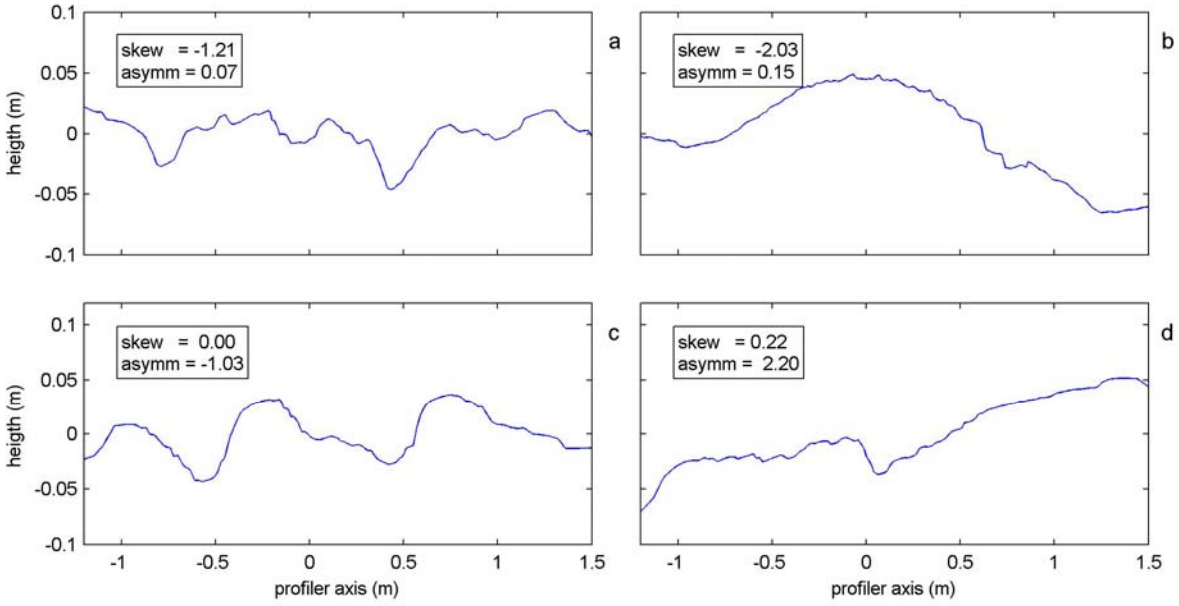

Fig.3.4. Skewness and asymmetry for four different bedlevel scans.

3.3 Type of flow conditions

The large mean currents measured at the Truc Vert frame (figure 3.1.f) indicate that the conditions were not always wave dominated. In an attempt to qualify the type of conditions present throughout the campaign, the data is plotted in a θ_c versus θ_w diagram according to Kleinhans (2005) and includes the separation criteria of Li & Amos (1998), figure 3.5. The U_{*w}/U_{*c} ratios of Li & Amos (1998) are converted to θ_w/θ_c by squaring the accompanying constant. The separation ratios of Zanke (2003) used by Kleinhans (2005) are also plotted. The criteria of Li & Amos (1998) and Zanke (2003) both distinguish between wave only, wave-dominated and current-dominated conditions. The boundaries between wave-only and wave-dominated are quite similar. However, Li & Amos also incorporate wave/current-dominated conditions while Zanke distinguish also current-only conditions making the other boundaries quite different. But, this does still lead to a similar condition differentiation, since no current-only conditions are measured and the wave/current-dominated condition class of Li & Amos (1998) can be seen as an extra classification. The shear velocities (U_{*w} and U_{*c}) used to calculate the Shields numbers (θ_w *and* θ_c) are calculated with Grand & Madsen (1986). $\sqrt{2}$ · horizontal rms velocity (high frequency) is used for the maximum wave induced bottom particle velocity, $Tm\text{-}_{10}$ is used for the period and d_{50} is used for the (median) grain diameter.

For distinguishing between no motion and sheet flow conditions a fixed Shields number is used, 0.0283 and 0.8 respectively. The Shields number for no motion is calculated with Soulsby (1997). This Shields number is fixed since the grain size is assumed constant throughout the campaign. The Shields number of 0.8 is the one used by van Rijn (1993) and Camenen (2009). To plot the Shields criteria for no motion and sheet flow into the θ_c / θ_w diagram, a method combining θ_c and θ_w to θ_{wc} had to be adopted. The method of Soulsby (1997) (see the literature review, 1.19) is very extensive but difficult to apply and also includes the angle between the wave and current component which varies in time. Therefore, Allen & Leeder (1980) (1.21) and the 'maximum' Shields number of Soulsby (1997) (1.22) are used. The largest deviation between the different methods is expected when $\theta_w = \theta_c$. Allen & Leeder (1980) give than for the sheet flow boundary $\theta_w = \theta_c = 0.4$, Soulsby (1997) maximum method gives $\theta_w = \theta_c = 0.57$ and Soulsby (1997) with a wave current angle of 100° gives $\theta_w = \theta_c = 0.58$. Since the wave current angle is mostly around 100 (or – 100) equation the maximum method of Soulsby & Whitehouse (1997) is also a good estimate for Soulsby (1997) for this data. Both methods for the no motion and sheet flow are plotted in figure 3.5.

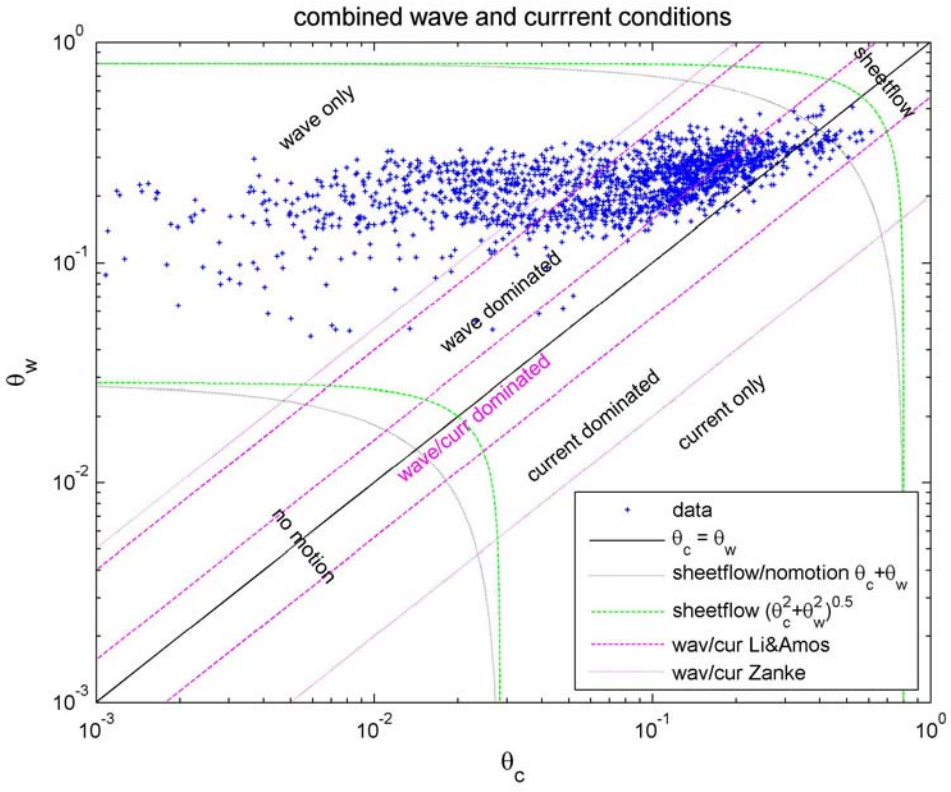

Fig.3.5. Distinguishing between different types of wave/current conditions.

The conditions during the campaign, according to the graph, varied between wave only and current dominated. Most conditions are wave dominated and according to Li & Amos a large part of the data is wave/current dominated. 'No motion' conditions have not been measured but sheetflow conditions, depended on which method is adopted, have. Which method should be adopted for distinguishing sheetflow conditions and whether the criteria of Li & Amos (1998) and or Zanke (2003) are valid will be analysed tide individually in the following section.

3.4 Hydrodynamic and bedform relations, tide specific

Based on the θ'_c/θ'_w diagram per tide, 7 tides (out of the 59 tides with both ripple as hydrodynamic data) are selected for further analysis. The selection tries to capture the versatile range of conditions and bedforms into a coupe of distinct tides. The characteristics of the tides and possible patterns will be discussed per subject rather than tide specific. For each tide a figure is made showing; the bedprofile in time, Hm_0 and relative waveheight, mean current, angle between wave and current direction and the angle between the wave direction and shore normal, bedform length and height, and the migration rate. Furthermore a type of flow condition (θ_c versus θ_w) graph analogue to figure 3.5 is included showing the conditions from the beginning to the end of the tide. The figure for tide 22 is show in figure 3.7, for the other selected tides the reader is referred to Appendix A. The black dashed line depicted together with Hm_0 and the relative waveheight is the breakpoint according to Price and Ruessink (2008).

Tides 5, 10 and 28 (appendix A) are tides with little to moderate evolution of the bedform dimensions but for three different flow conditions. The conditions during tide 5 are wave dominated with a very little changing Hm0 of 0.35 m and a mean current of 0.08 m/s on average. With the relative wave height being significantly smaller than the breakpoint, shoaling like conditions were present. The bedforms corresponding to such low energy wave dominated conditions are ripples. However, at the beginning of the tide, from 17:45 till 19:00, two dominant bedform lengths are present, ripples (L = 0.3 - 0.35 m) and larger bedforms (L = 0.7 m). This can be observed from the bedform length oscillating between 0.35 and 0.7 m and the presence of the green dots, the second wavelet spectrum maxima, in between. Since the larger bedform length is exactly twice the ripple length, this situation is probably induced by the growth of some ripples (in height and broader crest) making the smaller ripples to become less pronounced and thus less detected. This can also be observed in the bed profiles and is strengthened by the bedform height, being not significantly larger for the periods with L > 0.5. The tide average bedform length, height and steepness are 0.37m, 0.027m and 0.08 respectively, but when the larger (>0.5m) bedform lengths are disregarded the bedform lengths are between 0.2 – 0.3 m with maximum steepness of 0.13 (figure 3.7). Such lengths and steepness are indicative for vortex ripples. The presence of vortex ripples is supported by visual observations in the field at the beginning of the tide. The conditions during the tide are wave only except for just one moment in time according to Li & Amos (1998) and about three times according to Zanke (2003). The mean current is small < 0.2 m/s being largest at the beginning and end of the tide and changes direction (180°) a couple of times. These changes are, as expected for wave only conditions, not reflected in the bedform dimensions.

The conditions of tide 10 are more intense with an average Hm0 of 0.7 m and mean current of 0.35 m/s. Still, shoaling conditions except for a brief moment at the end of the tide are present. Both wave as current conditions change significantly during the tide, although this does not seem reflected in the bedform dimensions. Hm0 increase from 0.4 m to 0.9 and back again, while the mean current starts at 0.5 m/s at the beginning of the tide and decrease to 0.2 at the end of the tide. The conditions therefore change from wave dominated to wave only at the end of the tide. The mean current is in this tide in the ‘same’ direction (north

going) as the wave propagation. But, since the mean current starts at its maxim value and decreases while the wave height increases, it cannot only consist of a longshore current. However with an wave angle of around 30° a longshore current component is expected. Also, a north going (Slufter inwards) tidal current is only expected for the rising tide, therefore apart from the first one and a half hour the mean current maybe mainly wave induced. The bedforms at the beginning of the tide start small (L of 0.3-0.5 m) but rapidly increase to 1-2m in length and 0.1m in height with a corresponding steepness of about 0.07. The bedform length and accompanying height do show some variation during the tide, but remain on average the same (1.15 and 0.08 m). The bedform are therefore larger bedforms. So, although the conditions change significantly, the bedforms do not.

Tide 28 shows similar wave conditions as for tide 10, a Hm0 starting at 0.4 m increasing to 0.8 m (0.9 m for tide 10) and decrease to 0.4m again. The current conditions however are more intense starting at 0.6 m/s and a tidal average of 0.77 m/s. This does not only leads to a different type of conditions of current dominated according to Li & Amos (1998) and wave dominated at the begin changing to current dominated at the end of the tide according to Zanke (2003), but also lead to much larger bedforms compared to tide 10. The length varies between 1 m and 3 m, with an average of 1.7 m. The height varies between 0.02 and 0.2 m and averages 0.08 m. The bedform length and height varies much, but in an oscillatory type of way. This is properly due to the large bedforms and their position relative to the scanner in time as they migrate along. The lengths are much larger than for tide 10 but the heights are nearly the same. Apparently, as the minimum height also reflects, the height is washed out by the more intense current. Since the bedforms are quite different for tide 10 (wave dominated) but does not seem to really change during the tide while the type of conditions change according to Zanke (2003), this pleads for adopting Li & Amos (1998 Furthermore, the wave angle is small (10°) and opposite to the direction of the current. The current must therefore be tide originated. Although outside the scope of this thesis, it is interesting to look at the differences in behaviour of the mean current between tide 10 and 28. In figure 3.6, a 90 second section of y (longshore) direction of the lower EMF is shown for tide 10 (left) and 28 (right). The characterises are quite different, in tide 10 the mean current oscillates much with about the same period as the wave period (5.5 sec), while for tide 28 more but smaller oscillations and fewer but larger and wider oscillations are present. The latter larger oscillation can roughly be linked to wave period. Also, while the mean current of tide 28 is twice as large as for tide 10, the amplitude of the oscillations seems smaller on average.

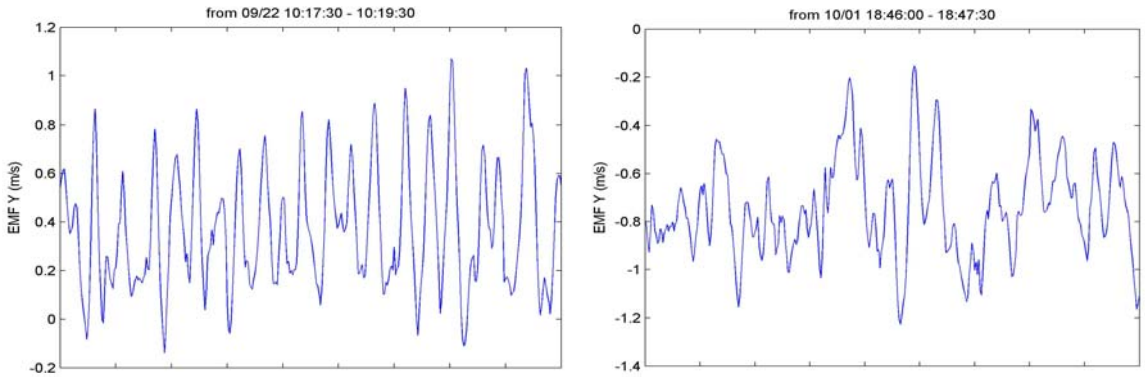

Fig.3.6. Distinguishing between different types of wave/current conditions.

This is strengthened by the tidal mean and standard deviation of the y component of the mean current: mean of 0.38 and 0.77 m/s and standard deviation of 0.24 and 0.21 m/s for tide 10 and 28 respectively. From this can conservatively concluded that a mean current induced by a longshore current is much more irregular than a tidal current. This difference may have a pronounced effect on bedform development.

Furthermore, in the bedprofile graphs are besides the differences in bedform dimension between tide 5, 10 and 28 reflected, also a distinct and for those three tides a different pattern visible. Tide 5 shows bedforms crests which can be followed in the graph for several hours in time. The (in the graph vertical) displacement is reflected in the migration rates which are in this tide positive, so shoreward migration. In tide 10 the bedform crests can also be followed in time, but seem to shift or change suddenly multiple times during the tide. These shifts are also reflected in the migration rate. However, the migration rate peaks cannot be linked to changes (peaks) in the flow conditions. The cross shore mean current which is expected to have a large influence on the migration rate, displayed in figure 3.7, does also not show large peaks which coincide with the migration peaks.

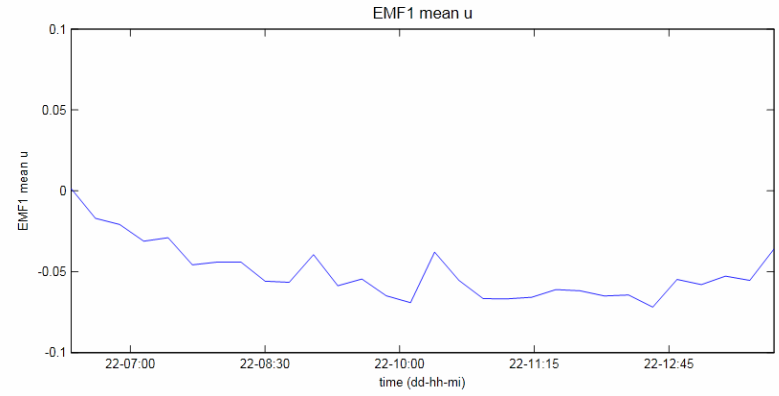

Fig.3.7. Cross shore mean current form EMF1 during tide 10.

A more convenient explanation for this feature is the presence of an irregular bedform pattern. Because, when the bed would have had bedforms with a completely 2D pattern and experiencing a more or less constant migration rate, a pattern like tide 5 would have been present. This is even the case when the direction of the crests is not longshore, since that would only result in larger observed bedform lengths and lower measured migration rate. When cross-shore ripples would have been present with the primary ripples crest having a longshore direction, flat area as large one ripple length would have been observed representing the cross ripples. While, an irregular bedform pattern results in lots of bifurcations and convulsions which can cause these shifts of crest locations. Although bifurcation cannot visually be distinguished from the process of split and merge in the case of 2D images, split and merge are not expected to occur for little changing bedform dimensions.

The bedforms in tide 28 are so large that is becomes harder to distinguish the type of bedform and pattern present since only one or two bedforms can are observed within the scans. But, an irregular pattern is likely to be present seen the irregular pattern and varying migration direction, which cannot be linked to the flow conditions. Furthermore, some crests do not seem to originate from or end to another bedform,

indicating the presence of 3D bedforms which do not have continues crests. But since most bedforms are not fully captured within the scan, this is hard to judge. For the other 5 tides given tides in appendix A it is more difficult to couple the bedprofile graph characteristics to bedform characteristics due to more and or rapid changing bedform dimension and or conditions. But, these and other tides strengthen the appearance of 2D bedforms for low intense wave-only conditions and irregular bedforms (patterns) for more intense wave-dominated or wave-current conditions. More 3D shaped bedforms may be present for intense wave-current conditions.

While in tide 5, 10 and 28 the bedforms change little with respect to the conditions, giving a good image of the bedforms present under 3 different type (wave vs mixed) conditions, in tide 22 it is the other way around. Tide 22 is characterised by the evolution of a rippled bed to larger bedforms with lengths > 1 m (figure 3.8). The ripples with lengths 0.25-0.30 m start to increase in length around 13:20 to 1 m around 14:40. The length stays roughly 1 m until 16:45 after which it increases to 1.5 m and decreases after 17:20 to 1 m again. The bedform height does follow the same pattern as the bedform length, only deviating from it after 17:00 were the height increases later and less pronounced and decreases later than the length. In contrast with the large change in bedforms, the flow (wave and current) conditions change very little. According to the θ'_c/θ'_w diagram the type of flow condition does not change significantly. The intensity of the conditions does increase somewhat and decrease again at the end of the tide. An explanation for the larger change in bedforms versus little change in conditions and longer period of little bedform evolution is relaxation time, the bedform development lacking behind the conditions and in this case already from the beginning of the tide. Or, another explanation, the transition from ripples to larger bedforms is marked by a small range of flow conditions. In the case of relaxation the question arises whether the bedform evolution is the consequence of 'normal' evolution, the relaxation time decreasing exponentially by increasing flow conditions, or the bedform evolution is constrained by a conditional threshold which rapids up the evolution to the larger bedforms. Regardless of the explanation for the larger change in bedforms versus little change in conditions, the specific conditions triggering this transition are of interest. Therefore, the conditions of tide 22 are taken a closer look at. The relative waveheight does not change much during the tide. Hm_0 increases from 0.4 m till 0.55-0.6 m around 13:30 and remains fairly constant until 16:30 hours. The mean current increases from little under 0.4 m/s to 0.55-0.6 m/s at 14:00 hours and decreases after 16:45 hours. The angle between the waves and current is constant around -100°. The wave angle oscillates 5° around 15° and steadily increases after 14:30 to 25°. The variables expected to have the largest influence on the bedform evolution are, seen the timing and increases of the variables, the absolute wave height and mean current. But, because both wave height and mean current increase nearly simultaneously (θ'_c/θ'_w ratio remains constant) and increase the same amount, one can not distinguish the effect of the different variables on the bedforms. Therefore, other tides also including a similar transition from ripples to larger bedforms as in tide 22 are analysed. 7 other tides are pointed out as having such transition from which two tides, tide 26 and 55, are shown in appendix A.

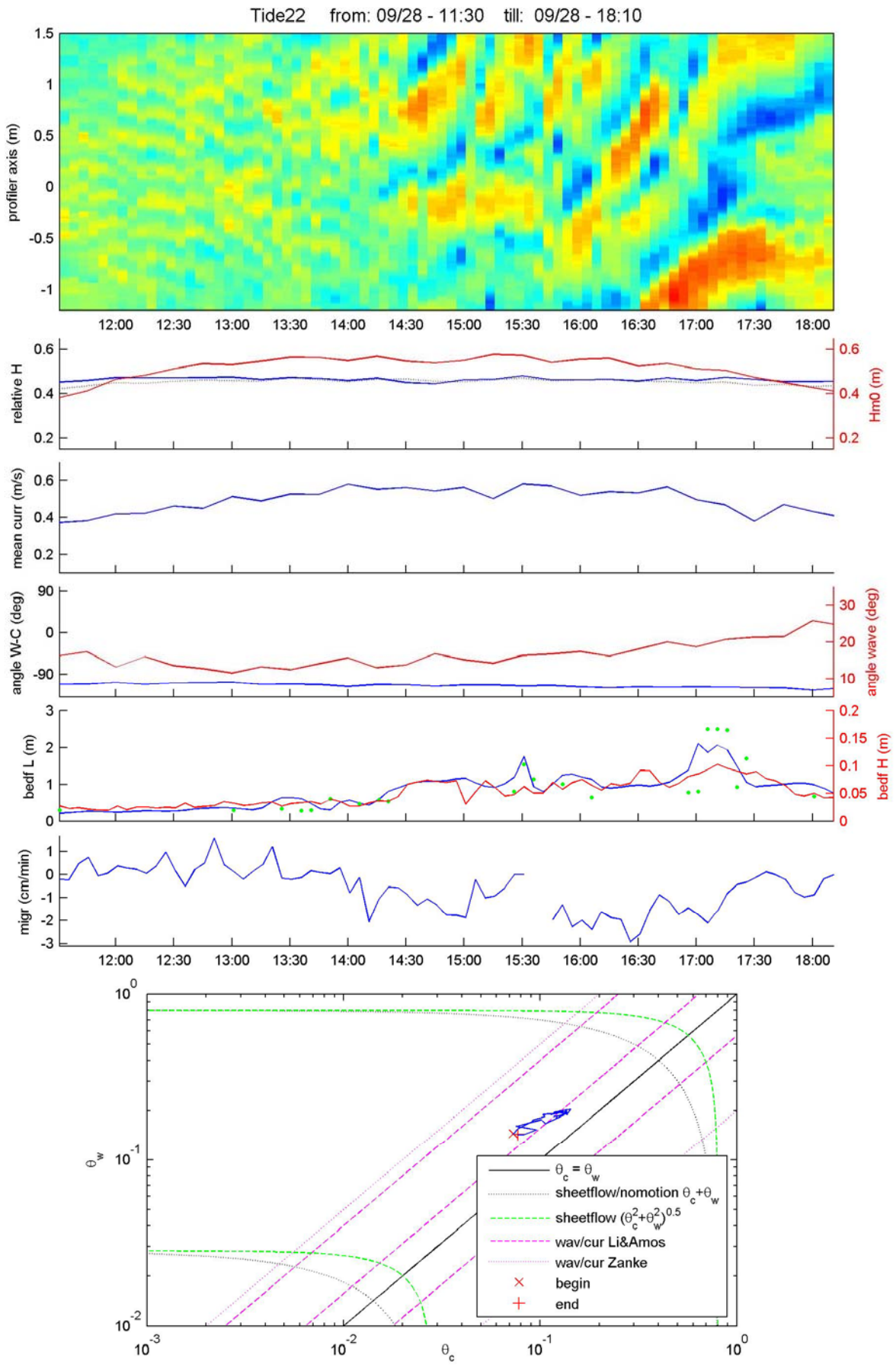

Fig.3.8. Bedform characteristics and hydrodynamic condtions during tide 22.

Tide 26 shows superimposed ripples on a larger bedform shape at the beginning of the tide. This superimposeness can be made up from the bedprofiles and bedform length graph, which shows two dominant wavelengths at the beginning of the tide. This is again shown by the spikiness of the graph and the presence of green dots, representing the second maxima of the wavelet spectrum, in between the spikes. The bed profiles at the end of tide 25 explain this superimposed situation by showing large bedforms (L > 1.5m) with crests at the same location as the larger bedform shapes at the beginning of tide 26. This makes the larger bedforms at the beginning of tide 26 relict bedforms. Having explained the larger bedforms, the wave / current driven bedforms at the beginning of tide 26 can be characterised as ripples. The ripples start to increase in size from about 15:40. The bedform length and height keep increasing until the end of the tide, the irregularity/spikiness of the increase not taken into consideration. This in contrast with tide 22 in which the increase is more rapid and stays steadier afterwards. The wave height, wave angle and wave-current angle of tide 26 are similar to those in tide 22. However, the mean current is different from tide 22. This is also expressed in the θ'_c/θ'_w diagram, the conditions of tide 26 are more wave- dominated at the beginning changing to even more current dominated at the end than for tide 22. The ripples show an increase in length after 15:40, when Hm0 exceeds 0.55 m and the mean current exceeds 0.5 m/s. This is similar to tide 22. But when the mean current decreases around 15:45 to 0.4 m/s at 16:10 the bedform length decreases. When the mean current increases again, the bedform length starts to increases as well. Meanwhile Hm0 is constant around 0.55. This is indicative for the bedform development not lacking much behind (relaxation) the flow conditions and the mean current having a possible key role in the bedform evolution from ripples to larger bedforms. Another observation of tide 26 supporting this argument; the bedform length and height increase according to the increasing mean current to maximal 0.7 m/s around 19:30, while Hm0 already decreases from the maximum of 0.6 m after 18:40. The bedform height follows a similar pattern as het bedform length, only less pronounced (showing less irregularity) and usually lacking behind the development of the bedform length.

In tide 55 the type of flow conditions varies largely. The conditions start very modest being wave dominated. During the tide the conditions become more intense but still being wave dominated until around 6:40 when the mean current increases from 0.35 to finally 1.2 m/s changing the type of flow conditions to current-wave dominated at the end of the tide. The wave-current angle changes from positive (from the south) to negative early in the tide. But, since the mean current is still small (> 0.15 m/s) not of great influence. The wave angle varies mainly between 5 - 10° increasing to 20° at the end of the tide. The bedforms start as ripples with lengths between 0.25-0.35 increasing temporarily two times (around 04:25 and 05:50) to 0.5 m and increase to larger bedforms after 06:30. While Hm0 is already above 0.5m from 03:00, the mean current reaches 0.4 m/s at 06:15 decreases a little and increases to beyond 0.5 m/s from 07:00. Although the development of larger bedforms after 06:30 does coincide with the maximum Hm0 (1m) with ‘only’ 0.4 m/s of mean current, the major bedform length development with lengths > 2m (07:20) coincides with the increase of the mean current to 1 m/s. Since no large delay between the change in conditions and the bedform development is present, relaxation is not likely to play a large role in the transition from ripples to larger bedforms in this tide. The development of larger bedforms seems

dominantly driven by the mean current and tend to develop when the current exceeds 0.4 - 0.5 m/s. Wave dominated conditions with Hm0 between 0.5 – 0.7 m did not develop (within the time span of 2 hours) larger bedforms.

The other five tides having a transition similar to tide 22 show similar results. In three tides larger bedforms develop when both Hm0 as the mean current exceed 0.5 - 0.6 (m and m/s respectively). In one tide the bedform development seems to be dominated by the mean current exceeding 0.45 m/s while Hm0 is 0.6m. But, in one tide larger bedforms do develop from ripples when Hm0 exceeds 0.7 m while the mean current is only 0.2 m/s.

From the 7 tides can be concluded that the transition from ripples to larger bedforms is likely to depend on a small change of flow conditions rather than largely influenced by relaxation times. However, relaxation can still play an important role in the rapid development during the 'transition', due to the decrease of relaxation times when the conditions increase in combination with the initially small bedforms (small volume). The transition seems insensitive to the relative waveheight, wave angle and wave current angle, but sensitive to Hm0 and the mean current. The mean current often plays a key roll when exceeding 0.5 m/s. But, larger bedforms are also found when Hm0 > 0.7 m and the mean current < 0.5 (m/s).

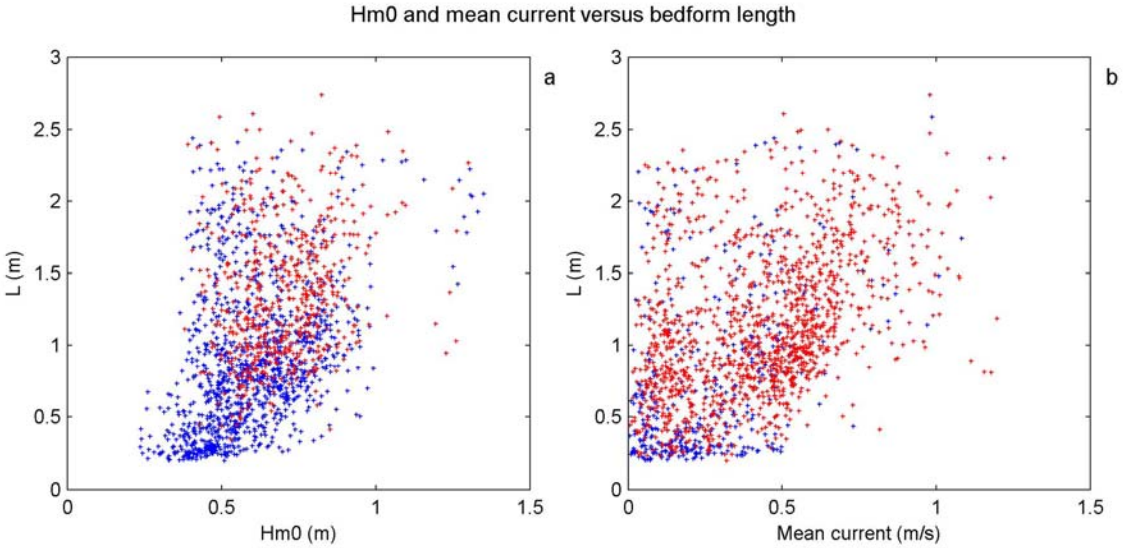

Fig.3.8. The bedform length plotted against Hm0 (a) and the mean current (b). The dots are bleu in figure a when the mean current is less than 0.5 m/s and red when the mean current is equal or larger than 0.5 m/s. In figure b the same hold for Hm0, bleu < 0.5 m, red >= 0.5.

In order to check the findings about this transition the bedform length is plotted against Hm0 and the mean current for all available data points (figure 3.8). From figure 3.8.a can be concluded that large bedforms do not develop when Hm0 < 0.4 and ripples are not likely to be present when Hm0 > 0.7. When the mean current exceeds 0.5 m/s larger bedforms are present (figure 3.8.a and b) regardless of Hm0, although the bedforms are on average larger when Hm0 exceeds 0.5 m. These findings support the conclusions drawn from the observation of the selected tides.

Besides the dependence of the transition from smaller to larger bedforms on absolute numbers for Hm0 and the mean current, it also seem to be related to bedform type criteria of Li & Amos (1998). Even though the bedform type does not significantly change in tide 22 the transition does takes place around the wave-dominated (W-d)/ wave-current (W-C) boundary. For tide 26, in which the conditions change from wave dominated to W-C conditions, the bedform transition does also take place around the W-d / W-C criteria of Li & Amos (1998). For tide 55 this is also the case, however the type of condition changes rapidly around that time to the W-d/ C-d (current dominated) boundary by Zanke (2003) making it hard to assign the transition to the Li & Amos (1998) criteria. Still, both three tides seem to plead for interference of the Li & Amos (1998) criteria on the transitions from smaller to larger bedforms. But, since the transitions from W-d to W-C is in these situations induced by an increase in mean current and therefore increase in overall flow intensity, the given image may be distorted. In figure 3.10 the bedform length is plotted against the shear velocity ratio on log scale. The Li & Amos (1998) W-o (wave-only) / W-d and W-d / W-C criteria together with the Zanke (2003) W-d / C-d criteria are also plotted in the figure. The W-o / W-d criterion of Zanke (2003) is not separately plotted since that is nearly equal to that of Li & Amos (1998). Larger bedforms (> 1m) are present for nearly all ratios of U_w/U_c but in a larger amount for small ratios, so larger wave influence. For small ratios ripples (<< 0.5m) are lacking and bedforms < 1m are also nearly not present. The boundary for which this occurs coincides with the W-d / W-C criteria of Li & Amos (1998). But, the lack of small bedforms for small ratios of U_w/U_c may also be the result of a lack of low energetic W-C conditions. Judging from figure 3.5, the conditions become increasingly intense for more current dominated conditions. Still, the found boundary pleats more for Li & Amos (1998) than for Zanke (2003).

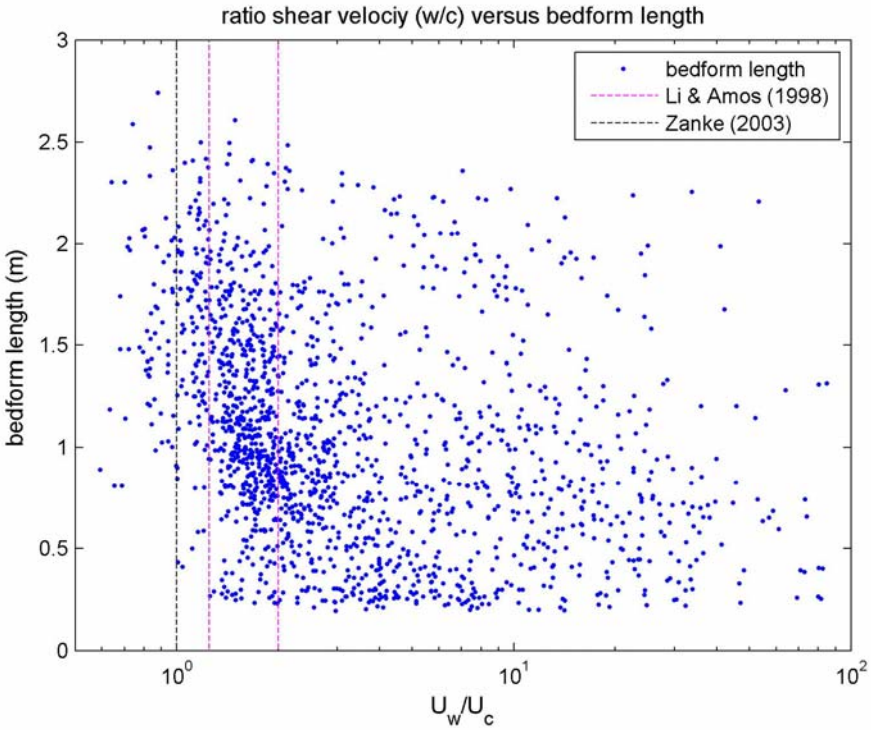

Fig.3.10. Ratio between the wave and current induced shear velocity versus the bedform length.

Another way to review the wave/current criteria is by looking at the bedform asymmetry and bedform steepness, since those bedform properties are influenced by current effects (van Rijn, 1993; Ribberink & Al-Salem, 1994; Wiberg and Harris 1994; Hay & Mudge, 2005, Kleinhans, 2005). Figure 3.11 shows the absolute bedform asymmetry plotted against the U_w/U_c ratio. The bedforms show larger asymmetry values for decreasing U_w/U_c ratios, so increasing current influence, as expected. But since small asymmetry values are also present for low U_w/U_c ratios and no distinctive boundary is found, one cannot judge the wave-current criteria based on bedform asymmetry. The smaller asymmetry values may be explainable by the fact that bedform asymmetry is mostly expected in the direction of the current which is mainly perpendicular to the scanned bedforms and is therefore not incorporated in the given asymmetry values.

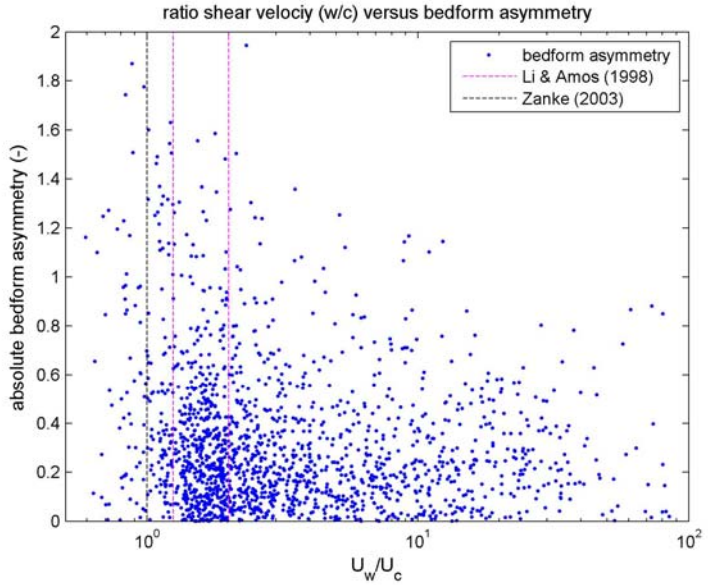

Fig.3.11. Ratio between the wave and current induced shear velocity versus beform asymmetry.

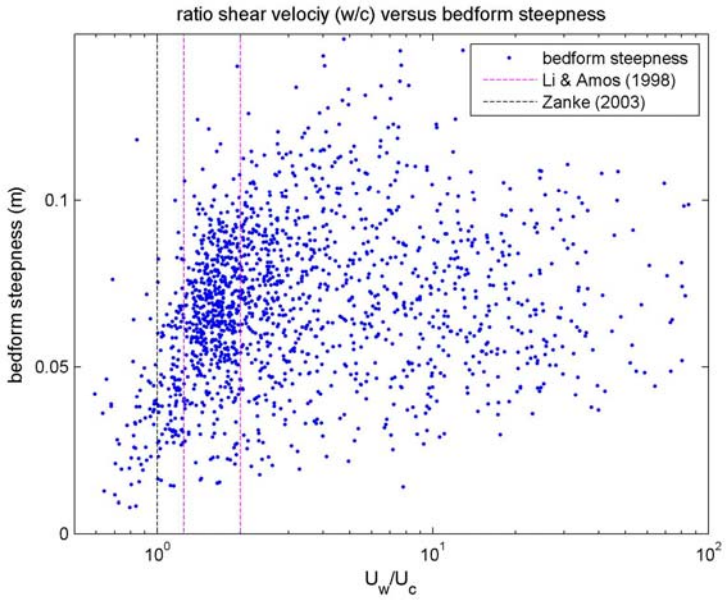

Fig.3.12. Ratio between the wave and current induced shear velocity versus beform steepness.

Figure 3.12 shows the bedform steepness against the U_w/U_c ratio. Li & Amos (1998) namely observed less steep bedforms for more current induced beforms. Also irregular (3D) bedforms, which are expected for more current induced bedforms according to Andersen & Faraci (2002), have lower steepness according to e.g. O'Donoghue et al. (2006). The maximum steepness value decrease indeed for decreasing U_w/U_c (increasing current influence). The ratio (U_w/U_c) for which this decrease starts or at least starts to decrease more rapidly coincides with the W-o / W-d criteria of Li & Amos (1998) or just above that ratio. This is indicative for the current effect being depended on the Li & Amos (1998) criteria.

In tide 38 the conditions start wave dominated according to Li & Amos (1998) with a mean current of 0.4 m/s and Hm0 of 0.4 m and rapid increase to wave-current conditions with a mean current of about 0.7 m/s and Hm0 of 0.7m at 06:00 hours. The bedform dimensions also grow rapidly, length from 0.5m to 1.5m and height from 0.05m to 0.1m, but after 06:00 hours. This indicates that the bedforms lack behind the flow conditions, relaxation. From 6:00 hours on the mean current decrease steady to 0.03 m/s at 09:10 hours and stays low, most of the time <0.1 m/s, the rest of the tide, changing the flow condition to wave-dominated according to Li & Amos (1998). Hm0 meanwhile oscillates around 0.8 m and starts to decrease steadily after 11:30. The bedform length however does not change much between 06:30 and 10:00 hours, where after it rapidly decreases towards 0.7m and stays around that for the rest of the tide. The bedform height does start to decrease earlier, after 08:10 hours to around 0.05 m at 10:00. This decoupling between the bedform length and height indicates the occurrence of split. This process can also be observed in the bedform graph. The duration of this bedform decrease in relation to the rapid bedform increase at the beginning of the tide and the constant (although some oscillatory variations) bedform length and height after 10:00 hours while Hm0 decreases form 0.8m to 0.4m again, indicate hysteresis: the bedform development differing for increasing and decreasing conditions. However, the bedform dimensions do change after the conditions decrease, at least in the period from 08:10 till 10:15 hours, this is in contradiction with the end of the tide where the flow conditions do decrease but the bedforms not. Especially remarkable is that for the period where the bedforms do decrease for decreasing conditions, the bedforms initially do not change much (for example hardly any migration) while for the period where the bedforms do not decrease, the bedforms do change much: migration. This non-decrease in bedform dimension at the end of the tide may be explained by the narrow band of conditions for which a large increase in bedform dimension is observed which is discussed earlier. The other way around: only when the conditions are below a certain narrow band of conditions the bedforms evolve back to ripples. Meaning that, the bedforms at the end of the tide may be in equilibrium with the forcing.

The process of hysteresis is even more clearly visible in tide 22 from the nearly symmetry in conditions but asymmetry in the bedform characteristics. Still, the bedform development does not come to a halt when the flow conditions decrease. After around 17:15 hours the bedforms decrease in height and soon thereafter the bedform length decreases sharply to lengths around 0.7 m. During tide 10 the bedforms dimensions, after a rapid increase at the beginning of the tide, do no change significantly. Besides hysteresis a more or less freeze of the bedforms at the end of the tide can be observed. Such freeze is also

found at the end of tide 26. The reason for this difference found between tide 22 and 10 is properly the rate of the decrease in flow conditions. In tide 22 Hm0 changes at the end of the tide 0.11 m and the mean current 0.1 m/s over the span of $1^1/_2$ hours, while this is 0.28 m and 0.3 m/s for tide 10. Since the relaxation time is found to decrease for decreasing conditions (Smit & Sleath, 2004; Doucette & O'Donogue, 2006; Traykovski, 2007) rapid decreasing conditions may lead to decoupling of the bedforms from the conditions. This seems also to be the case for tide 26 in which the bedforms at the end of the tide seem to freeze, induced by a decrease of 0.15 m in Hm0 and 0.2 m/s in the mean current within an hour. Also in other tides freezed bedforms are found for fast decreasing conditions and decreasing bedform dimensions are observed for more slowly decreasing conditions. The large variety of conditions makes it difficult to quantify a boundary between 'freeze' and still decreasing bedform dimensions for decreasing flow conditions. Also, when only the wave height or only the mean current decreases, the conditions may still be intense enough for the bedform dimensions to change. This effect is more pronounced for a decrease in mean current. A fast decreasing wave height leads most of the time to a freeze. But, a general rule of thump could be defined, when both the Hm0 as the mean current decrease 0.2 m versus 0.2 m/s within an hour, the bedform dimension freeze. The bedform length is found to be more sensitive to such freezes. Some tides do show a freeze in the bedform length but decreasing bedform height for decreasing flow conditions. Such process was also observed at the middle of tide 38 during the process of split. At the middle of tide 38 the bedforms also seem to freeze after a rapid decrease in conditions, but the bedforms do decrease in length sharply eventually. Looking at the end of tide 22, just before the decrease in bedforms, a similar but less pronounced process as in tide 38 can also be observed. These observations indicate that the observed freezes may be a temporary process ending with a rapid decrease in bedform length. If that is the case, the tides in which the freezes are observed lasted just not long enough for that to happen.

In section *3.3 Type of flow conditions* has already been observed that sheet flow conditions may have been present. Only during four tides the conditions reached or exceeded the critical flow conditions according to the wave and current Shields number combining method of Allen & Leeder (1980), during tide 32, 55, 56 and 57. During tide 55 the conditions exceeded the sheetflow criteria between 08:55 and 09:40 hours as can be observed from the θ_c versus θ_w graph. At the beginning of that period large bedforms were present with a bedform length of about 2m and height of 0.1m. The bedform height rapidly decrease to below 0.05m while the length keeps varying between 1 and 2m. At the end of the sheet flow period the bedform height is decreased to 0.02 m with an accompanying length of 0.07. Due to the impossible presence of such small ripples during those conditions and the visual interpretation of the bedform graph, these bedform characteristics are indicative for flat bed or closely to it. This indicates that the method of Allen & Leeder (1980) should be adopted. In order to validate this, the bedform graph, dimensions and θ_c versus θ_w graph are also shown for tide 56 and 57 in figure 3.13. During tide 56 the conditions are according to the method of Allen & Leedder (1980) most of the time just below or just above the sheet flow conditions. Judging from the bedform length and height, length often > 2m and height < 0.05 m, the bedforms are or close to flat bed. Furthermore, three white bands are visible in the bedform graph

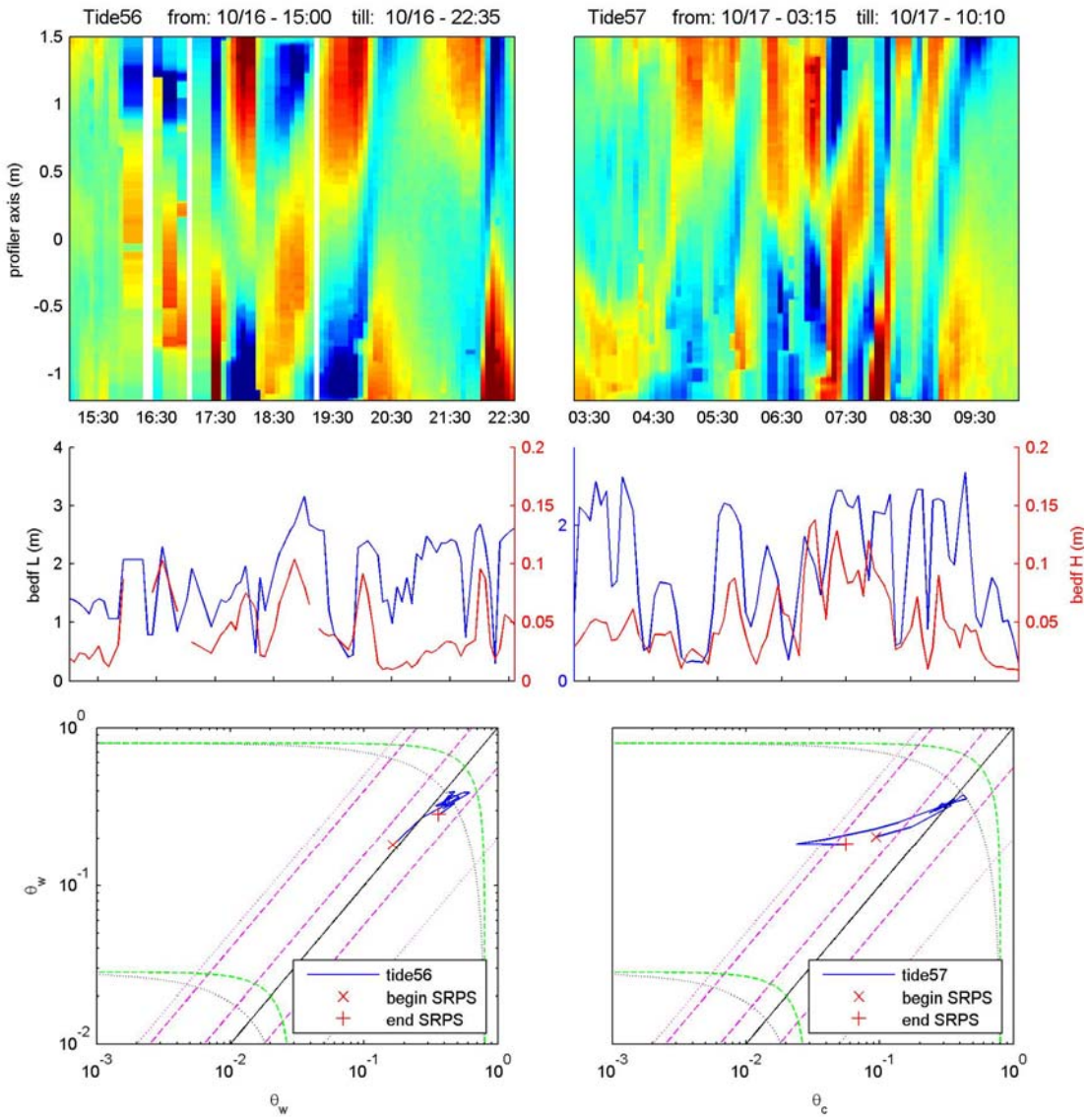

Fig. 3.13. Bedform graph, bedform length/height and type of flow conditions for tide 56 and 57.

indicating that the algorithm was not able to produce a bedform image. The source of this failure can be found in the raw SRPS data. Figure 3.13 shows two extremes found within the scans for tide 56. Scan 3371 corresponding to 17:05 on 16 October shows a nearly empty scan, little bed could be detected. Scan 3431 corresponding to 22:15 on 16 October shows a bed profile but with much scatter above it. Both scans can result from the same effect, much sand suspension. Because, the ripple profiler was fully submerged during both scans and the scans show relative instead of absolute reflection. Although the bed profiles are interpolated within and between scans, multiple adjacent scans with little or bad (scatter due to suspension) bed detection can result in failure of the bedform algorithm. The sand suspension leading to this failure is indicative for sheet flow conditions. This pleads again for adopting the method of Allen & Leeder (1980) above Soulsby (1997). The individual sweeps of tide 55 also show some large gabs and suspension clouds as in figure 3.14 during the period the conditions exceeded sheetflow. This strengthens the concluded sheet flow conditions during that period.

The conditions of tide 57 are most of the time just below the sheet flow criteria method of Allen & Leeder (1980). The bedform length is on average smaller than for tide 56 and the height on average larger. Some gabs in the individual scans are still found but smaller than for tide 56 and 55. These facts combined with the presence of larger bedforms with significant height before exceeding sheetflow conditions in tide 55, confirms the usage of Allen & Leeder (1980) by bounding the lower limit of the criteria.

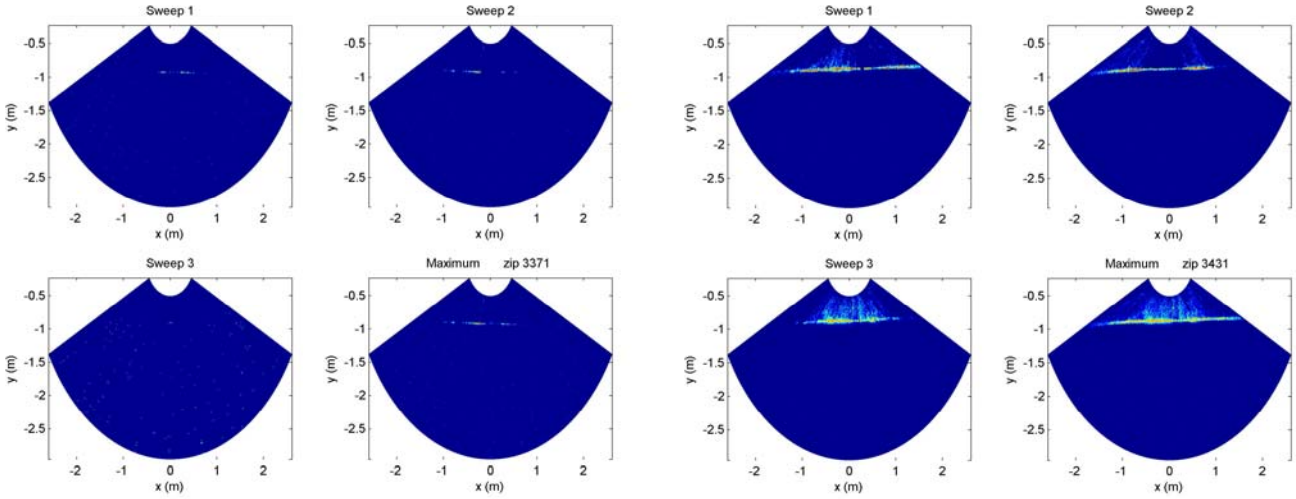

Fig. 3.14. Three successive SRPRS sweeps and there combined maxima for tide 56 on 16 October at 17:05 (left) and 22:15 (right).

3.5 Performance of bedform predictors

Figure 3.15 shows the observed bedform lengths against the predicted lengths by Nielsen (1981), Grant & Madsen (1982), Soulsby & Whitehouse (2005) and Khelifa & Ouellet (2000). $\sqrt{2} \cdot$ horizontal rms velocity (high frequency) is used for the maximum wave induced bottom particle velocity for the mobility number in Nielsen (1981). The bedform dimensions are averaged per 15 min to equal the period of the wave condition parameters. Since Nielsen (1981) and Grant & Madsen (1982) are purely wave predictors the plots distinguish the different flow conditions according to the separation criteria of Li & Amos (1998). In the plot of Soulsby & Whitehouse (2005) only wave and current induced bedforms are distinguished in line with their predictor. From first glance can be concluded that all predictors do not perform great. Nielsen (1981) predicts lengths between 0.35 and 3m which is in line with the observations. Bedforms > 2.5m have been present but have been averaged out and were difficult to capture due to the limited length of the bedform profile captured by the SRPS in the first place. But, little bedform lengths are correctly predicted by Nielsen (1981). Most of the lengths are under predicted, predicting a length of around 0.5 m while lengths of 0.7 to 2 m are present. Even thought Nielsen (1981) is a wave based bedform predictor, little difference between the performance for wave-only, wave-dominated or wave-current conditions is present. However, the wave-current conditions are the most under predicted. Which is expected since the current induced flow intensity is not taken into account.

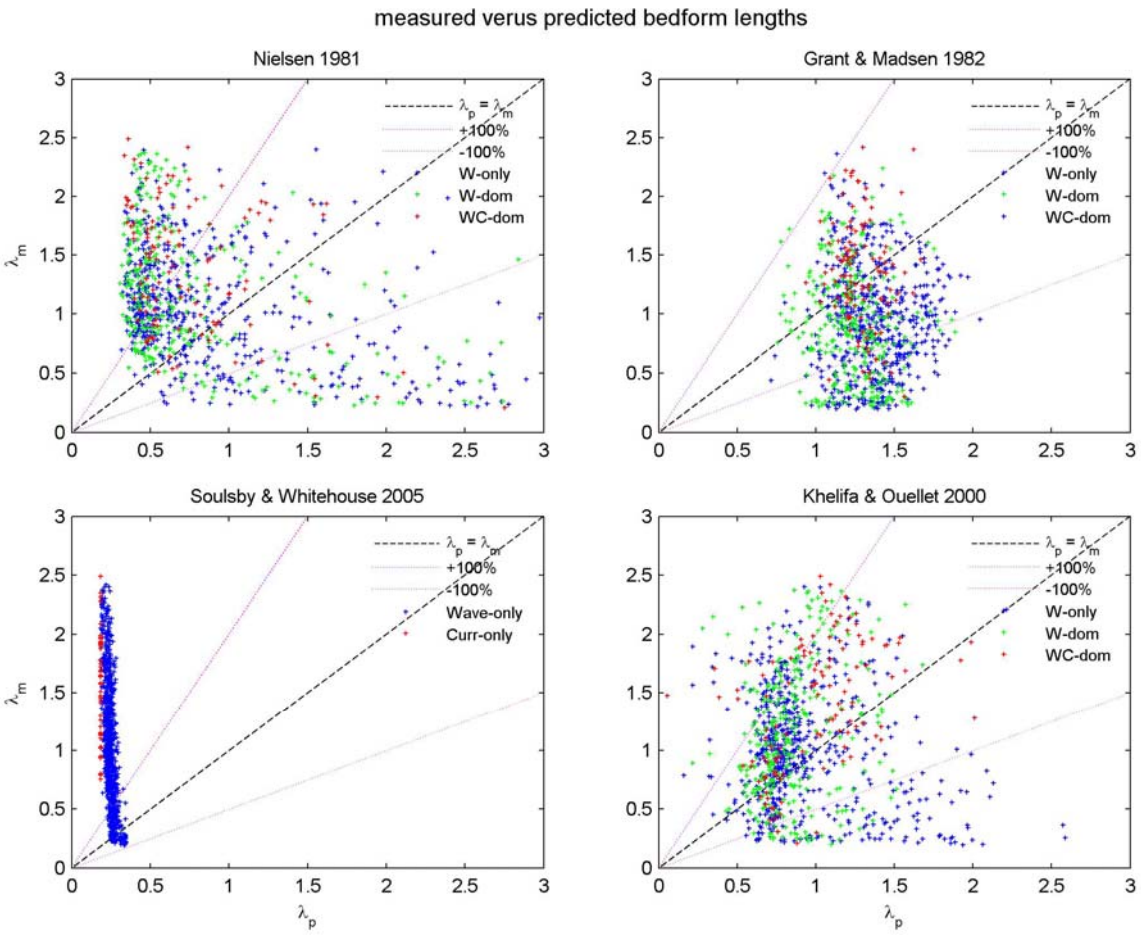

Fig. 3.15. Measured against predicted bedform heights for four different predictors. Wave-only, wave-dominated and wave-current conditions are distinguished and wave-only and current-only for Soulsby & Whitehouse (2005).

The majority of the predicted lengths by Grand & Madsen (1982) lay between 0.7 and 1.8m, hereby both under- and over predicting the lengths largely. The majority of the lengths are over predicted. The wave-current but especially the wave-dominated bedform lengths are more under predicted in compared with the wave-only bedforms, therefore having a slight better performance. This difference in performance between the different types of conditions is larger than for Nielsen (1981). Soulsby & Whitehouse (2005) predict lengths between 0.18 and 0.35m for wave conditions and lengths of 0.184m for current conditions. Nearly all lengths are therefore under predicted. Khellifa & Ouellet (2000) predict bedform lengths mainly between 0.2 and 2.2m with the majority between 0.6 and 1.4m. The lengths are more under- than over predicted, but for a more or less equal ratio for the different condition types. Khellifa & Ouellet (2000) perform the best out of the four tested predictors with most of the predicted lengths within a factor 2 (100% range in the figure) and also correctly predicting the range of lengths. Moreover, Khellifa & Ouellet (2000) does not only perform the best for all type of conditions, but also for the wave only conditions. The predictions of Soulsby & Whitehouse (2005) are the poorest. Unexpected is the small range of lengths predicted by Soulsby & Whitehouse (2005). However, it can be explained. In Soulsby & Whitehouse (2005) λ/A depends on Δ (A/d_{50}). For the given d_{50} and the found orbital diameter range of 0.6 – 2.6m Δ varies between 2000 and 8000. Since Soulsby & Whitehouse (2005) state that for $\Delta > 3000$ λ is

proportional to the d_{50} (anorbital ripples) and the sediment properties are assumed and expected to be constant during the campaign, the predicted bedfrom length range is small. As already concluded from the literature, the correctness of anorbital ripples scaling only to the sediment size for field (irregular wave) conditions is questioned.

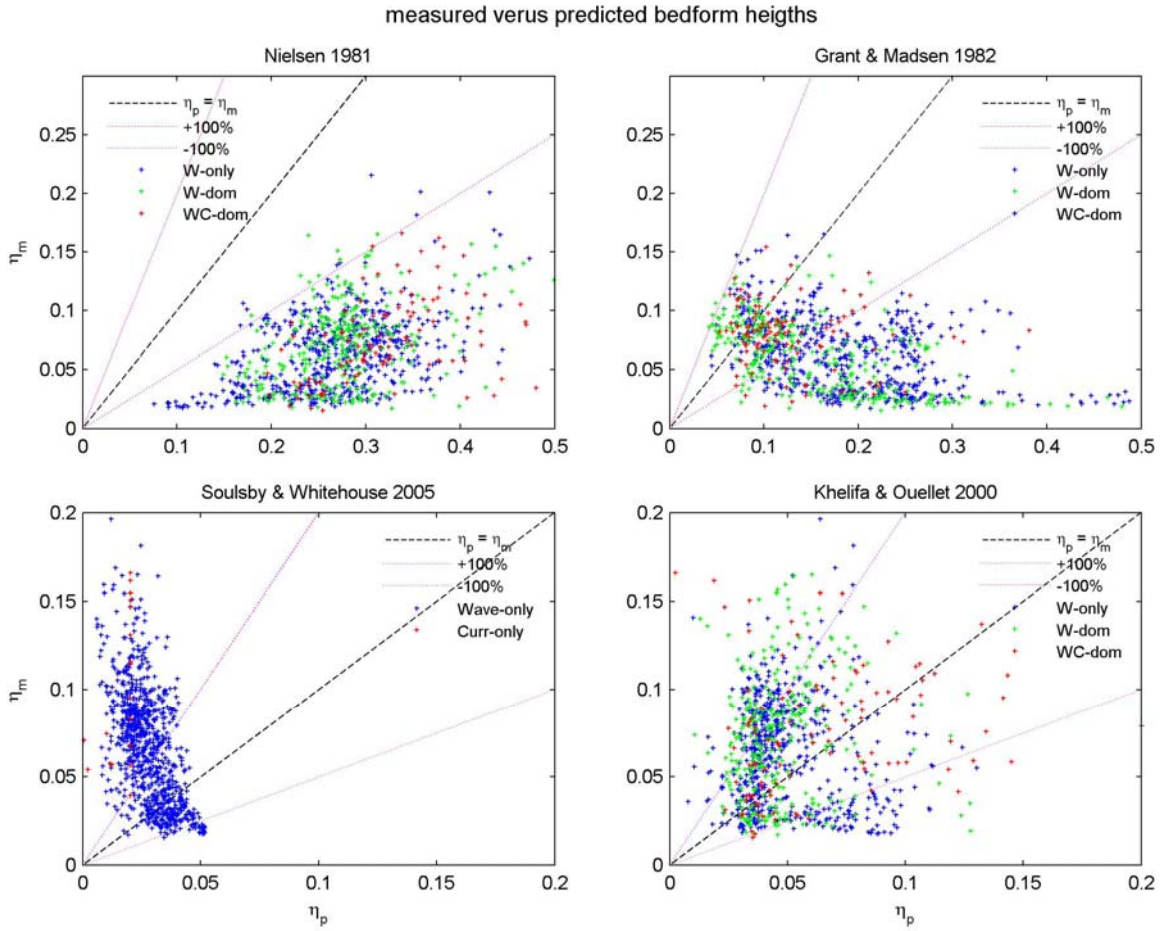

Fig. 3.16. Measured against predicted bedform lengths for four different predictors. Wave-only, wave-dominated and wave-current conditions are distinguished and wave-only and current-only for Soulsby & Whitehouse (2005).

Figure 3.16 shows the measured bedform height versus predicted bedform height. Nielsen (1981) over predicts all bedform lengths by at least a factor 2. No real difference between the predictions for the different condition types can be observed. Grant & Madsen (1982) performs better with about half of the bedform height within the 100% range and the rest being over predicted. Grant & Madsen (1982) over predict, like with the bedform length, the wave-dominant and wave-current conditions less than the wave-only conditions. Note the scale of the lower two graphs, which is different from the upper two for better details. Soulsby & Whitehouse (2005) also predicts a small range of bedform heights performing much better than for the bedform lengths. Khelifa & Ouellet (2000) perform again the best with a major part of the measurements within a factor 2. The wave-current heights seem to be the best distributed around the η_m-η_p line while the wave-only and wave-dominated bedforms are more under predicted. The (large) over prediction of the bedform height by Nielsen (1981) and Grant & Madsen (1982) would be expected for

wave-current conditions and in less amount for wave-dominated conditions due to the lower steepness for current induced bedforms by not incorporating the wash out effect for more intense flow conditions induced by a additional mean current. But, this over prediction is also present for wave-only conditions.

The poor performance may besides be caused by the predictors not being able to capture the hydraulic properties on which the bedforms depend on, also be induced by the way the bedform dimensions are measured and by relaxation for (rapid) changing conditions. Because the bedprofile scans were taken in cross shore direction, bedforms not having crests parallel to the longshore direction are under predicted by the measurements (observation) leading to under prediction by the predictors. For the bedform height measurements this bedform orientation is not relevant. When the bedform lengths would be compensated for this effect, which cannot been done since the angle between the crests and longshore direction cannot be measured, this would lead to a better length prediction performance for Nielsen (1982), Khelifa & Ouellet (2000) and Soulsby & Whitehouse (2005) since these predictors generally under predict the observed lengths. The performance of Grant & Madsen (1982) would further decrease since that predictor over predicts most lengths already.

Relaxation times alter the bedforms to be out of equilibrium with the forcing. Since the predictors predict equilibrium bedform dimensions, relaxation times causes over or under prediction for increasing versus decreasing conditions respectively. This effect can be observed in figure 3.17 for the Nielsen (1982) and Khelifa & Ouellet (2000). Because, the bedforms are expected to lack behind the conditions at the beginning and end of the tide when the conditions increase or decrease rapidly, while the bedforms are expected to be more or less in equilibrium with the flow conditions in between. The bedforms are in this study expected to be out of equilibrium with the conditions for the first- and fifth fifth part of the total duration of the tide. Those three periods are ‘separately’ plotted in figure 3.17 which do show the expected

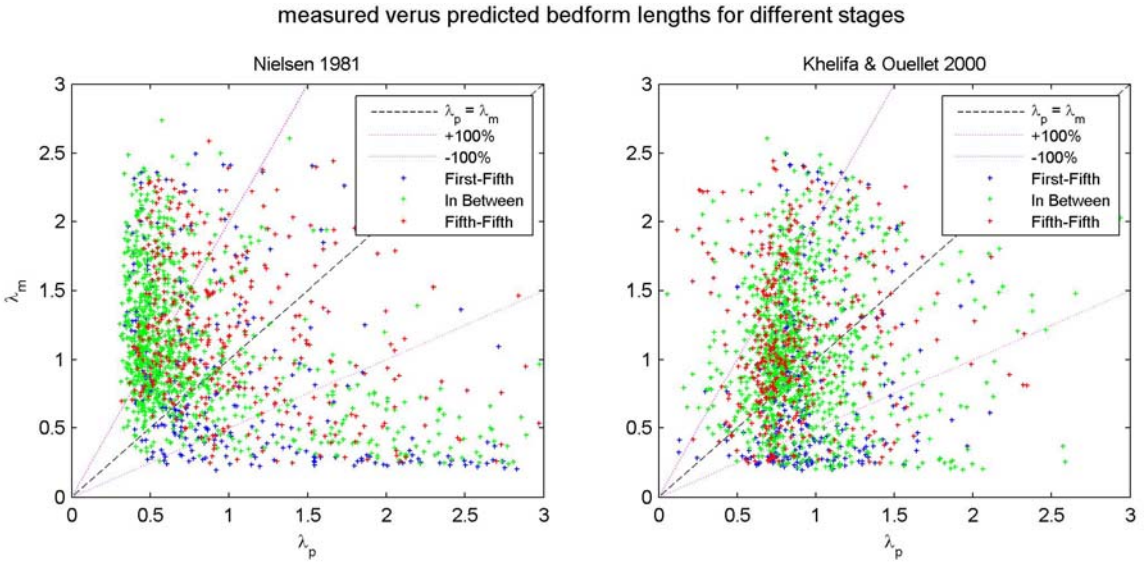

Fig. 3.17 Measured versus predicted bedform length for three different stage during the tides: the first fifth, fifth fifth and in between period of each tide.

behaviour: more overestimation at the beginning of the tide and more under estimation at the end of the tide with respect to the 'in between' period. Nielsen (1982) is plotted in addition to Khelifa & Ouellet (2000) because a pronounced effect was expected due to the large spread in predictions, which is indeed the case.
To correct for this effect a relaxation time model should be included to the predictor, like Soulsby & Whitehouse (2005), Doucette & O'Donogue (2006) or Traykovski (2007). But, a relaxation time model requires the equilibrium bedform height for the accompanying conditions to be known a priori. In order to assess how well the two best height predictors (Grant & Madsen, 1982; Khelifa & Ouellet, 2000) are able to predict the equilibrium bedform heights, the observed bedform heights are plotted against the predicted bedform heights for the different tide periods, figure 3.18. Although over prediction for the first fifth period and under prediction for the fifth fifth period in relation with the 'in between' period can be observed, ignoring those parts does not majorly improve the prediction performance. Since the scatter is for the in between period still very large, with a large part of the heights not correctly predicted within a factor two, comparison between different relaxation time models will difficult. Besides, the performance of the relaxation models will also depend on the choice of the predictor as can be noticed form the different behaviour of the first and fifth fifth periods in comparison to the in between period for the two predictors.

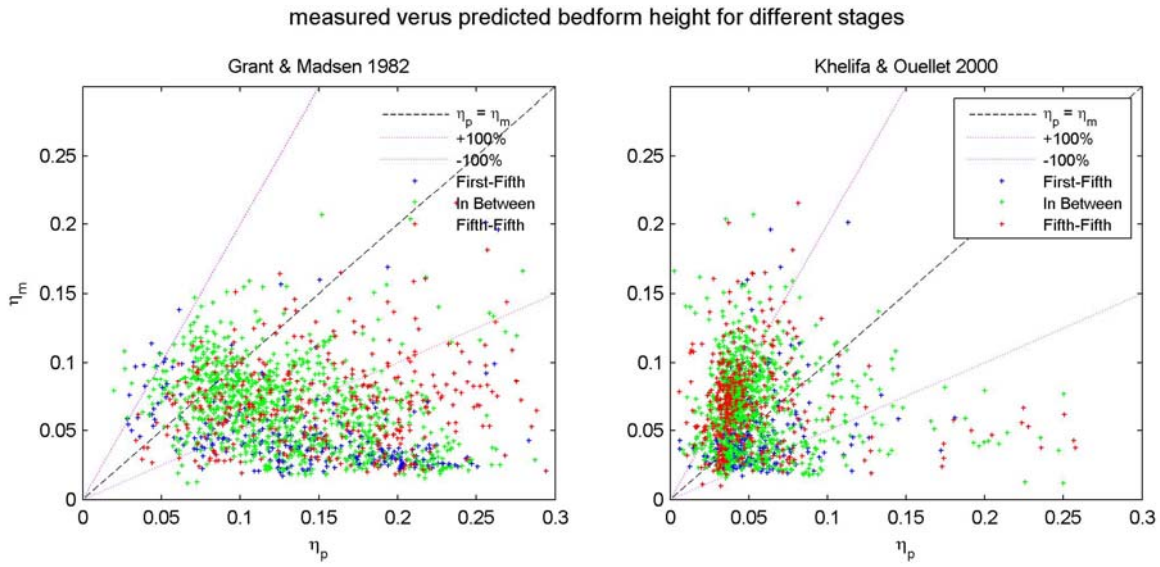

Fig. 3.18. Measured versus predicted bedform height for three different stage during the tides: the first fifth, fifth fifth and in between period of each tide.

Another observation can be made in figure 3.18 confirming the already formulated hypothesis about hysteresis. The fifth fifth part of the bedform heights shows more extreme under prediction than the first fifth part shows over predictions. And, the majority of the fifth fifth part shows a larger spread in over / under prediction in relation to the 'in between part' compared with the first fifth part. This is especially the case for Grant & Madsen (1982). This indicates that the response of the beforms to changes in flow conditions is different for an increase than for a decrease in flow conditions: hysteresis. Also the extreme under predictions in the fifth fifth part indicate the occurrence of bedform 'freeze' occasionally.

4. Discussion

The patterns in the bedprofile graphs indicate the presence of irregular (3D) bedforms. Although it is an interpretation of the bedprofile in time and could not be verified, visual observations confirm the presence of (relict) irregular (3D) bedforms during the campaign. This 3D occurrence is in contradiction with the criteria of O'Donoghue et al. (2006) who argue that 2D bedforms will appear for $d_{50} > 0.30$ mm while 3D bedforms will appear when $d_{50} < 0.22$ mm, since the d_{50} found to be 0.316 mm. However, O'Donoghue et al. (2006) also argue that turbulence is the key mechanism causing the formation of 3D bedforms. Turbulence is greater for more intense flow conditions, both larger $\hat{A}_\delta$ and mean current. This could explain the presence of 2D bedforms (ripples) for low intensity wave conditions and 3D for more intense mixed wave current conditions. This is in line with the dependency of the bedform type on the flow intensity found by Hay & Mudge (2005), although they found dependency on the orbital velocity and not on the longshore current. But, in relation to the conditions of Hay & Mudge (2005) the mean current was, due to the Slufter influence, much more intense. The observation are also to some extend in line with Andersen & Faraci (2002), according to which an increasing perpendicular current results in serpentine, segmented and irregular bedforms. The serpentine pattern is not observed directly. But, the ripples at the beginning of tide 22 and 55 do show some forward and backward moving behaviour which could indicate a serpentine pattern. Although this movement could be caused by reversing migration, this is not likely seen the conditions. However, such movement can also be the result of the growing processes split and slide. And, since the serpentine behaviour is accompanied with an increase of both the wave and current conditions, the distinction between a serpentine pattern and growing bedforms cannot be made. Still, the presence of irregular bedforms for intense currents, as in Andersen & Faraci (2002), is observed.

The transition from ripples to larger bedforms is found to depend on a small change of flow conditions. This transition is sensitive to Hm0 and the mean current with the mean current often playing a key role when exceeding 0.5 m/s. Such increase in bedform dimension depending on a small range of flow conditions has not been found in the literature. But, such nearshore type of conditions combined with a large mean current are new either, especially for such large tidal induced currents. This makes it even more plausible that the mean current plays a key role in the transition. Also, the tidal current is found to differ in flow characteristics from wave induced currents.

It was not possible to classify each bedform states into different wave / current induced classes due to the lack of 3D images of the bed. Although some 2D / 3D bedform characteristics have been indentified, on a timescale of one tide the conditions changed often too much to couple the bed characteristics to one type of condition, while on the timescale of an hour too little bedform characteristics could be identified. Though, the transition to larger bedforms did often coincide with the wave-dominated / wave-current boundary of Li & Amos (1998). But since such transitions were accompanied with an increase in flow intensity, the effect of changing flow conditions type cannot be judged separately. Low intensity mixed

wave current conditions did not occur at all during the field campaign, making it difficult to compare the mixed wave current bed characteristics to that of wave only bedforms. Furthermore, the different proposed criteria to separate wave / current induced bedforms / conditions are tested on different hydrodynamic versus bedform relations. Bedform length, steepness and asymmetry are plotted versus the shear velocity U_w/U_c ratio. Since the criteria of Andersen & Faraci (2002) comprehend orbital and mean current velocity instead of shear velocity, it could not be compared. None of the given bedform characteristics; bedform length, asymmetry or steepness, was separated by the U_w/U_c ratio. This can be explained by the fact that those three bedform characteristics are also influenced by wave only conditions. And, the fact that those characteristics are calculated from 2D images in one direction while the bedform may be directed in another direction, leads to anomalies. Still, some characteristics in the plotter graphs indicate dependency of the bedform characteristics on the criteria of Li & Amos (1998) above that of Zanke (2003). This combined with the found bedforms transitions occurring around the Li & Amos (1998) criteria pleads for adopting Li & Amos (1998).

The evolution of bedforms is found to differ for increasing versus decreasing condition: hysteresis. This effect becomes more pronounced for rapid changing conditions. For increasing conditions the bedforms evolve equal rapidly although some relaxation is often present. While for decreasing conditions the bedforms may, for a decrease in Hm0 of 0.2 m and mean current of 0.2 m/s per hour, freeze. However, such freeze is also found to be a temporally result of the process split. The 'freeze' of bedforms is also found by Austin et al. (2007), but for every tide. The larger tidal range and shorter duration of frame submergement (for the tides given in the paper maximal 4 hours versus 6-7 hours on average in this study) for Austin et al (2007) in comparison with this study may explain the found differences. Namely, the larger tidal range makes that the conditions change more rapidly inducing more easily an 'freeze' and the shorter duration makes that the bedforms do not get the time to further evolve (split) as for example observed in tide 38.

The found bedform evolution behaviour found for decreasing flow conditions does not stroke with the relaxation time predictors given in the literature. Smit & Sleath (2004), Soulsby & Whitehous (2005), Doucette & O'Donoghue (2006) and Traykovski (2007) state that the relaxation time depends negatively on the flow intensity and on the departure from equilibrium factor. For increasing flow conditions this is expected to be the case, as the data of Austin et al. (2007) also obeyed the predictor of Doucette & O'Donghue (2006). But, for decreasing conditions a different behaviour is found. (Temporary) freeze of the bedform dimension is not predicted by the different relaxation predictors. The departure from equilibrium factor is therefore believed to be invalid for decreasing conditions. Larger relaxation times for larger differences between present and equilibrium bedform dimension for decreasing conditions are expected.

The observed upper stage plan beds indicate that the method of Allen & Leeder (1980) should be adopted above Soulsby (1997) with a critical Shields number of 0.8. The difference between the two methods is reflected in the shape of the curves in the θ_w/θ_c graph, which deviates the most from each other

around the $\theta_w = \theta_c$ line. But since all sheet flow observations cluster around this $\theta_w = \theta_c$ line one cannot conclude that the method of Allen & Leeder (1980) is better than Soulsby (1997). Because, no sheet flow conditions for wave-only, wave-dominated, current-dominated or current-only conditions (according to the criteria of Li & Amos (1998)) are observed, the curvature of the combined Shields criteria is not constrained. Therefore, the method of Soulsby (1997) could also be adopted with a lower critical Shields number corresponding to a wave and current induced Shields number of 0.4, adding up to a critical Shields number of 0.57. So, adopting the method of Allen & Leeder (1980) with a critical Shields number of 0.8 or adopting Soulsby (1997) with 0.57? Although Soulsby (1997) is the most physical correct, a critical Shields number for wave only induced conditions of 0.57 is low in comparison with other researches, 0.8 by Rijn (1993) and Camenen (2009) and 1.0 by Nielsen (1992). Therefore, the method of Allen & Leeder (1980) $\theta_{\mathrm{wc}} = \theta_w + \theta_c$ is adopted with a critical Shields number of 0.8.

None of the reviewed predictors, Nielsen (1981), Grant & Madsen (1982), Soulsby & Whitehouse (2005) and Khelifa & Ouellet (2000), managed to predict the dimensions within a factor 2. Even, when disregarding the first fifth and fifth fifth duration of each tide which are expected to deviate due to relaxation. Besides the lack of capturing the bedform behaviour for the observed conditions, such as the observed large bedform length increase for a small range of conditions, errors in the length measurements also alter the predictions. Correcting for these errors, which is not possible, would improve the predictions of Nielsen (1981), Soulsby & Whitehouse (2005) and Khelifa & Ouellet (2000) since those predictors generally under estimate the bedform lengths. The predictions of Soulsby & Whitehouse (2005) are the poorest. This is induced by the assumption that anorbital ripples only scale to the sediment size. This is not the case, and probably does not count for any field (irregular) condition either. The predictor taking into account the current effects, Khelifa & Ouellet (2000), performs the best even for wave only conditions. The differences in predictions between wave and mixed conditions are small anyway, even for the wave only predictors.

5. Conclusion

The wave conditions at the instrument location during the campaign were mostly just prior to breaking having shoaling characteristics, due to its location behind an inner bar at roughly the same height as the bar. The significant wave height varied mainly between 0.5 m and 1.0 m exceeding to 1.35 m. The mean current averaged 0.4 m/s with a maximum of 1.2 m/s. The current was most of the time mainly tidal induced due to the presence of the Slufter. The accompanying bedforms varied in length between 0.17 and 3 m with an average of 1.0 m. The heights, mostly following the same pattern as the length, varied between 0.01 and 0.23 m with an average of 0.07 m. The bedform steepness mainly varying between 0.02 and 0.17 decreased for increasing bedform length, nearly linearly.

The transition from ripples to larger bedforms is found to depend on a small change of flow conditions. This transition is sensitive to Hm0 and the mean current and is found to occur when both Hm0 and the mean current exceed 0.5 - 0.6 (m and m/s respectively), but the mean current often plays a key role. 2D bedforms (ripples) for low intensity wave conditions and 3D for more intense mixed wave current conditions are observed. This observation is based on an interpretation of the 2D bedprofiles in time. The observation are in line with Hay & Mudge (2005) and Andersen & Faraci (2003), but further bedform classification like Hay & Mudge (2005) and Andersen & Faraci (2003) is not possible due the limitations of the 2D ripple profiler. So are the growing and decaying bedform processes split and merge indistinguishable form an irregular bedform pattern.

Due to this lack of distinguishable bedform classes the wave and mixed wave-current induced bedforms could not be separated by proposed criteria directly. But several observations and relations indicate that the criteria proposed by Li & Amos (1998) are applicable. So did the transition to larger bedforms often coincide with the wave-dominated / wave-current boundary of Li & Amos (1998) and did the bedform length and bedform steepness show characteristics which could be linked to the criteria of Li & Amos (1998).

Bedforms were not always present. Lower stage plane bed has not been observed or measured but upper stage plane bed, sheet flow conditions, did. Since sheet flow conditions were only present for wave-current conditions, the sheet flow criteria method of Allen & Leeder (1980) with a critical Shields number of 0.8 and the method of Soulsby (1997) with a critical Shields number of 0.57 both distinguish a bed covered with beforms and upper stage plane bed. But, since the critical Shields number of 0.57 is quite low and 0.8 is more widely adopted for wave only conditions (e.g. Rijn, 1993; Camenen, 2009) the method of Allen & Leeder (1980) is adopted.

The evolution of bedforms is found to differ for increasing versus decreasing condition: hysteresis. This effect becomes more pronounced for rapid changing conditions. For increasing conditions the bedforms evolve equal rapidly although some relaxation is often present. For decreasing conditions the bedforms dimensions delay the conditions significantly and may, for a decrease in Hm0 of 0.2 m and mean current of 0.2 m/s per hour, ‘freeze’. This freeze may be a temporarily result of the process of split. The occurrence of freeze and quite different behaviour for increasing versus decreasing conditions indicate that

relaxation time predictors given in the literature; Soulsby & Whitehous (2005), Doucette & O'Donoghue (2006) and Traykovski (2007) are not valid for decreasing conditions. These predictors state that the relaxation time depends negatively on the flow intensity and departure from equilibrium factor. For increasing flow conditions this is expected to be the case, as the data of Austin et al. (2007) also obeyed the predictor of Doucette & O'Donghue (2006). But, for decreasing conditions the departure from equilibrium factor is expected to be invalid. Larger relaxation times for larger differences between present and equilibrium bedform dimension for decreasing conditions are expected. The always 'freezed' bedform dimensions for decreasing conditions observed by Austin et al. (2007) may be caused by the rapid decreasing conditions and short available time for the bedforms to adjust.

The bedform predictor of Khelifa & Ouellet (2000) preformed the best with predicting the correct range of dimensions and predicting a large part of the dimensions within a factor 2 of the observations. Soulsby & Whitehouse (2005) preformed the poorest especially for the bedform length predicting a maximum length of 0.35m. This error is induced by the prediction that anorbital ripples were present which only scale to the sediment size. This is not the case, and probably does not count for any field (irregular) condition either. Disregarding the bedforms from the first fifth and fifth fifth duration of each tide, which are expected to deviate due to relaxation, did not lead to major improvements of the predictors. Also, the differences in performance for wave versus wave-current conditions were small even for wave based predictors. The prediction of wave only induced bedform dimensions were surprisingly also best performed by Khelifa & Ouellet (2000).

References

Andersen, K.H. and C. Faraci (2003), The wave plus current flow over vortex ripples at an arbitrary angle, *Coastal Engeneering, Vol 47, p 431-441.*

Austin, M.J., G. Masselink, T.J. O'Hare and P.E. Russell (2007), Relaxation time effects of wave ripples on tidal beaches, *Geophysical Research Letters, Vol 34.*

Bagnold, R.A. (1946), Motion of waves in shallow water Interaction between waves and sand bottoms, *Proc. R. Soc. London, Ser. A, Vol. 187*, 1-15.

Camenen, B. (2009), Estimation of the wave-related ripple characteristics and induced bed shear stress, *Estuarine, Coastal and Shelf Science, 84*, 553-564.

Clifton, H.E. (1976), Wave-formed sedimentary structures: A conceptual model, *SEPM Spec. Publ.*, 24, 126-148.

Dolphin, T., C. Vincent (2009), The influence of bed forms on reference concentration and suspension under waves and currents, *Continental Shelf Research, 29,* 424 – 432.

Doucette, J.S., and T. O'Donoghue (2006), Response of sand ripple to change in oscillatory flow, *Sedimentology, 53,* 581-596

Durieux, M.X., 2004, *De stabiliteit van de Slufter op Texel*, MSc thesis (unpublished)

John D'Errico 4/15/06 (inpaint_nans)

Jenkins, G.M. and D.G. Watts (1968), Spectral analysis and its applications, *Holden-Day*, *San Francisco*, 525 pp.

Garrett, C.J.R. and B. Toulany (1981), Variability of the flow through the Striat of Belle Isle. *Journal of Marine Research*, 39, 163 – 189.

Grant, W.D. and O.S. Madsen (1986), The continental shelf bottom boundary layer. *Annual Review of Fluid Mechanics*, Vol. 18, 265-305.

Grasmeijer, B. and M.G. Kleinhans (2004), Observed and predicted bed forms and their effect on suspended sand concentrations, *Coastal Engineering, 51,* 351-371

Hay, A.E., and T. Mudge (2005), Principal bed states during SandyDuck97: Occurrence, spectral anisotropy, and the bed state storm cycle*, J. Geophys. Res.*, 110, C03013.

Khelfa, A. And Y. Ouellet (2000), Prediction of sand ripple geometry under waves and currents, *Journal of Waterway, Port, Coastal, and Ocean Engineering, Vol 126, p 14-20.*

Kleinhans, M.G. (2005), Phase diagrams of bed states in steady, unsteady, oscillatory and mixed flows, *report Q of Sandpit book.*

Lee Young, J.S. and J.F.A. Sleath (1990), Ripple formation in combined transdirectional steady and oscillatory flow, *Sedimentology, Vol 37, p 509-516.*

Li, M.Z. and M.Z. Amos (1998), Predicting ripple geometry and bed roughness under combined waves and currents in a continental shelf environment, *Continental Shelf Research, 18,* 941-970.

Masselink, G. (1995), Group bound long waves as a source of infragravity energy in the surf zone, *Continental Shelf Research,* Vol 15, No.13, pp. 1525-1547.

Masselink, G., M.J. Austin, T.J. O'Hara, and P.E. Russell (2007), Geometry and dynamics of wave ripples in the nearshore zone of a coarse sandy beach, *Journal of Geophysical Research,* Vol.112, C10022.

Nielsen, P. (1992), Coastal bottom Boundary layers and sediment transport

O'Donoghue, T., J.S. Doucette, J.J. Van der Werf, J.S. Ribberin (2006), Dimensions of full-scale sand ripples in oscillatory flow, *Coastal Engineering, 53*, 997–1012.

O'Donoghue, T. and Clubb, G.C. (2001), Sand ripples generated by regular oscillatory flow, *Coastal Engineering*, 44, 101–115.

Osborne, P.D. and C.E.Vincent (1993), Dynamics of large and small scale bedforms on a macrotidal shoreface under shoaling and breaking waves, *Marine Geology, 115,* 207-226.

Ribberink, J. S. and A.A. Al-Salem (1994), Sediment transport in oscillatory boundary layers in case of rippled beds and sheet flow, *J. Geophys Res*, 99(C6), 12707-12727.

van Rijn, L.C., 1993, Principles of sediment transport in rivers, estuaries, seas and oceans. *Aqua Publications.*

Sherman, D.J. and B. Greenwood (1984), Boundary roughness and bedforms in the surf zone, *Marine Geology, 60,* 199-218.

Smith, D. and J.F.A. Sleath (2004), Transient ripples in oscillatory flows, *Continental Shelf Research, 25*, 485 – 501.

Soulsby, R.L. (1997), Dynamics of marine sands, *Thomas Telford,* p.249.

Soulsby, R.L., and R.J.S. Whitehouse (2005), Prediction of ripple properties in shelf seas, *Final Tech. Rep. TR154*, HR Wallingford, Wallingford, U.K.

Stegner, A. and J.E. Westfreid, Dynamical evolution of sand ripples under water, *Phys. Rev. E*, *Vol. 60(4),* pp. 3487-3490, 1999.

Torrence, C., and G.P. Compo (1998), A practical guide to wavelet analysis, Bulletin *of the American Meteorological Society*, Vol. 79, No. 1.

Traykovski, P. (2007), Observation of wave orbital scale ripples and a nonequilibrium time-depended model, *Journal of Geophysical research, Vol 112, C06026.*

van der Werf, J.J. (2006), Sand transport over rippled beds in oscillatory flow.

Styles, R., S.M. Glenn (2002), Modelling bottom roughness in the presence of wave-generated ripples, *Journal of geophysical Research, VOL 107, C8.*

Vincent, V.R., D.M. Hanes, and A.J. Bowen (1991), Acoustic measurements of suspend sand on the shore face and the control of concentration by bed roughness, *Marine Geology.*, 96, 1-18.

van der Werf, J.J. (2006), Sand transport over rippled beds in oscillatory flow.

van der Werf, J.J., J.S. Doucette, T.O'Donoghue, and J.S. Ribberink (2007*),* Detailed measurements of velocities and suspended sand concentrations over full-scale ripples in regular oscillatory flow, *Journal of Geophysical Research*, *VOL. 112*, F02012.

Wiberg, P.L., and C.K. Harris (1994), Ripple geometry in wave-dominated environments, J. *Geophys. Res., 99,* 775-798.

Williams, J.J., P.S. Bell and P.D. Thorne (2005), Unifying large and small wave-generated ripples, *Journal of Geophysical Research, 110,* C02008.

Yoshikawa, H.N., G. Rousseaux, J. Kruithof, A. Stegner, and J.E. Wesfreid (2004), Flow structure over rolling-grain ripples – laboratory experiments and theoretical study, *Marine Sandwave and River Dune Dynamics*, 346-351.

Zanke, U.C.D. (2003), On the influence of turbulence on the initiation of sediment motion, *International J. of Sediment Research*, 18(1), 1-15

Appendix A

Tide 5

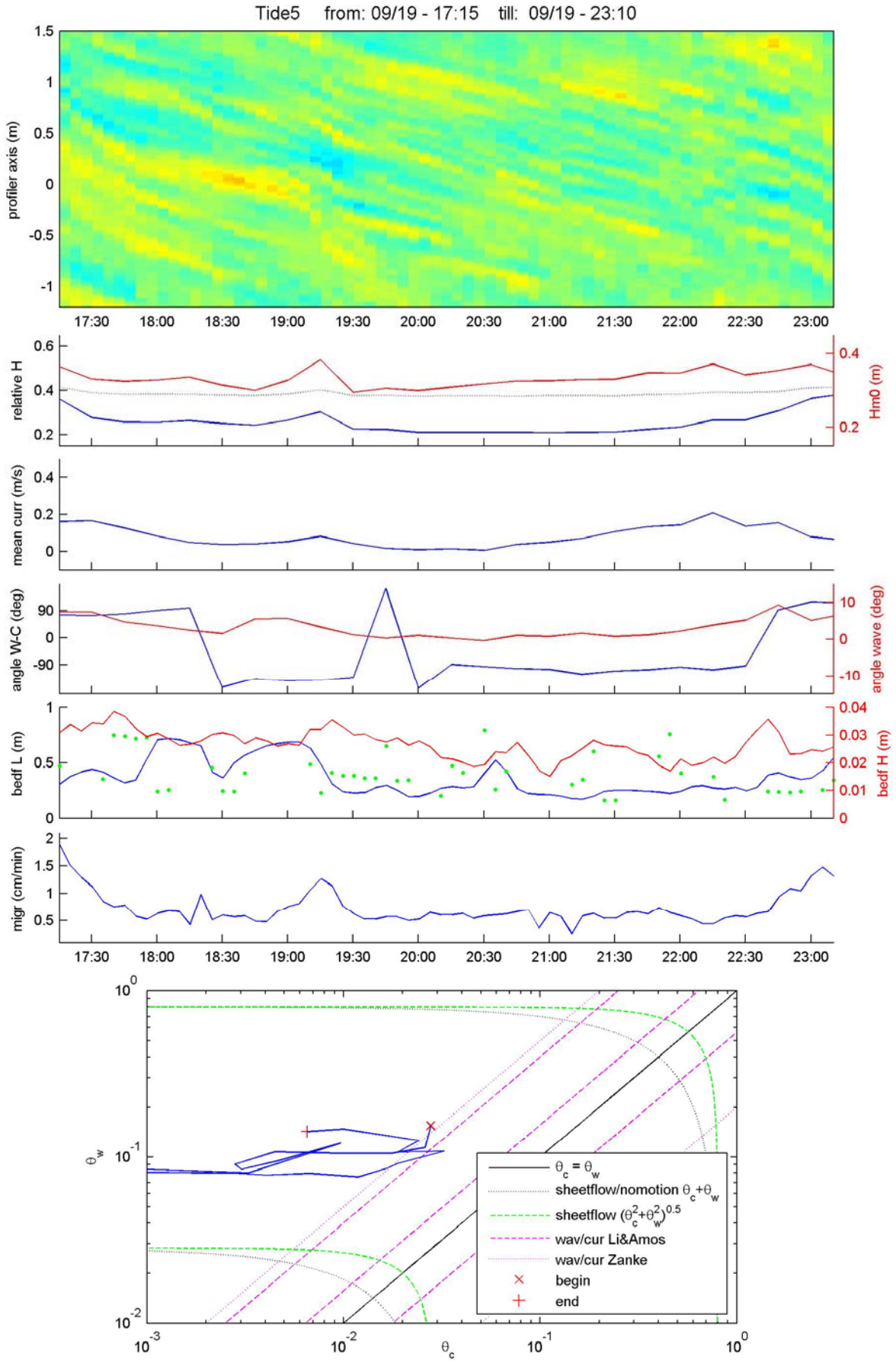
Tide5 from: 09/19 - 17:15 till: 09/19 - 23:10
profiler axis (m)
relative H
Hm0 (m)
mean curr (m/s)
angle W-C (deg)
angle wave (deg)
bedf L (m)
bedf H (m)
migr (cm/min)
17:30
18:00
18:30
19:00
19:30
20:00
20:30
21:00
21:30
22:00
22:30
23:00
θw
θc
θc = θw
sheetflow/nomotion θc+θw
sheetflow (θc²+θw²)^0.5
wav/cur Li&Amos
wav/cur Zanke
begin
end

Tide 10

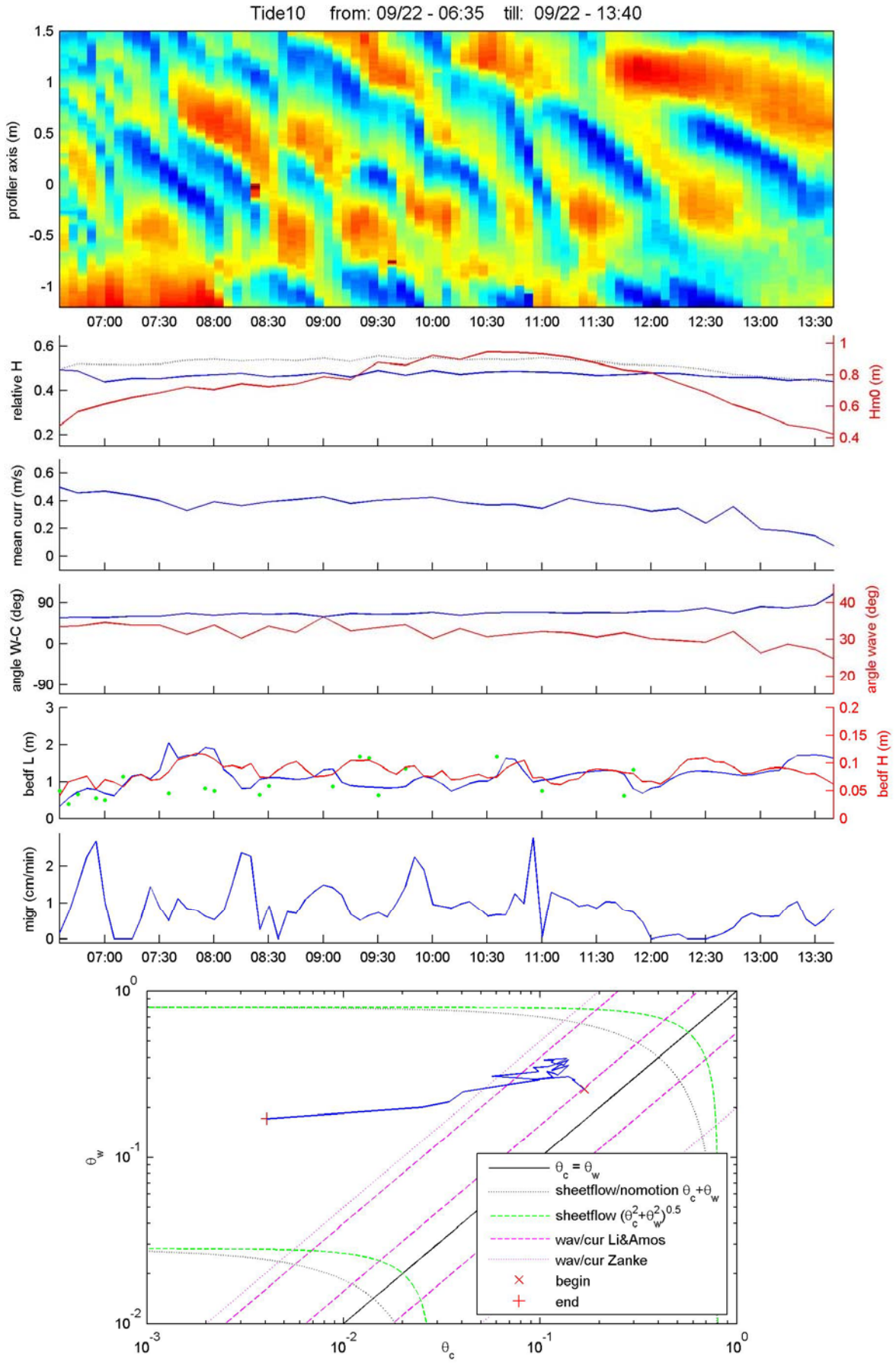
Tide10 from: 09/22 - 06:35 till: 09/22 - 13:40
profiler axis (m)
relative H
Hm0 (m)
mean curr (m/s)
angle W-C (deg)
argle wave (deg)
bedf L (m)
bedf H (m)
migr (cm/min)
07:00 07:30 08:00 08:30 09:00 09:30 10:00 10:30 11:00 11:30 12:00 12:30 13:00 13:30
θw
θc
θc = θw
sheetflow/nomotion θc+θw
sheetflow (θc2+θw2)0.5
wav/cur Li&Amos
wav/cur Zanke
begin
end

Tide 26

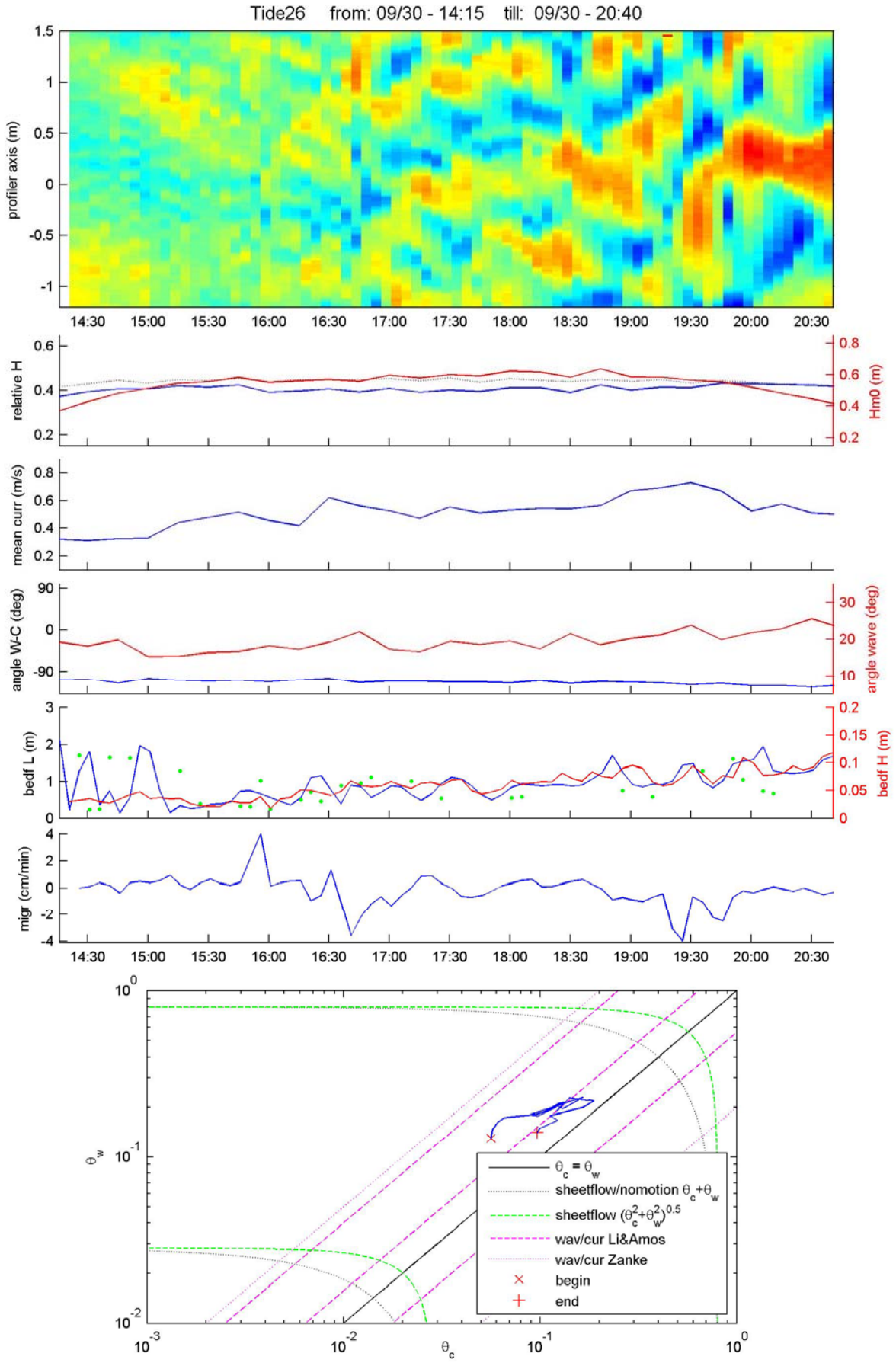
Tide26 from: 09/30 - 14:15 till: 09/30 - 20:40
profiler axis (m)
relative H
Hm0 (m)
mean curr (m/s)
angle W-C (deg)
argle wave (deg)
bedf L (m)
bedf H (m)
migr (cm/min)
14:30
15:00
15:30
16:00
16:30
17:00
17:30
18:00
18:30
19:00
19:30
20:00
20:30
θw
θc
θc = θw
sheetflow/nomotion θc+θw
sheetflow (θc²+θw²)^0.5
wav/cur Li&Amos
wav/cur Zanke
begin
end

Tide 28

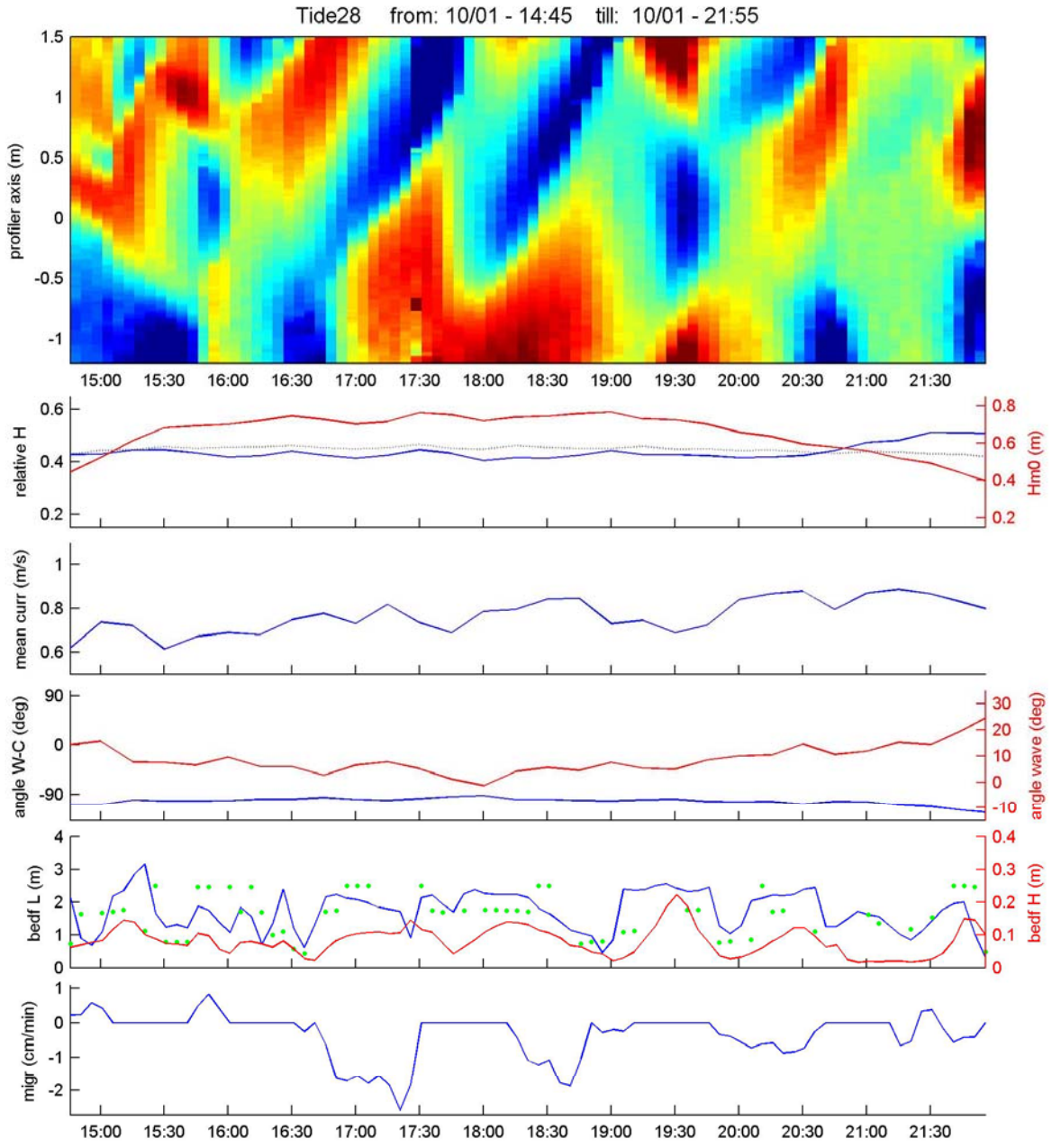
Tide28 from: 10/01 - 14:45 till: 10/01 - 21:55
profiler axis (m)
relative H
Hm0 (m)
mean curr (m/s)
angle W-C (deg)
angle wave (deg)
bedf L (m)
bedf H (m)
migr (cm/min)
15:00
15:30
16:00
16:30
17:00
17:30
18:00
18:30
19:00
19:30
20:00
20:30
21:00
21:30

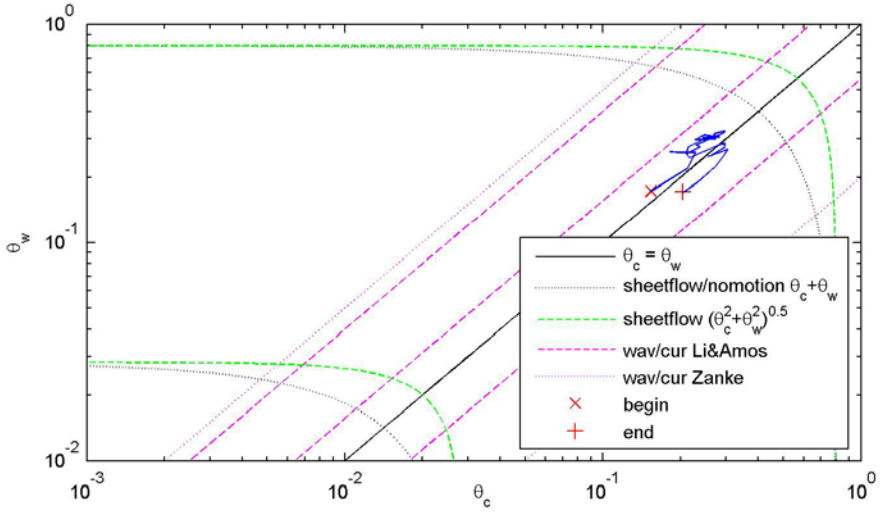
θc = θw
sheetflow/nomotion θc+θw
sheetflow (θc²+θw²)^0.5
wav/cur Li&Amos
wav/cur Zanke
begin
end
θw
θc

Tide 38

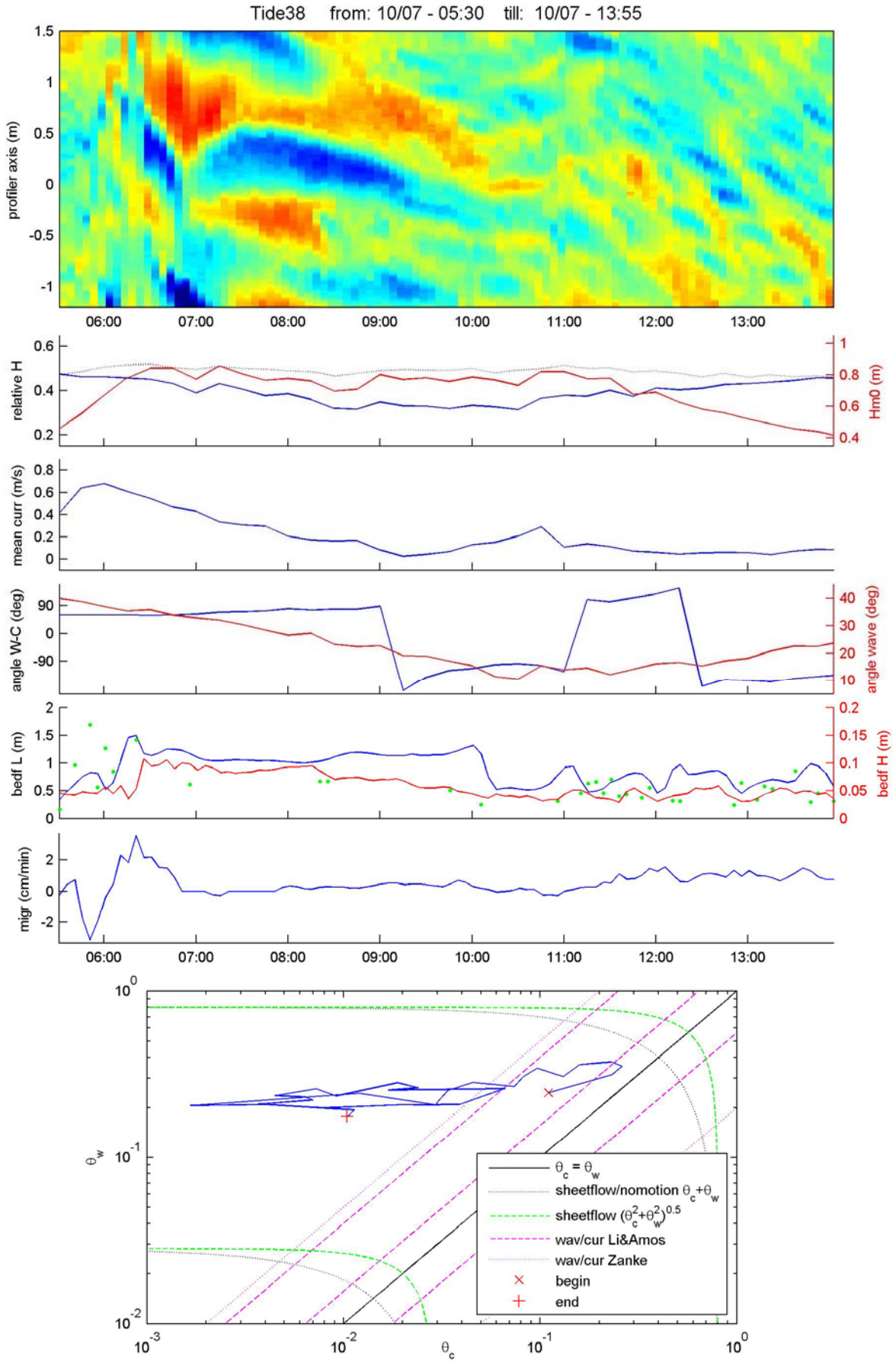
Tide38 from: 10/07 - 05:30 till: 10/07 - 13:55
profiler axis (m)
relative H
Hm0 (m)
mean curr (m/s)
angle W-C (deg)
argle wave (deg)
bedf L (m)
bedf H (m)
migr (cm/min)
06:00
07:00
08:00
09:00
10:00
11:00
12:00
13:00
θw
θc
θc = θw
sheetflow/nomotion θc+θw
sheetflow (θc²+θw²)^0.5
wav/cur Li&Amos
wav/cur Zanke
begin
end

Tide 55

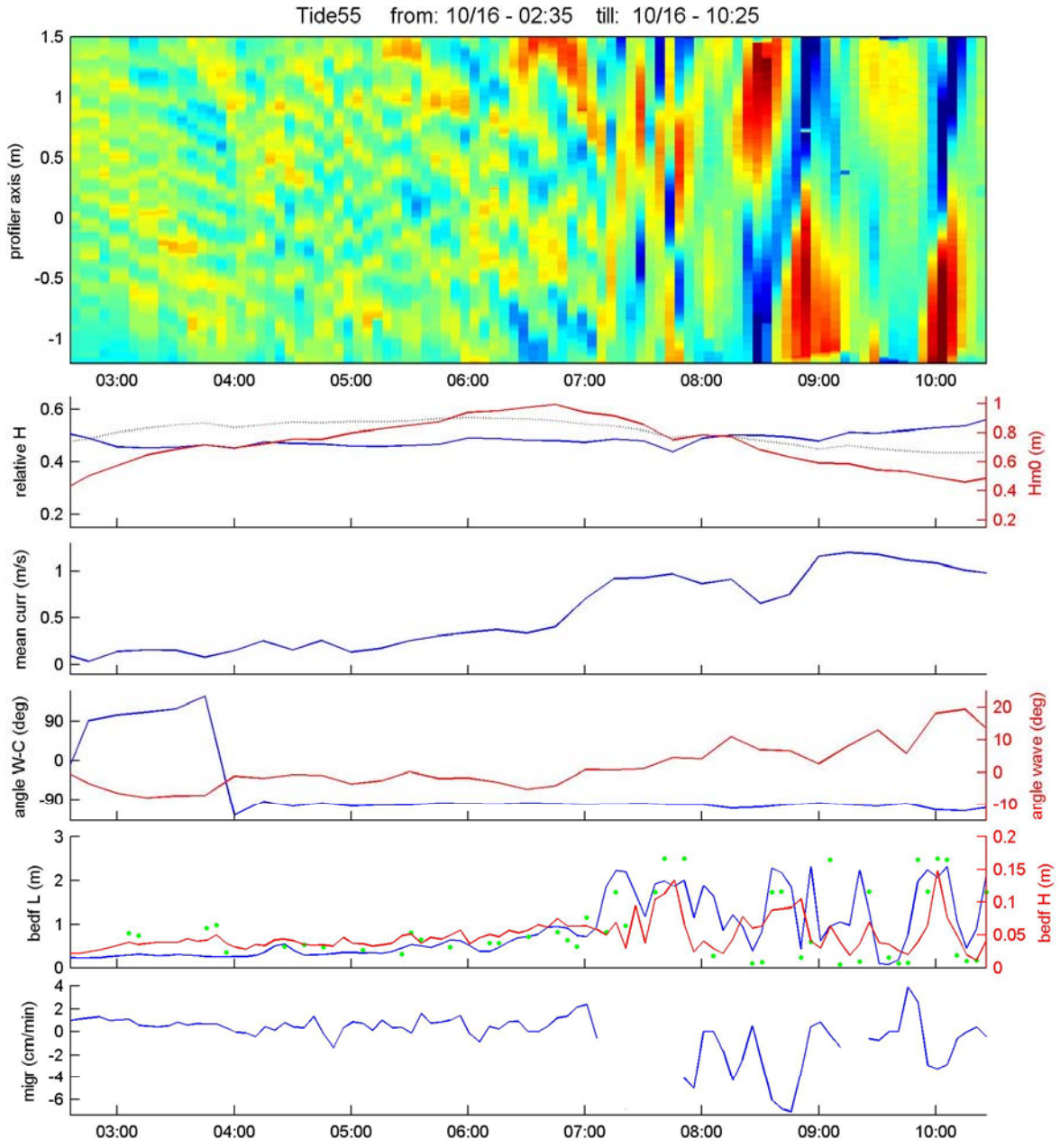
Tide55 from: 10/16 - 02:35 till: 10/16 - 10:25
profiler axis (m)
relative H
Hm0 (m)
mean curr (m/s)
angle W-C (deg)
angle wave (deg)
bedf L (m)
bedf H (m)
migr (cm/min)
03:00
04:00
05:00
06:00
07:00
08:00
09:00
10:00

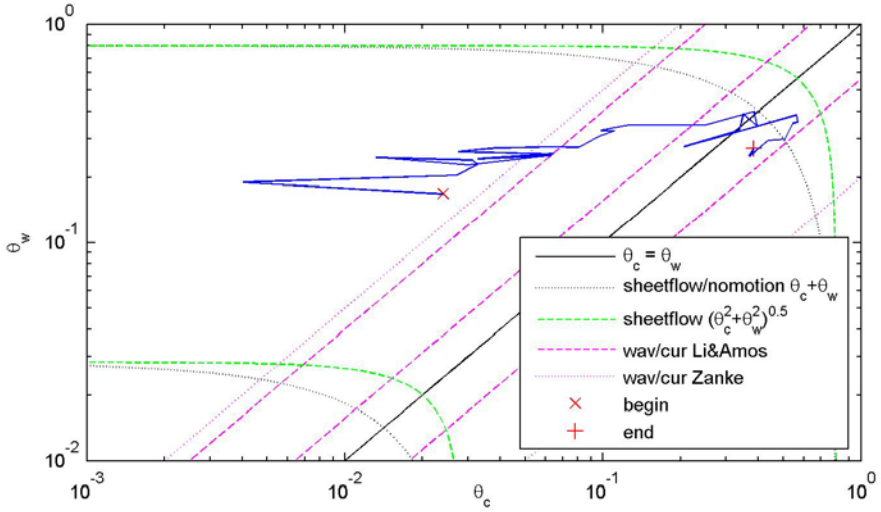
θc = θw
sheetflow/nomotion θc+θw
sheetflow (θc²+θw²)^0.5
wav/cur Li&Amos
wav/cur Zanke
begin
end
θw
θc